UNIVERSITY OF CALIFORNIA SAN DIEGO
SAN DIEGO STATE UNIVERSITY

Neotectonics in San Diego, California: Paleoseismology, Slip Rate, and Offshore Structure of the Rose Canyon Fault

A dissertation submitted in partial satisfaction of the requirements for the degree

Doctor of Philosophy

in

Geophysics

By

Drake Moore Singleton

Committee in charge:

San Diego State University:
Professor Jillian M. Maloney, Chair
Professor Trent W. Biggs
Professor Thomas K. Rockwell

University of California San Diego
Professor Duncan C. Agnew
Professor Joel P. Conte

2020

The dissertation of Drake Moore Singleton is approved, and it is acceptable in quality and form for publication on microfilm and electronically:

_____

_____

_____

_____

_____

Chair

University of California San Diego

San Diego State University

2020

DEDICATION

To my mom and dad,
Thanks for all the hard work

EPIGRAPH

We're building something here, detective.
We're building it from scratch.
All the pieces matter.

- Det. Lester Freeman
(The Wire S01-E06)

TABLE OF CONTENTS

Signature Page iii
Dedication iv
Epigraph v
Table of Contents vi
List of Figures viii
List of Tables ix
Acknowledgements x
Vita xii
Abstract of the Dissertation xiii

1. Introduction....1
   1.1. References....6

2. Late-Holocene rupture history of the Rose Canyon fault in Old Town, San Diego: Implications for cascading earthquakes on the Newport-Inglewood-Rose Canyon fault system....9
   2.1. Abstract....10
   2.2. Introduction....11
   2.3. Methods....14
      2.3.1. Site Selection 14
      2.3.2. Trench Investigation 15
      2.3.3. Radiocarbon Dating 16
   2.4. Stratigraphy 16
      2.4.1. Trench 1....16
      2.4.2. Trench 2....19
         2.4.2.1. Historical alluvial and fluvial deposits 20
         2.4.2.2. Holocene alluvial and fluvial deposits 21
         2.4.2.3. Pleistocene deposits 23
   2.5. Age Dating of Units 23
      2.5.1. T1 24
      2.5.2. T2 24
   2.6. Interpretation and Correlation of Stratigraphic units in T1 and T2 25
   2.7. Evidence of Earthquakes 29
   2.8. Discussion 33
      2.8.1. Earthquake Magnitudes and Late-Holocene Recurrence Interval 33
      2.8.2. Effect of Fault Structure on Earthquake Occurrence 37
      2.8.3. Cascading Seismicity of the Newport-Inglewood-Rose Canyon Fault System .39
   2.9. Conclusions 42
   2.10. Data and Resources 43
   2.11. Acknowledgements 43
   2.12. References 44

3. Slip rate for the Rose Canyon fault through San Diego, CA based on analysis of new GPS data: Evidence of a potential Rose Canyon-San Miguel-Vallecitos fault connection?....63
   3.1. Abstract 64

3.2. Introduction 65
3.3. Methods 70
3.3.1. GPS data collection and processing 70
3.3.2. Deformation models 72
3.3.2.1. Deformation models–homogeneous elastic half-space 72
3.3.2.2. Deformation models–asymmetric elastic half-space 73
3.3.3. Reprocessing legacy MCS data 74
3.4. Results 75
3.4.1. Stability of campaign survey sites and GPS data quality 75
3.4.2. Single and double fault homogeneous elastic half-space model 76
3.4.3. Asymmetric elastic half-space model....78
3.4.4. Legacy MCS profiles 79
3.5. Discussion 80
3.5.1. Slip rate on the Rose Canyon Fault 80
3.5.2. A Rose Canyon – San Miguel-Vallecitos fault connection? 81
3.5.3. Rheological contrasts across the southern Newport-Inglewood-Rose Canyon fault 85
3.5.4. Seismic hazard for San Diego-Tijuana region 86
3.6. Conclusions 87
3.7. Acknowledgements 88
3.8. References 88

4. Recency of faulting and subsurface architecture of San Diego pull-apart basin, California USA 107
4.1. Abstract 108
4.2. Introduction 109
4.3. Regional Geology and Local Tectonics 111
4.4. Methods 116
4.5. Results 119
4.5.1. Observations from nested MCS and chirp datasets with age control 119
4.5.2. Structural Analysis 127
4.6. Discussion....130
4.6.1. Subsurface architecture, fault linkage, and stratigraphic controls beneath San Diego Bay 130
4.6.2. Conceptual model for the San Diego Bay pull-apart basin 134
4.6.3. Recency of faulting and seismic hazard 138
4.7. Conclusion 140
4.8. Acknowledgments 141
4.9. References 142

5. Conclusion....171

LIST OF FIGURES

Figure 1.1 Map of faults in southern California....6

Figure 2.1 Map of faults in southern California....51
Figure 2.2 Faults and geomorphic features of the San Diego Region....52
Figure 2.3 1927 Aerial photograph of Old Town, San Diego, CA....53
Figure 2.4 Log of the south face of trench T1....54
Figure 2.5 Log of the south face of trench T2....55
Figure 2.6 Log of the north face of trench T2....57
Figure 2.7 Trench wall photographs....59
Figure 2.8 Age model for Old Town....61
Figure 2.9 Earthquake dates for the Newport-Inglewood-Rose Canyon fault system....62

Figure 3.1 Overview map of the Inner Continental Borderland....97
Figure 3.2 Map of San Diego Region....98
Figure 3.3 Fixed height campaign station....99
Figure 3.4 Baseline components between STG1 and STG2....100
Figure 3.5 Homogeneous elastic half-space models....101
Figure 3.6 Asymmetric elastic half-space model....103
Figure 3.7 X^2 contour plot of asymmetric elastic half-space model....104
Figure 3.8 MCS profiles in San Diego Bay....105
Figure 3.9 Map of surface velocity in San Diego region....106

Figure 4.1 Map of faulting in the San Diego region....150
Figure 4.2 Map of San Diego Bay....151
Figure 4.3 MCS profile T196-098....152
Figure 4.4 MCS profile T196-c092....153
Figure 4.5 MCS profile T196-088....154
Figure 4.6 Horizon 5 gridded surface....155
Figure 4.7 D1 and Chollas Creek fence diagram....156
Figure 4.8 MCS profile T196-083....157
Figure 4.9 Gridded surface of paleochannels in San Diego Bay....158
Figure 4.10 Nested chirp profile SSB03 and MCS profile T196-a792....159
Figure 4.11 Fault SB1 fence diagram....161
Figure 4.12 Chirp profile SSB06....162
Figure 4.13 Chirp profile SSB02....163
Figure 4.14 Chirp profile SSB05....164
Figure 4.15 Map of Crown Cove....165
Figure 4.16 Crown Cove cores....166
Figure 4.17 OxCal age model for Crown Cove cores....167
Figure 4.18 Regional fault orientations and plate boundary parameters....168
Figure 4.19 Conceptual model for San Diego Bay pull-apart basin....169
Figure 4.20 Conceptual kinematic block model for San Diego region....170

LIST OF TABLES

Table 2.1 Old Town radiocarbon samples.....50

Table 3.1 Intracluster horizontal and vertical baselines.....95
Table 3.2 GPS velocities relative to ITRF14.....95
Table 3.3 Slip rate and asymmetry parameter model estimates.....96

Table 4.1 Radiocarbon dates for Crown Cove cores.....149
Table 4.2 Average fault trends and plate motion boundary conditions.....149

ACKNOWLEDGEMENTS

I would like to thank my advisor, Jillian Maloney, for providing opportunities to collaborate on research projects as well as the freedom to pursue my own research interests. I am especially grateful for the opportunity to take leadership roles on research cruises and her guidance when developing research projects, which has helped me become a better scientist. Thomas Rockwell and Duncan Agnew generously provided their expertise and guidance, as well as considerable patience during our discussions on the Rose Canyon fault. I would also like to thank Trent Biggs and Joel Conte for making time and providing guidance during my dissertation.

I would like to thank Daniel Brothers for our discussions about marine geophysics and faulting in San Diego Bay. His early work as a graduate student at Scripps provided the foundation for the conceptual models of the San Diego Bay pull-apart basin. I would also like to thank Shannon Klotsko and Neal Driscoll for their support and assistance in collecting and processing the seismic data in San Diego Bay. Diane and Monte Murbach made the paleoseismic trenches in Old Town possible, and their efforts during the series of winter storms that were determined to flood our trench were much appreciated.

I would like to thank my family for providing never-ending support, love, and encouragement at all times, but especially over the last five years. I am fortunate to have such a strong support system. I am grateful to all the friends I have made at Scripps and SDSU who have made my time in San Diego so enjoyable. I feel lucky to have studied geophysics at IGPP as part of the 2015 Keller cohort, whose varied personalities and comradery formed what will no doubt be life-long friendships. A special thanks to my friends Yuval Levy and Susheel Adusumilli for their enthusiastic help in the field and discussions over coffee. Lastly and most

importantly, I want to say thank you to Maya Becker for being at my side through all the ups and downs over the past five years. I look forward to our future together.

Chapter 2, in full, is a reformatted reprint of the material as it appears in: Singleton, D.M., Rockwell, T.K., Murbach, D., Murbach, M., Maloney, J.M., Freeman, T. and Levy, Y., 2019. Late-Holocene rupture history of the Rose Canyon fault in Old Town, San Diego: Implications for cascading earthquakes on the Newport–Inglewood–Rose Canyon fault system. *Bulletin of the Seismological Society of America*, *109*(3), pp.855-874. The dissertation author was the primary investigator and author of this paper.

Chapter 3, in part is currently being prepared for submission for publication of the material. Singleton, D. M., Maloney, J. M., Agnew., D., C., Rockwell, T. K., Brothers., D., Slip rate for the Rose Canyon fault through San Diego, CA based on analysis of new GPS data: Evidence of a potential Rose Canyon – San Miguel-Vallecitos fault connection? The dissertation author was the primary investigator and author of this material.

Chapter 4, in part is currently being prepared for submission for publication of the material. Singleton, D. M., Maloney, J. M., Brothers. D., Klotsko, S., Driscoll, N., Rockwell, T. Recency of faulting and subsurface architecture of the San Diego Bay pull-apart basin, California USA. The dissertation author was the primary investigator and author of this material.

VITA

2012-2013	Undergraduate Research Assistant Department of Geological Sciences University of Colorado Boulder
2013	Bachelor of Arts, Geological Sciences University of Colorado Boulder
2020	Doctor of Philosophy, Geophysics University of California San Diego San Diego State University

Publications

Singleton, D.M., Rockwell, T.K., Murbach, D., Murbach, M., Maloney, J.M., Freeman, T. and Levy, Y., 2019. Late-Holocene rupture history of the Rose Canyon fault in Old Town, San Diego: Implications for cascading earthquakes on the Newport–Inglewood–Rose Canyon fault system. *Bulletin of the Seismological Society of America*, *109*(3), pp.855-874.

Cerchiara, A., Fukuchi, R., Gao, B., Hsiung, K., Jaeger, D., Kaneki, S., Keller, J., Kimura, G., Kuo, S., Lymer, G., Maison, T., Motohashi, G., Regalla, C., Singleton, D. M., & Yabe, S., 2018. IODP workshop: Core-Log-Seismic Investigation at Sea – Integrating legacy data to address outstanding research questions in the Nankai Trough Seismogenic Zone Experiment. *Scientific Drilling*, 24, 93-107.

ABSTRACT OF DISSERTATION

Neotectonics in San Diego, California: Paleoseismology, Slip Rate, and Offshore Structure of the Rose Canyon Fault

by
Drake Moore Singleton

Doctor of Philosophy in Geophysics
University of California San Diego, 2020
San Diego State University, 2020

Professor Jillian M. Maloney, Chair

The Newport-Inglewood-Rose Canyon (NIRC) fault system is a major structural boundary that extends along coastal southern California from Los Angeles to San Diego. The material presented in this thesis provides new data that resolve uncertainties in fault behavior for the southern segment, the Rose Canyon fault (RCF).

Stratigraphic evidence from newly opened paleoseismic trenches are used to interpret six surface-rupturing earthquakes on the RCF in the past 3,300 years. Paleoearthquake ages constrained by radiocarbon dating suggest a late-Holocene recurrence interval of ~700 years, with the most recent large-magnitude event occurring in the mid-1700s. When combined with previous paleoseismic studies, the new paleoearthquake ages show an apparent temporal correlation of earthquake occurrence between the southern and northern segments of the NIRC fault system, suggesting a possible northward-cascading sequence of earthquakes.

The RCF includes a significant onshore segment, which provides an opportunity to use traditional geodetic techniques to resolve slip rate. Surface velocities from a combined

campaign and continuous GPS network that spans the RCF are used to constrain elastic half-space models. The best-fitting model suggests a rate that is toward the higher end of geologic estimates, as well as a potential rheological contrast across the fault trace. The GPS surface velocities further suggest a more easterly trace for the RCF, and a possible connection with the San Miguel-Vallecitos fault system.

South of downtown San Diego, the RCF splays out into a complex network of faults that accommodate the subsidence beneath San Diego Bay. Using legacy multi-channel seismic data and recently collected high-resolution chirp profiles, the fault structure and stratigraphic character beneath San Diego Bay is examined. Gridded surface horizons and fault maps show widespread down-to-the-east displacement. Fault orientations in the western portion of the San Diego Bay pull-apart basin are well described by a Rose Canyon–Descanso pull-apart basin, but faults in the eastern portion of the basin lie outside of this model and exhibit the wrong sense of displacement. A separate but related Rose Canyon–San Miguel-Vallecitos pull-apart basin may explain the faulting seen in the eastern portion of the basin.

1. Introduction

In Southern California, the Big Bend in the southern San Andreas fault system dominates the tectonic environment and results in a diffuse plate boundary that stretches ~200 km from the Salton Sea to the Channel Islands offshore. The Inner Continental Borderland (ICB) represents the offshore portion of the Big Bend domain (Wetmore et al., 2018). The ICB is composed of a complex tectonic fabric that has undergone all three types of plate boundary deformation; mid-Cenozoic subduction-related structures are overprinted by Miocene extension, which in turn is overprinted by Plio-Quarternary dextral shearing (Atwater, 1970; ten Brink et al., 2000; Oskin and Stock, 2003; Legg, 1991). Similar to its terrestrial counterpart, the ICB consists of a series of northwest-trending right-lateral strike-slip faults that together accommodate 10–15% of the total plate boundary motion (Figure 1) (Legg, 1991; Platt and Becker, 2010).

The Newport-Inglewood-Rose Canyon fault system is the easternmost fault in the ICB and represents a major structural boundary between the ICB and Peninsular Range tectonic province (Figure 1) (e.g., Wright, 1991; Boles et al., 2015). The fault zone is relatively well mapped from western Los Angeles to downtown San Diego and is located beneath or within ~8 km of the heavily populated southern California coastline (Moore, 1972; Wright, 1991; Sahakian et al., 2017). The 1933 Long Beach earthquake, which ruptured the southern onshore section of the northern Newport-Inglewood segment, demonstrates the fault's potential lethality and devastating effects on infrastructure. However, despite evidence of a connection to the clearly active northern Newport-Inglewood fault segment as early as the 1970s, prior to 1990, San Diego was perceived as a relative safe haven from the otherwise shifting ground of southern California. However, in 1989, new paleoseismic data provided evidence for Holocene

surface ruptures on the Rose Canyon fault that prompted a renewed interest in the seismic hazard of the San Diego region (Rockwell et al., 1991).

In the following decades, additional studies started to address some of the outstanding questions regarding the characteristics of the Rose Canyon fault. However, several key parameters required for an accurate seismic hazard assessment, such as the fault's Holocene earthquake history, slip rate, and southern continuation, remain uncertain. In addition to improved seismic hazard assessment, constraining these parameters on the Rose Canyon fault addresses fundamental questions of earthquake science. For example, how are earthquakes spaced in time and how are fault characteristics and stress conditions related to temporal patterns? Some earthquake models predict that event recurrence is quasi-periodic (e.g., Reid, 1910; Shimazaki and Nakata, 1980), but much more variability has been observed including temporal clustering and cascading (e.g., Grant and Rockwell, 2002; Marco et al., 1996; Pondard et al., 2007; Rockwell et al., 2009; Stein et al., 1997). Additionally, how and why do ruptures start and stop and what controls branching or triggering of earthquakes from one fault zone to another? Several recent earthquakes on fault systems around the world involved highly complex rupture patterns that have called into question previous assumptions about rupture propagation across fault steps (e.g., 2016 Kaikoura, NZ (Hamling et al., 2017); 2010 El Mayor-Cucapah, MX (Fletcher et al., 2014); 2016 Central Italy (Scognamiglio et al., 2018). The Rose Canyon fault is a low slip rate, complex fault system, that represents a structural boundary across a wide strike-slip plate boundary. These characteristics make it an excellent fault system to approach these fundamental questions. The following chapters resolve some of the remaining uncertainties on the Rose Canyon fault zone in the context of improving seismic hazard assessment and understanding fault processes.

Chapter 2 is focused on the Holocene earthquake history of the Rose Canyon fault. New results are presented from recently opened paleoseismic trenches across the main trace of the Rose Canyon fault in Old Town San Diego. The stratigraphy exposed in the trench walls provides evidence for six surface-rupturing earthquakes in the past ~3,300 years, and a late-Holocene recurrence interval of ~700-800 years. Combining these new results with previous paleoseismic studies in San Diego suggests a quasi-periodic behavior for the Rose Canyon fault, in contrast to a possible cluster-mode behavior suggested by the prior incomplete paleoseismic history. The new earthquake dates are then compared with other published paleoseismic histories along the entire Newport-Inglewood-Rose Canyon fault system, and a potential sequence of northward-cascading earthquakes is interpreted.

In Chapter 3, a combined campaign and continuous GPS network is used to resolve an upper bound for the slip rate across the Rose Canyon fault. Surface velocities from the GPS network are used to constrain elastic half-space models of the San Diego region. The best-fitting model indicates a rate of ~2.4 mm/yr, which is towards the higher end of geologic estimates. GPS surface velocities relative to a station centered on the Rose Canyon fault point to a more easterly southern extension of the fault zone, and may be evidence for a southern connection between the Rose Canyon fault and the San Miguel-Vallecitos fault.

The material presented in Chapter 4 examines the southern continuation of the Rose Canyon fault. South of downtown San Diego, the fault splays out into a complex network of faults that together accommodate the subsidence seen in San Diego Bay. A pull-apart basin between the Rose Canyon fault and the offshore Descanso fault is typically invoked to explain the fault orientations and subsidence of the Bay (Legg, 1991; Rockwell, 2010). However, several northwesterly oriented faults in the southern portion of San Diego Bay, as well as the

associated La Nacion fault zone, do not fit this model. Using a combination of reprocessed legacy multi-channel seismic data, high-resolution chirp surveys, and borehole/core lithology, the subsurface fault architecture and stratigraphic character beneath San Diego Bay are examined. Several sub-parallel and potentially linked fault structures, along with localized depositional basins, are observed in the combined datasets, and are consistent with models of pull-apart basins. To explain the different orientation of fault groups observed in San Diego Bay, a conceptual model is developed to provide a structural framework for the San Diego Bay pull-apart basin.

In summary, this thesis presents a more complete understanding of the characteristics of the Rose Canyon fault through San Diego, California. The material presented in the following chapters provides not only key parameters required for a more accurate seismic hazard assessment of the San Diego-Tijuana metropolitan area but also constraints on how strain may be distributed throughout the ICB.

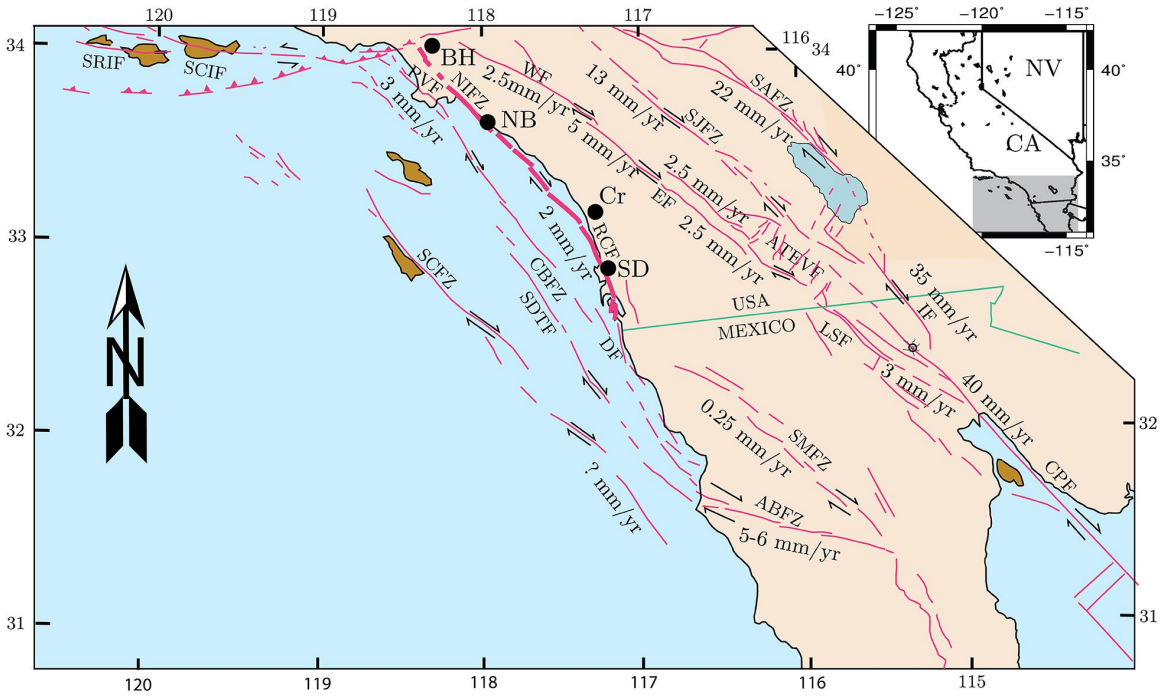

Figure 1.1. Active faults of southern California with their corresponding slip rates. Shaded box in inset shows location in California. The trace of the Newport-Inglewood-Rose Canyon fault system is bolded, and marks the eastern boundary of the ICB. Circles are locations of urban centers: BH=Beverly Hills, NB=Newport Beach, Cr=Carlsbad, and SD=San Diego. SAFZ=San Andreas fault zone, IF=Imperial fault, SJFZ=San Jacinto fault zone, EF=Elsinore fault zone, CPF=Cerro Prieto fault, LSF=Laguna Salada fault zone, SMFZ=San Miguel fault zone, ABFZ=Agua Blanca fault zone, DF=Descanso Fault, RCF=Rose Canyon fault zone, NIFZ=Newport Inglewood fault zone, PVF=Palos Verde fault zone, CBFZ=Coronado Bank fault zone, SDTF=San Diego Trough fault, SCFZ=San Clemente fault zone, WF=Whittier fault zone, SCIF=Santa Cruz Island fault, and SRIF=Santa Rosa Island fault.

1.1 References

Atwater, T. 1970. Implications of plate tectonics for the Cenozoic tectonic evolution of western North America. *Geological Society of America Bulletin*, *81*(12), 3513-3536.

Boles, J. R., Garven, G., Camacho, H., & Lupton, J. E. 2015. Mantle helium along the Newport-Inglewood fault zone, Los Angeles basin, California: A leaking paleo-subduction zone. *Geochemistry, Geophysics, Geosystems*, *16*(7), 2364-2381.

Fletcher, J.M., Teran, O.J., Rockwell, T.K., Oskin, M.E., Hudnut, K.W., Mueller, K.J., Spelz, R.M., Akciz, S.O., Masana, E., Faneros, G. and Fielding, E.J., 2014. Assembly of a large

earthquake from a complex fault system: Surface rupture kinematics of the 4 April 2010 El Mayor–Cucapah (Mexico) Mw 7.2 earthquake. Geosphere, 10(4), pp.797-827.

Grant L. B. and Rockwell, T. K. 2002. A northward propagating earthquake sequence in coastal southern California: Seismological Research Letters, v. 73, no. 4, p. 461-469.

Hamling, I.J. et al., 2017, Complex multifault rupture during the 2016 M w 7.8 Kaikōura earthquake, New Zealand: Science, v. 154, doi:10.1126/science.aam7194

Legg, M.R., 1991. Developments in understanding the tectonic evolution of the California continental borderland: Society for Sedimentary Geology Special Publication 46.

Moore, G. W. 1972. Offshore extension of the Rose Canyon fault, San Diego, California. *Geol. Surv. Profess. Pap*, 800-2.

Marco, S., Stein, M., Agnon, A., and Ron, H. 1996. Long-term earthquake clustering: A 50,000-year paleoseismic record in the Dead Sea Graben, *J. Geophys. Res.*, 101(B3), 6179– 6191, doi:10.1029/95JB01587.

Oskin, M., & Stock, J. 2003. Pacific–North America plate motion and opening of the Upper Delfín basin, northern Gulf of California, Mexico. *Geological Society of America Bulletin*, *115*(10), 1173-1190.

Platt, J. P., & Becker, T. W. 2010. Where is the real transform boundary in California?. *Geochemistry, Geophysics, Geosystems*, *11*(6).

Pondard, N., Armijo, R., King, G.C.P., Meyer, B., Flerit, F. 2007. Fault interactions in the Sea of Marmara pull-apart (North Anatolian Fault): earthquake clustering and propagating earthquake sequences, *Geophysical Journal International*, Volume 171, Issue 3, 1185–1197, https://doi.org/10.1111/j.1365-246X.2007.03580.x

Reid, H. F. 1910. The California Earthquake of April 18, 1906 Report of the state earthquake investigation commission Vol. 2, Carnegie Institute, Washington DC

Rockwell, T. K. 2010. The Rose Canyon Fault Zone in San Diego *Fifth International Conference on Recent Advances in Geotechnical Earthquake Engineering and Soil Dynamics and Symposium in Honor of Professor I.M. Idriss*, no. 7.06c: 1–9.

Rockwell, T., J. Fonseca, C. Madden, T. Dawson, L. A. Owen, S. Vilanova, and P. Figueiredo 2009. Paleoseismology of the Vilariça Segment of the Manteigas-Bragança Fault in Northeastern Portugal. Reicherter, K., Michetti, A.M. and Silva, P.G. (eds)

Paleoseismology: Historical and Prehistorical Records of Earthquake Ground Effects For Seismic Hazard Assessment. The Geological Society of London Special Publications, 316, 237-258. DOI: 10.1144/SP316.15

Rockwell, T. K., Lindvall, S. C., Haraden, C. C., Hirabayashi, C. K., Baker, E., Abbott, P. L., & Elliott, W. J. 1991. Minimum Holocene slip rate for the Rose Canyon fault in San Diego, California. *Environmental Perils San Diego Region*, 37-46.

Sahakian, V., Bormann, J., Driscoll, N., Harding, A., Kent, G., & Wesnousky, S. 2017. Seismic constraints on the architecture of the Newport-Inglewood/Rose Canyon fault: Implications for the length and magnitude of future earthquake ruptures. *Journal of Geophysical Research: Solid Earth*, *122*(3), 2085-2105.

Scognamiglio, L., Tinti, E., Casarotti, E., Pucci, S., Villani, F., Cocco, M., Magnoni, F., Michelini, A. and Dreger, D., 2018. Complex fault geometry and rupture dynamics of the MW 6.5, 30 October 2016, Central Italy earthquake. Journal of Geophysical Research: Solid Earth, 123(4), pp.2943-2964.

Shimazaki, K. & Nakata, T. 1980. Time-predictable recurrence model for large earthquakes. *Geophys. Res. Lett.* 7, 279–282

Stein, R. S., A. A. Barka, and J. H. Dieterich 1997. Progressive failure of the North Anatolian fault since 1939 by earthquake stress triggering, Geophys. J. Int. 128, 594–604.

ten Brink, U. S., Zhang, J., Brocher, T. M., Okaya, D. A., Klitgord, K. D., & Fuis, G. S. 2000. Geophysical evidence for the evolution of the California Inner Continental Borderland as a metamorphic core complex. *Journal of Geophysical Research: Solid Earth*, *105*(B3), 5835-5857.

Wetmore, P.H., Malservisi, R., Fletcher, J.M., Alsleben, H., Wilson, J., Callihan, S., Springer, A., González-Yajimovich, O. and Gold, P.O., 2019. Slip history and the role of the Agua Blanca fault in the tectonics of the North American–Pacific plate boundary of southern California, USA and Baja California, Mexico. Geosphere, 15(1), pp.119-145.

Wright, T.L., 1991. Structural Geology and Tectonic Evolution of the Los Angeles Basin, California: Chapter 3: PART 1.

2. Late-Holocene rupture history of the Rose Canyon fault in Old Town, San Diego: Implications for cascading earthquakes on the Newport-Inglewood-Rose Canyon fault system

2.1 Abstract

We present new results from paleoseismic trenches excavated across the main trace of the Rose Canyon fault zone (RCF) in Old Town-San Diego, California to determine the timing of late Holocene earthquakes. There is evidence for four large surface-rupturing events, as well as two smaller events, the youngest of which cuts the early historical living surface that contains glass, ceramics, and a historical era foundation. This youngest event is likely related to the 1862 San Diego earthquake, which had an estimated magnitude close to M6. The age of older ruptures are constrained by 36 radiocarbon dates that exhibit good stratigraphic order. The four larger events produced substantially more ground deformation, and over a broader width of the fault zone, than the 1862 event. The youngest of the four larger events is found immediately below the historical horizon and likely correlates with the most recent event recognized at multiple trench sites along the RCF in San Diego and dates to the mid-1700's. The three older events have all occurred in the past 3,300 years, with the penultimate large event dated to about 1300 AD.

The results of this paleoseismic study indicate that the RCF has sustained activity throughout the late Holocene and into the Historical period. These results also suggest that the RCF has a late-Holocene recurrence interval of ~700 years, which is several hundred years shorter than previous estimates. Comparison of RCF paleoseismic results with paleoseismic data from the Newport-Inglewood fault zone (NIF) indicates that some RCF earthquakes have similar timing with NIF events, most likely indicating the occurrence of a sequence or cluster of events on the coastal system of strike-slip faults. The alternative explanation – very large earthquakes rupturing both faults simultaneously – is unlikely when both the slip rate and recurrence intervals for these faults are considered.

2.2 Introduction

The Rose Canyon fault zone (RCF) in San Diego, California follows the broader northwest-striking right-lateral strike-slip motion that characterizes much of southern California's seismic landscape (Figure 1) (Kennedy, 1975; Rockwell et al., 2016). The Newport-Inglewood fault zone (NIF) and the RCF have long been speculated of connectivity offshore southern California (Moore, 1972; Fischer and Mills, 1991). Recent high-resolution marine seismic surveying from Dana Point to La Jolla have imaged four offshore segments separated by three structural step-overs, none of which exceeds 2 km in width, thereby extending the NIF to connect with the RCF (Sahakian et al. 2017). Thus, the RCF is interpreted as the southern onshore expression of the larger Newport-Inglewood-Rose Canyon fault system (NIRC).

The NIRC stretches southeast from its northernmost extent in the Los Angeles basin near Beverly Hills, trends offshore at Newport Bay to cross the continental shelf adjacent to southern Orange and northern San Diego counties, and terminates in San Diego Bay. In total, the NIRC extends for some 170 km, and runs adjacent to many of southern California's most heavily populated coastal communities. Fault systems further to the east of the NIRC, such as the Elsinore, San Jacinto, and San Andreas fault systems, have received more attention because their progressively higher slip rates and slip per event impose high seismic hazards to onshore infrastructure and communities. Recent research continues to demonstrate that despite a lower slip rate and slip per event the NIRC still represents a significant seismic hazard to much of coastal southern California (Rockwell, 2010a; Sahakian et al., 2017; Leeper et al., 2017). However knowledge gaps in the paleoseismic data for the NIRC remain, both for the offshore

and coastal segments beneath major metropolitan areas (e.g. along the RCF through San Diego) indicating the need for additional studies on the earthquake history along the NIRC, particularly for the RCF in San Diego.

The primary fault traces and associated geomorphic features in the San Diego region are shown in Figure 2. It is thought that some portion of slip is potentially distributed to the RCF by the Agua Blanca fault system of northern Baja California, Mexico, of which the Descanso and Coronado Bank faults are associated strands (Rockwell, 2010a; Maloney, 2013) (Figure 1). South of San Diego, the RCF steps onshore via a releasing right-step from the Descanso fault (and possibly from the Coronado Bank fault), accomplished through a series of fault segments whose motion partially down-drops San Diego Bay (Moore and Kennedy, 1975; Rockwell, 2010a; Maloney, 2013) (Figure 2). North of downtown San Diego, the various fault strands that splay across San Diego Bay have consolidated into a narrow fault zone. The fault then trends along the I-5 freeway corridor until it makes a restraining bend, resulting in the uplift of Mount Soledad, before trending offshore at La Jolla (Kennedy, 1975; Rockwell, 2010a; Rockwell and Murbach, 1999). Throughout its onshore trace, the RCF exhibits predominantly horizontal displacement except in locations where segment obliquity results in oblique motion (Lindvall and Rockwell, 1995).

The RCF was first shown to be Holocene active by Rockwell et al. (1991) and Woodward Clyde (1985) whose paleoseismic trenches at Rose Creek and geotechnical survey in downtown San Diego clearly exhibited faulted stratigraphy of Holocene age. Additional 3-D trenching at the Rose Creek site by Lindvall and Rockwell (1995) revealed that the RCF has sustained at least four surface rupturing earthquakes, with possibly more, in the past 11,000 years as well as having accumulated a minimum of 8.7 m of right-lateral displacement in less

than the past 8.1 ka, resulting in a minimum slip rate of ~1.1 mm/yr throughout the Holocene (Lindvall and Rockwell, 1995; Murbach and Rockwell, 1999). A higher slip rate of ~2 mm/yr was suggested by Rockwell (2010a) based on deflected stream channels that are inferred to incise the last interglacial marine terrace deposits in Old Town and north of the San Diego River. Of the earthquakes previously documented for the RCF, three events and possibly as many as five, appear to be clustered in time from ~9.3 ka to ~5.3 ka, after which a period of quiescence of about ~5 ka was inferred, based on a moderately developed soil that overlies several of the early Holocene fault strands at the Rose Creek site (Rockwell, 2010a; Lindvall and Rockwell, 1995). This "quiet period" was apparently followed by a return to activity with an earthquake displacing the modern topsoil A horizon at Rose Creek, indicating an event date sometime in the past ~400 years (Lindvall and Rockwell, 1995; Rockwell, 2010a). These observations, combined with those from a paleoseismic site in La Jolla and geotechnical surveys in downtown San Diego, support the occurrence of at least one surface rupturing earthquake along this strand of the RCF in the last ~400 years (Rugg et al., 2013; Rockwell and Murbach, 1999; Lindvall and Rockwell, 1995).

However, there was uncertainty as to whether the trenches excavated at the Rose Creek site captured the complete seismic history of the RCF because deposition ceased at the site more than 7 ka and there is more than one mapped strand through that area (Lindvall and Rockwell, 1995; Rockwell, 2010a; Rugg et al., 2013). Of particular interest is the apparent absence of any notable earthquakes being documented on the RCF from ~5.3 ka until the most recent event that occurred prior to the establishment of the San Diego Mission and Presidio by the Spanish in 1769 AD. The occurrence of surface rupturing earthquakes on the RCF during the mid-to late-Holocene has important implications for the seismic hazard of San Diego and

nearby coastal regions, as well as the evolving understanding of southern California's coastal fault systems. Therefore, a paleoseismic investigation to resolve the discrepancy in earthquake occurrence during the mid- to late-Holocene was warranted. This paper presents results on the earthquake activity of the RCF from two paleoseismic trenches at Old Town in San Diego, California. We present evidence for six earthquake surface ruptures along this segment of the RCF in the past ~3,300 years, and discuss the impact these new findings have on estimates of the recurrence interval for earthquakes along the RCF. Furthermore, we discuss possible patterns in the temporal and spatial distribution of reported paleo-earthquakes along southern California's NIRC fault system, and the possible implications that this pattern may have on future seismicity of the Los Angeles Basin.

2.3 Methods

2.3.1 Site Selection

Paleoseismic investigations in urban areas are typically very limited due to removal of stratigraphic evidence by mechanical grading and inaccessibility due to modern infrastructure. Analysis of historical aerial photography of San Diego from 1927 AD identified Old Town's Presidio Hills Golf Course site as an area that has sustained minimal anthropogenic modification, has a high probability of a Holocene sedimentation record, and contained geomorphic indicators of active faulting (Figure 3). In addition, it is inferred that the distributed faulting that is present across San Diego Bay (Kennedy and Welday, 1980; Kennedy and Clarke 1999) has largely coalesced into a sufficiently narrow zone of faulting just south of Old Town (Rockwell, 2010a) such that a paleoseismic site in Old Town should capture most or all Holocene ruptures.

2.3.2 Trench Investigation

In order to minimize the impact of excavations, two trenches were opened along the boundaries of the Presidio Hills Golf Course. Trench one (T1) was located along the northern boundary of the course, while the second trench (T2) was located along the southern boundary at a slightly higher topographic position in the landscape (Figure 3).

The trenches were excavated by a backhoe and stabilized with hydraulic trench shores. T1 was excavated first from northeast to southwest, but contact with a Spanish Colonial era wall foundation at the western-most portion of the trench abruptly halted further excavations by mechanical equipment before the main fault trace could be encountered. The trench did expose a secondary strand of the fault, and the trench was deepened by hand across this fault (Figure 4). It is also possible that a trace of the fault exists east of T1.

A trench-wall grid of half-meter by half-meter spacing was emplaced for a reference frame. Etching of some contacts and fault strands was done because of the poor light conditions for photography, as well as the generally similar color of the stratigraphic units. Two trench mosaics were constructed of the south wall, one photographed under natural light and a second with a halogen light source, as the trenching was done in late November when light conditions were poor. The northern trench face was only photographed once.

The photomosaics were used as the base for logging, which was conducted in the field. Following the logging and backfilling of the T1 excavation, a second trench, T2 was initiated along the southern margin of the golf course. A one-meter by half-meter grid was emplaced on the southern trench face for the entire length of the trench, and on the northern trench face across the main fault zone, both of which were photographed to construct a mosaic for logging. The weakly to massively bedded silt stratigraphy at this location required significant hand

etching of all contacts and faulted surfaces so that they would be easily identifiable on the photo-mosaics of the trench faces, as the stratigraphy was generally the same color and dark, and light conditions in December and January were generally poor.

2.3.3 Radiocarbon Dating

Detrital charcoal was collected for radiocarbon dating, and sample locations on trench walls were flagged, logged, and photographed. In the lab, samples were washed with deionized water, separated from sediments, dried, weighed, and inspected under a microscope. Sample analysis by Accelerated Mass Spectrometry (AMS) was done at the University of California Irvine's Keck Carbon Cycle Laboratory. The radiocarbon dates were then entered into OxCal v4.3.2 and calibrated with the Intcal13 radiocarbon calibration curve (Bronk Ramsey, 2009; Reimer et al., 2013) to construct a time versus depth profile of sedimentary units, which would be used to constrain the ages of interpreted paleoearthquakes.

2.4 Stratigraphy

The stratigraphy observed in both trenches is consistent with a predominantly fluvial flood plain environment of the nearby San Diego River (Figure 3), with some additional alluvial fan deposits in trench T2 from a nearby small canyon. The separation in trench locations results in a slightly different stratigraphic expression in the trenches, as trench T1 is topographically lower and closer to the river. Common to both trenches are packages of fine- to coarse-grained light-colored sand, massive bedded sandy-silt sections, and several buried soil A horizons which we use to help correlate stratigraphy between the two trenches.

2.4.1 Trench 1

The natural stratigraphy seen in the trench exposures of T1 consisted of stratified sand, sandy-silt, and clayey-silt deposits; the observed finer sediment packages are interpreted as primarily the result of overbank sedimentation likely the result of T1's lower position in elevation on the San Diego River flood plain, discussed in more detail below. Above the natural deposits lie approximately 1.5 meters of mechanical fill apparently emplaced during the grading and construction of the golf course as the historical imagery shows natural depositional surfaces four years prior to construction of the golf course (Figures 3 and 4).

The upper mechanical fill section is divided into three subsections. Unit 1, the top most 30 cm, is an organically-enriched, dark sandy-silt containing abundant shell fragments and scattered brick fragments; an abrupt lower contact is also observed. The organic enrichment, dark coloration, and abrupt lower contact suggests that unit 1 represents a reworked A horizon with intermixed Native American midden deposits, which are locally present in the Old Town area. Below unit 1, unit 2a is a 1 m-thick dense, reddish brown layer of cobbles with clay films and an abrupt upper and lower contact. Based on similarity in grain size, composition, and local availability we interpret unit 2a to likely be derived from either the San Diego or Linda Vista Formations. The clay films are interpreted to be inherited from the soil developed in the source deposit. Scattered among the cobbles are brick fragments demonstrating its' artificial fill origin. The base sequence of unit 2, unit 2b, is composed of dark, fine-grained sandy-silt and clay that is organic rich and dense, suggesting some component of mechanical compaction. A partial ear of an earthenware urn handle (or a similar cooking artifact) was recovered from within this stratum, indicating a historical age. Unit 2b also contained localized clusters of angular blocks of B horizon material (oxidized, clay-enriched) and the upper portion buries a Spanish or Mexican era foundation structure. The dark coloration, organic component, and inclusion of

anthropogenic artifacts suggests that unit 2b is the result of locally, redistributed topsoil mixed during grading of the golf course; whereas based on the abrupt upper and lower contacts, together with the distinctive composition the upper unit 2a was likely brought in from an outside source to raise this area of the golf course up to a desired grade level. Hence, we use unit 2b as an historical living surface to correlate to the stratigraphy in trench T2 in later discussions.

Unit 3 and 4 comprise natural strata of T1 and are exposed for the length of the trench, however unit 4 is mostly exposed in the hand-excavated portion of the trench, which was excavated down below the original base of T1. Unit 3a is composed of light brown, clean (well-sorted) sand, about 30 cm thick, and is interpreted as the result of overbank sedimentation from the adjacent San Diego River. The top of unit 3a lacks a developed A horizon and is seen to pond against or bury the Spanish era wall foundation, although it is likely, based on stratigraphic order and composition, that unit 2b is the disturbed A horizon for this stratum. Together these observations suggest a very young historical age for unit 3a.

Unit 3b is characterized by stiff, dark brown sandy silt with minor clay, and is interpreted to be of alluvial origin. The top of unit 3b is likely a buried A horizon, which represents the early historical living surface prior to flooding and deposition of unit 3a. (Note, both the buried A horizon at the top of unit 3b and the redistributed A horizon of 2b may represent historical living surfaces, with historical sedimentation at trench T1 separating the two. Trench T2, as discussed below, exposed only a single historical living surface, which collectively correlates to these two.) Unit 3c is a 1.3 m thick section of sand, which based on the presence of several buried weakly-formed A horizons, likely represents multiple flooding events. Unit 3c is further subdivided based on the best developed A horizon. The lower unit 3c

is composed of clean, well-stratified cross-bedded sand with sparse krotovina (filled burrows), while the upper part of unit 3c is massive, organic-rich, dark brown, silty-sand with many krotovina and has at least one, but possibly two, buried A horizons. Together these two subunits are interpreted to represent at least two flooding events, with a depositional hiatus when the soil A horizons formed. The Spanish era wall foundation footing appears to have been excavated into units 3b and 3c suggesting that unit 3b was the historical ground surface at that time. Unit 3a is therefore best interpreted as a historical flood deposit capped by another A horizon.

Unit 4 is subdivided into four subunits based on stratigraphic and structural factors, and is the stratum that contains all evidence for faulting in T1. Generally, unit 4 is a sequence of stratified silty-clay, clayey-silt, sandy-silt, and muddy-sand with abundant krotovina that is interpreted as a result of overbank sedimentation on the San Diego River floodplain. When not obscured by bioturbation, individual strata can be traced for several meters. The stratigraphy is relatively better preserved on the south face of the trench, especially near the faulted surfaces; on the north face the stratigraphy is more massive making interpretations more difficult.

2.4.2 Trench 2

The stratigraphy exposed in T2 can be divided into three distinct sections: 1) well-bedded, oxidized gravelly sand strata loaded with historical debris interpreted as post-1850 alluvial fan and fluvial deposits (units 30-85); 2) bedded to massive clayey and sandy silt deposits with some gravelly sand or sandy gravel deposits interpreted to be Holocene alluvial fan and fluvial deposits (units 95-300); and 3) an older silty and sandy gravel deposit with a well-developed clay-enriched soil interpreted to be Pleistocene alluvial deposits (Figures 5 and 6). Each is discussed in more detail below, starting with the uppermost unit.

2.4.2.1 Historical alluvial and fluvial deposits

The topmost 1-1.5 m of T2 exposed predominantly coarse- to medium- to fine-grained oxidized sandy strata. Units 30-60 (Figure 5a and 6) are composed of sub-rounded, poorly sorted, coarse- to fine-grained, yellow to light-brown sand with intermixed clusters of rounded to well-rounded, poorly-sorted pebble and cobble clasts with scattered boulders. Abundant historical artifacts such as brick, tile, glass, pottery, and bone were found in-situ within units 30-60. Units 70-95 (Figure 5a and 6) are composed of coarse- to fine-grained, light brown to reddish-brown sand with localized cross bedding, and clusters of pebble-sized clasts concentrated at the thalwegs of small lenses interpreted to be channels. Scattered fragments of historical artifacts, such as brick and iron bars, were observed in units 70-95 (Figure 7b). Together these units appear to make up several small alluvial channels that have locally eroded into the underlying strata, unit 100 (Figure 7a,b). We interpret these units to represent deposition from the alluvial drainage immediately to the south, and onto the alluvial fan seen in historical imagery (Figure 3).

Unit 100, at the base of the historical deposits, is a 10-15 cm thick, stiff, brown, fine-grained silty sand interpreted as a buried A horizon that has been heavily bioturbated, and has been faulted by the main fault strand as well as several auxiliary strands (Figure 5a and 6). The uppermost section of unit 100 hosted rare bone and glass fragments, as well as evidence for burn pits filled with cow bone excavated into the stratum. Based on the clean contact with the overlying historical alluvial sands, except where the largest alluvial drainages have eroded into and below unit 100, as well as the inclusion of anthropogenic artifacts, we interpret unit 100 to represent the living surface at the time of Old Town's founding sometime after 1769 AD. This

surface and A horizon likely correlate to either or both unit 2b (redistributed A horizon) and the A horizon that caps unit 3b in trench T1, discussed in more detail below.

2.4.2.2 Holocene alluvial and fluvial deposits

A section of Holocene-aged deposits lie directly below an erosional to depositional contact (depending on the locations of interpreted small drainages) at the base of the historical-aged sand and gravel. The Holocene section, the age of which is based on numerous radiocarbon dates as discussed below, consists of massively bedded brown to dark-brown, sandy-silt units bedded with several deposits composed of well-rounded, poorly-sorted, pebble- to cobble-sized clasts supported by a coarse-grained sand matrix and interpreted to be alluvial channel deposits. Several buried A horizons, identified based on dark coloration, abrupt upper contact, and increased krotovina, can be recognized in this section, implying periods of non-deposition and surface stability. The relatively massive nature of sections separating the buried A horizons is apparently due to bioturbation associated with the periods of non-deposition, as several distinct, thinly bedded silt strata are locally obscured by krotovina, and other parts of the section display clearly identifiable krotovina.

The Holocene units are capped by the bottom portion of unit 100 and unit 105, below which is a 0.5 m thick sequence of brown to dark brown, sandy silt strata, units 110 and 115. Below these units is a gravelly deposit, unit 120, composed of pebble to gravel clasts supported by a light-brown, fine-grained sandy-silt matrix. Unit 120 is clearly expressed in the westernmost portion of the trench as a laterally continuous unit, which progressively thins eastward towards the fault zone. Based on the increase in grain size, lateral variation, and proximity of T2 to alluvial drainages, unit 120 is interpreted to be a channel deposit that likely flowed at an oblique angle to the trench.

Unit 130 is a dark brown, fine-grained sandy silt stratum interpreted as a buried A horizon. Unit 130 can be traced for the length of the trench through the faulted section (except where obscured by krotovina), and exhibits a small northeast up component of vertical separation across the fault. Below unit 130 and within another sequence of massively bedded, brown sandy silt sediments (units 140-160) is a relatively well-expressed package of thinly bedded strata mapped as unit 150, which is composed of several yellow to light-brown sand and silt layers (stringers) that are preserved sporadically for the length of the fault study area (the length of which corresponds to the logged sections represented in Figures 5a and 6). Unit 200, based on its darkened color, is interpreted as another buried A horizon that caps a lower sequence of sandy-silt beds, units 205-220, and was again identified by the dark coloration, porosity, its massive, fine grained texture, and by its abrupt upper contact.

Units 225 through 290 were exposed in the deepest portion of the trench, ~1.5 m directly below the deepest portion of the historical alluvial channel, and are composed of poorly-sorted, rounded clasts, pebble to cobble in size, with intermixed fine-grained sandy-silt strata. Finally, unit 300 lies at the base of the trench and is interpreted as a possible fourth weakly developed buried A horizon. It crops out at the western and eastern edges of the area of detailed fault zone study, but has been removed towards the center likely by erosion of younger alluvial channels of unit 225-290 (Figures 5a and 6).

We interpret the entire section of massively bedded, sandy-silt units, units 100-300, to represent deposition by overbank sedimentation from the San Diego River or from the nearby small drainage immediately to the south of T2 (Figure 3). The intermixed strata that support large clasts, such as units 120 and 225-290, are interpreted to be the result of alluvial channel deposition from the small drainage because they trend towards the San Diego River, parallel to

the trend of the small drainage and slope of the alluvial fan, as observed in early photography. In contrast, the well-defined silty strata of unit 150 are likely to be the result of San Diego River overbank deposition as they are sub-horizontal where not disrupted by faulting and laterally continuous where not disrupted by bioturbation.

2.4.2.3 Pleistocene deposits

East of the fault-zone, the Holocene deposits erode into and buttress against the older, Pleistocene deposits (Figure 5b). The older deposits exposed towards the eastern half of the trench are interpreted to be Pleistocene in age because they express a reddish argillic (Bt) horizon developed into the upper section of the soil profile and contain a secondary calcium carbonate (Bk horizon) in the lower section, below the argillic horizon. These deposits likely date to the last interglacial period (MIS 5), as post-MIS 5 climate in coastal southern California is known to have been wetter and cooler than present (Heusser, 1978), and no late Pleistocene San Diego area soils that post-date MIS 5 contain secondary carbonate. Because the fault does not cut these deposits, they are not described further.

2.5 Age Dating of Units

Sediment ages were determined through radiocarbon analysis of detrital charcoal collected in situ (Table 1, Figure 8). Age determination of sediments using detrital charcoal is limited in temporal accuracy by the effects of carbon inheritance during growth, death, initial burn, and subsequent transport to the depositional location. This inheritance can be compensated for, to a degree, by the collection and analysis of a large number of samples so that suspected inheritance of one sample can be identified by comparing its age to that of neighboring samples. However, age estimates determined using detrital charcoal will inevitably

have some amount of inheritance associated with them and will thus be at least slightly older than the actual age of the sediment from which they are collected.

2.5.1 T1

In T1, the detrital charcoal samples that were dated came primarily from the hand-excavated section. Beginning towards the top of the natural section, sample #19 was collected from unit 3a and yielded a calibrated date range of 267-291 years before present (yrs BP), but construction of the Derby Dike (to protect Old Town from flooding) limits the likely upper age bound to 1853-1867 (Abbott, 1991). No radiocarbon samples were dated from unit 3b, but below in unit 3c three samples (#27, #45, #29) returned a calibrated date range of 957-1174 yrs BP. Approximately 4 cm above the base of unit 4a, sample #8 was dated to 1326-1407 yrs BP. Below unit 4a, sample #12 was collected ~4 cm above the contact between units 4c and 4b and was dated to 1377-1519 yrs BP. Two samples were collected from unit 4c, #13 and #35, returning a calibrated date range of 1566-1855 yrs BP. Lastly, sample #5 was collected ~7 cm from the base of the trench T1, well within unit 4d, and yielded a calibrated date range of 2215-2346 yrs BP. These dates were run through OxCal (Bronk Ramsey, 2009), resulting in the age model presented in Figure 8.

2.5.2 T2

The abundance of historical artifacts found in units 30-90 suggests a historical age decades after first settlement of the Old Mission in 1769 AD. Additionally, the inclusion of scattered fragments of pottery, bone, and brick within the top 1-3 cm of unit 100 suggest that the uppermost portion of this horizon represents the living surface at the time of Old Town's founding and very early settlement. Therefore, we interpret an approximate age of circa ~1800 AD and younger for those units which make up the coarser grained alluvial sands.

From the Holocene age deposits a total of 34 detrital charcoal samples were dated from T2, collected from both the north and south faces (Table 1). Samples that were collected from units 100-110 returned an age range of 65-455 yrs BP. Above unit 120, sample C19S was collected from unit 115 and was dated to 796-925 yrs BP. Sample C38S was collected within unit 120 and yielded a calibrated age of 1065-1173 yrs BP. Below unit 120 and at the contact between unit 130 and the overlying unit 125, two samples returned an age range between 1187-1377 yrs BP, while samples C71N and C70N returned a date range of 1345-1405 yrs BP for unit 130. Three samples were collected and dated from unit 140, resulting in a date range of 1396-1616 yrs BP. Above unit 200, three samples were collected from unit 160, which yielded a radiocarbon date range of 1823-2093 yrs BP.

From unit 200 two samples resulted in calibrated ages of 2000-2298 yrs BP. Samples collected throughout units 210 to 225 yielded a calibrated date range of 2341-2923 yrs BP. Finally, at the base of T2 located approximately 2-3 cm below the top of unit 300 sample C65N returned a calibrated age of 2974-3216 yrs BP, in good agreement with neighboring samples. As discussed previously, sediments exposed in the eastern portion of the T2 likely date to the Pleistocene based on the presence of the well-developed soil capping the alluvium and no further dating was attempted for this unit.

Both trenches returned radiocarbon samples that exhibited excellent stratigraphic temporal consistency, with calculated ages generally becoming younger from the base of the trench to the top (Figure 8). Seven radiocarbon samples showed evidence for some amount of inheritance and were excluded from the age model (Table 1).

2.6 Interpretation and Correlation of Stratigraphic units in T1 and T2

Overall, we interpreted the stratigraphy seen in each of the trenches to be the result of their relative position on the San Diego River flood plain. T2's location higher in elevation on the San Diego River flood plain allowed for the intermixing of overbank sediments, auxiliary fluvial channels, and outflow of alluvial drainages to occur. In contrast T1 is located lower and closer to the San Diego River in a position to experience a higher frequency of flooding. The presence of buried soils indicates periods of non-deposition and surface stability, and combining the presence of these soils with the general characteristics of each section and close relative spacing of the two trenches allows for an initial correlation of units, which can then be confirmed by radiocarbon dates to strengthen the stratigraphic correlations.

For instance, the "living surface" atop unit 100 in T2 most likely correlates with the pair of buried top soils in T1, represented by units 2b and 3b. We base this correlation of the observation that the unit 2b strata in T1 buries the early Spanish or Mexican era wall foundation and floor, and therefore must be historical in age, and again as T1 is lower and closer to the San Diego River, it makes sense that the T1 site would sustain more frequent flooding, resulting in an extra depositional unit that is not observed in T2. Additionally, based on the interpretation of unit 2b as redistributed or reworked natural topsoil capping unit 3a, the observed floor of the Spanish or Mexican Colonial Era structure at a similar stratigraphic level as the lowest portion of unit 3a (with the upper portion ponding against the foundation), and the base of the foundation excavated into unit 3b, we are confident in the interpretation that the upper two sections of unit 3 (3a and 3b) and unit 2b were the historical living surfaces at the time of first historical occupation of Old Town and in the decades thereafter.

A single radiocarbon date from unit 3a in T1 confirms a young age of 1660-1950 AD. The presence of glass, iron bar, and bone found in the upper most portion of units 100-110 in

T2, as well as radiocarbon dates indicating an age of 1500-1892 AD, suggests that these units also represent the historical living surface and shallow (~15 cm) subsurface during the earliest periods of occupation. We therefore confirm the interpretation that units 2b, 3a, and 3b in T1 are time synchronous with units 100-110 in T2.

Similarly to units 3a and 3b, unit 3c appears to be a major flood deposit associated with flooding of the San Diego River, and as unit 3 contains at least one weakly-formed buried A horizon, it must represent more than one flood event separated by some time, probably years, in order to form a weak soil. Based on stratigraphic order and similarities we correlate the silty-sand of unit 115 in T2 with the upper portion of unit 3c in T1, which is also represented by a massive section of silty-sand. We interpret the clean cross-bedded sands of unit 3c in T1 to represent higher flow during overbank sedimentation, perhaps as a consequence of a more southerly course of the San Diego River through Old Town. This period of higher flow deposition in T1 is expressed in T2 as the gravelly deposit of unit 120 which likely represents aggradation of the drainage to the south of T2. Thus, the similarity in stratigraphy, mostly alluvial sand and gravel, interpreted to represent high flow, suggests that the lower portion of unit 3c in T1, correlates to unit 120 in T2, which is confirmed by the close agreement of radiocarbon ages.

In T1, marine shells of almost certain Native American origin were found laying on top of unit 4, indicating that the top of unit 4 was a ground surface for at least a short period of time, although there is only very weak soil development based on darkening of the top of unit 4a. Considering that these strata are thinly bedded in T1 and although locally bioturbated, they retain the finely bedded characteristics of repeated overbank sedimentation, and so likely represent an environment that was too wet for occupation by burrowing animals most of the

time. In contrast, correlative stratigraphy in T2 are higher on the flood plain and may exhibit more A horizon soil development because of lower frequency of flooding reaching to the topographic level of T2.

Therefore, for the following correlations we lean more heavily on the close agreement of radiocarbon dates to assist in correlating these more massively bedded silty sand strata. We interpret the bedded, gray silty clay and clayey silts of unit 4a in T1 that exhibit some A horizon development to correlate with the buried A horizon of unit 130 in T2, which likely formed during a period of non-deposition at T2 and reduced overbank sedimentation at T1. This correlation is confirmed by several detrital charcoal samples collected from unit 4a in T1 and unit 130 in T2 which yield very similar dates of 544-624 AD and 574-763 AD, respectively.

Similarly, the heavily bioturbated silty sand of unit 140 in T2 is correlated with the bedded brown clayey silts of unit 4b in T1, both of these units contained agreeable radiocarbon date ranges of 344-535 AD and 432-573 AD, and are therefore interpreted to represent the same depositional time period. Unit 4c in T1 is composed of a sequence of silty clays and clayey silt with a few distinct brownish clay stringers that can be traced laterally throughout the fault zone; this stratigraphy is similar to the distinctive silty-sand stringers of unit 150 in T2. Therefore, we interpret the finer grained clay stringers in T1 to be correlated with coarser grained silty-sand deposits in T2. Lastly, we correlate the massive to weakly bedded muddy fine sands of unit 4d at the base of T1 with massive silty sands of unit 210-220 in T2, which is confirmed by the agreement of radiocarbon dates, which yielded date ranges of 397-266 BC and 389-235 BC, respectively.

By correlating the stratigraphy in the two trenches in this manner, the independent evidence of paleoearthquakes preserved in the separate trenches can be combined. This increased the overall strength of interpretations by supplementing the full width of the fault zone investigation of T2 with the high stratigraphic resolution of T1 on a secondary splay fault. Additionally, comparing the results from the two trenches acts as a check in our interpretations; events seen in trench T1 can be checked against the timing of independently interpreted events in T2.

2.7 Evidence of Earthquakes

From the trench exposures in T1 and T2, there is evidence for six surface ruptures in the past ~3,300 years at Old Town, although they do not appear to have all been the same size. In T1, the exposed part of the fault zone, which constituted a secondary fault strand only, is confined to a couple meter wide zone, but the finer stratigraphic resolution facilitated the identification of two events that are closely spaced in time. In T2, where the entire width of the fault zone could be investigated, the fault zone is broader with faulted stratigraphy seen across a ten-meter wide zone. Dates for paleoearthquakes were determined using the radiocarbon calibration program OxCal v 4.3.2, which employs a Basyian statistical framework on calibrated radiocarbon ages of the confining sediments to estimate probability density functions of the interpreted event horizons (Bronk Ramsey, 2009; Reimer et al., 2013) (Figures 7 and 9a).

Evidence for the youngest event captured in the trench exposures is event E0, which appears as a thin fissure or crack filled with historical-aged sand into the underlying unit 95, as exposed on the north face of T2 (Figure 7a). We named this event E0 as it is unknown whether this fracture is the result of fault creep, settlement, or some other mechanism; a non-tectonic

cause is plausible. The stratigraphic position of the infilling sediment, 20-25 cm above unit 100, suggests an age for this event that is substantially younger than 1769 AD, and likely well after 1850 AD by which time Old Town was firmly established. Although the historical sediments are fissured, there is no recognizable offset or mismatch of stratigraphy indicating only very minor motion, if any. Due to the uncertainty in the cause of E0, it was not included in the age model.

Event E1 is expressed as fissure infilling and small scale folding of historical-aged alluvial sands on the south face of T2 (Figure 7b) as well as a small (2-4 cm) displacement of a clayey-silt unit directly above unit 100, the top of which is the early historical living surface, and fissure infilling on the north face of T2 (Figure 7a). The evidence for event E1 is concentrated in an area directly above the main fault strand. The faulting of sediments containing abundant anthropogenic artifacts indicate a historical age (post-1769 AD), and as it displaces the living surface (top of unit 100) which probably saw occupation for some period of time, this event is probably at least several decades younger than the San Diego Mission and Presidio and likely dates to the Rancho Period (1834-1849 AD) or younger.

Evidence for event E2 is expressed over an approximately 9-m-wide fault zone with stratigraphy generally observed to be faulted up into or through unit 100 and being capped by the alluvial sands of historical age. On the south face of T2 and directly beneath the deepest small alluvial channel incisions, event E2 is seen as fissure infilling of lighter-colored coarser sediments than the surrounding units. These infilling sediments are derived from the deepest alluvial channels that have eroded into, and well below unit 100 and so lay at a deeper stratigraphic level then the historical sandy strata, which were likely deposited by the historical alluvial fan system seen in historical imagery (Figure 3 and 5a). In sections of the trench away

from the small deep alluvial channels, event E2 is seen as upward-terminating fault strands capped by the upper few centimeters of unit 100, as well as tilted alluvial channel deposits (Figure 5a and 7b). The north face of T2 has similar evidence for event E2 with fissure infilling of overlying lighter-colored sediments, again directly below the same deepest, small alluvial channel, and upward terminating fault strands capped by unit 100 or the historical age alluvial sands (Figure 6 and 7a). Radiocarbon analyses and historical records of seismicity place the occurrence of event E2 between 1708 and 1769 AD, using the timing of Mission establishment as a prior, yielding a mean date of ~1744 AD.

Event E3 is well expressed in T2 and is seen on both trench faces as upward-terminating fault strands, capped by unit 105-110 (Figures 5a, 6, and 7a), as well as fissure infilling to a similar stratigraphic level. The timing of event E3 is the least well-constrained event date of our study, due to the lack of reliable radiocarbon dates at this stratigraphic horizon. As a result, the age of event E3 is best constrained by age of unit 110 above and unit 115 below with a best estimate date range of 1077-1588 AD.

Event E4 is clearly identifiable only in T1 due to the more detailed stratigraphic resolution of T1 when compared to the more massively bedded stratigraphy of T2 for this time period. Event E4 is seen as a single fault strand that offsets the unit 4b/4a contact by about 5 cm, and terminates at the top of unit 4a and is capped by the unfaulted, clean cross-bedded sands of unit 3c (Figure 4). Thus, the age of unit 3c provides an upper bound for event E4, while unit 4a provides a lower. This results in a date range of 675-835 AD. It should be noted that evidence for event E4 is likely present in T2, but has been amalgamated with event E5 because of the poorer stratigraphic resolution of T2 sediments when compared to T1.

Event E5 is seen at multiple locations on both faces of T2 as well as in T1, although as mentioned above, some of the deformation observed in T2 may be attributable to event E4. On the north and south faces of T2, event E5 is expressed as upward terminating fault strands, all capped by unfaulted sections of unit 130, as well as fissure infilling of overlying sediment. At the eastern- and western-most sections of the south face of T2, event E5 is expressed as ~25-15 cm vertical displacement of unit 200 capped by unfaulted unit 130 (Figure 7c). In T1 event E5 is expressed as significant faulting and folding of units 4d through 4b, with deformation observed across a ~2-m-wide zone. This deformation is then planed off and capped by horizontally deposited strata of unit 4a (Figure 4). Event E5 is interpreted to have occurred sometime between 486 AD and 588 AD and appears to be a larger rupture than event E4 based on the associated folding and width of damage zone in T1.

The oldest event recorded at the Old Town site is event E6 and is observed near the base of trench T2. On the south face, evidence for event E6 includes the tilting and deformation of several fine-grained units including unit 215, which are then capped by the horizontal deposition of unit 200 (Figure 5a). Additionally, upward terminating fault strands with ~8-12 cm of displacement are observed and again capped by unit 200 (Figure 7c). The stratigraphy at the base of the northern face of T2 is more massive than the southern face and thus does not exhibit the same well-developed auxiliary channel features. However, away from the auxiliary channel deposits we still observed tilted fine-grained silt stringers as well as upward terminating fault strands, all capped by unit 200 (Figure 6). Event E6 is interpreted to have occurred sometime between 371 BC and 199 BC. The event ages and their uncertainties are summarized in Figure 9a.

2.8 Discussion

2.8.1 Earthquake Magnitudes and Late-Holocene Recurrence Interval

The paleoseismic trenches at Old Town show that the RCF has sustained repeated surface rupturing earthquakes throughout the late Holocene and into the Historical period. The extent of deformation associated with each individual event at Old Town can be used to estimate a relative magnitude of the causative earthquake.

Event E0 is a crack with no recognizable offset. Its origin is unclear; it may represent a small component of creep, a small triggered slip event, or it may represent settlement in the fault zone due to percolating surface water, as the presence of several small rills incised into unit 100 and the subsequent deposition of the historical-age alluvial fan sediments clearly demonstrate that this area has sustained repeated flooding. In any case, we do not attempt to relate this to a specific historical earthquake, although intensity VII shaking was recorded in San Diego from the M7.2 1892 AD Laguna Salada earthquake (Agnew et al., 1979; Hough and Elliot, 2004; Rockwell et al., 2015) and is a candidate if the crack is a result of triggering by strong ground shaking.

Event E1 displaces historical-aged sediments and the top of the unit 100 "living surface" and likely represents displacement from a historical earthquake, probably at least several decades after the arrival of the Spanish colonist in 1769 AD. From the historical records of seismicity there are two earthquakes with reported felt effects more intense, or equal, in San Diego when compared to other locations in southern California: April 12th 1852 AD, and May 27th 1862 AD (Agnew et al., 1979). The event reported in 1852 AD has a suspect seismic source based on the highly localized reports of damage (on only one adobe structure) from "a very severe shock" with no documented damage to other near-by structures (Anderson et al.,

1989; Agnew et al., 1979). As this event was not reported from areas to the north, we infer that if this was a bonafide earthquake, it likely occurred to the south.

Thus, the most likely candidate for event E1 is the May 27th 1862 AD earthquake, reported as the "Day of Terror in San Diego" by the regional newspaper the Los Angeles Star (*The Los Angeles Star,* 1862; Legg and Agnew, 1979). This event, preliminarily located along the Spanish Bight fault in San Diego Bay or an adjacent fault offshore, is estimated at about M6, which is about the threshold for surface rupture and is consistent with the amount of observed deformation for this event. The reported felt effects of this event, although inconclusive by themselves, when combined with the young surface rupture observed at Old Town support the occurrence of an earthquake on the RCF in 1862 AD (Legg and Agnew, 1979).

The penultimate event seen at Old Town, event E2, has caused displacement across the entire fault zone up to but just below the historical living surface, and represents a much broader zone of faulting than seen for E1. Furthermore, E2 correlates well with the most recent event (MRE) reported at other paleoseismic sites in San Diego (Rockwell, 2010a). North of Old Town, at Lindvall and Rockwell's (1995) Rose Creek site, a cleanly faulted modern topsoil A horizon indicates an event date in the past ~400 years. A young surface rupture for the northern most section of the RCF was confirmed by later work in La Jolla using material, partially derived from a Native American shell midden, from an infilled fissure that provided a more reliable date of 1650 ± 125 AD (Rockwell and Murbach, 1999). South of Old Town, multiple geotechnical reports in the downtown area have documented displacement of the topsoil A horizon as well as calibrated radiocarbon dates between 1420 and 1769 AD for the most recent event (Woodward and Clyde, 1985 and 1994, as reported in Rockwell and

Murbach, 1999). As discussed previously, radiocarbon dates from our Old Town trenches indicate that this event occurred between 1704 and 1769 AD, well within the radiocarbon uncertainty from other sites. Thus, with evidence for event E2 being documented for the length of the onshore segment of the RCF, we infer that event E2 represents a significantly larger earthquake than E1 that ruptured at least from La Jolla to San Diego Bay.

Events E3, E5, and E6 all exhibit similar styles of deformation, e.g., tilted beds, 5-25 cm vertical displacements, and deep fissure infillings over a broad ~10-m-wide zone, similar to that observed for event E2. Based on the similarities in deformation it is likely that events E3, E5, and E6 also ruptured most of, if not all of the onshore section of the RCF. Thus, based on the amount of deformation and width of the affected fault zone, we interpret events E2, E3, E5 and E6 all to be the result of relatively larger magnitude earthquakes.

The localized, small vertical displacement (~1-5 cm) associated with event E4 is similar to that observed for event E1 and is therefore also interpreted to be the result of a relatively smaller magnitude earthquake, possibly in the M6-6.4 range. Evidence that it may have been a little larger than the 1862 AD earthquake is inferred because it ruptured a secondary fault splay in T1 that did not re-rupture in 1862 AD. In contrast, the evidence for the 1862 AD earthquake is concentrated directly above the main fault zone in T2 with no displacement seen on secondary fault splays. Hence, it appears that E4 may have ruptured a slight wider area of the fault zone than E1 and thus the larger inferred magnitude range.

We attribute the difference in observed earthquakes between the two trenches to two factors. First, as mentioned previously, the excavation into a culturally significant structure in T1 possibly prevented an investigation of the main fault at that location. We believe that the main fault trace is likely located beneath, or slightly west of the Spanish Colonial era structure

and was just missed by the mechanical excavations at T1 (Figure 4). It is possible that a minor trace of the fault also exists east of T1. As a result, additional strands and the primary fault that would have ruptured in past earthquakes were not observed. Second, the higher stratigraphic resolution at T1 enabled us to distinguish E4 and E5 as separate events despite the close separation in time of approximately 100-200 years. Except for a few select locations, this kind of stratigraphic resolution between closely spaced, smaller and larger magnitude events was not possible in trench T2 due to the more massive nature of the silty bedding. Therefore, the possibility exists that evidence for additional, smaller late Holocene earthquakes on the RCF was not recovered at Old Town.

The six earthquakes interpreted at Old Town have important implications for the understanding of the seismic behavior of the RCF. The period of quiescence previously interpreted to have taken place from ~5.3 ka to ~500 years ago led Rockwell (2010a) to postulate a possible cluster mode behavior for the RCF. However, our results demonstrate that the RCF has sustained activity throughout the late Holocene, and seemingly into the Historical Period. While there remains a several thousand-year gap in the paleoseismic record of well-dated events, geotechnical reports from the San Diego airport suggest additional earthquakes in the mid-Holocene (Rugg et al., 2013). Thus, it would appear that the RCF has ruptured with quasi-periodic frequency for the periods over which a record has been preserved.

Previous estimates of the recurrence interval on the RCF have a broad range of about 3,000 to 800 years, depending on considerations of assumed quasi-periodicity, clustered behavior, and characteristic slip per event (Lindvall and Rockwell, 1995; Rockwell, 2010a). Rockwell (2010a) determined an intercluster recurrence interval of approximately 800 years for the early Holocene events observed at Rose Creek. Using the methods of Biasi et al. (2002), the

event dates recovered at Old Town suggest a similar recurrence interval for the inferred larger events of ~700 years during the late Holocene. With the suggested mid-Holocene seismic activity at the San Diego Airport, along with the close agreement between the early Holocene recurrence interval of Rockwell (2010a) and that of Old Town, these observations suggest that the Holocene recurrence interval for the RCF is closer to ~700-800 years rather than the 1,000-1,500 years determine from the Rose Creek events alone (Lindvall and Rockwell 1995; Rockwell 2010a, 2010b). However, it is possible that the earthquake sequence seen at Old Town represents the tail end of the most recent cluster, with a shorter quiescence period discussed above. More accurate paleoseismic dating targeting the mid-Holocene will be required to sufficiently resolve this question.

The apparently shorter recurrence interval at Old Town has important implications for slip per event and the average size of earthquakes when combined with slip-rate estimates of the RCF. A previously estimated slip per event of 3 m implies a slip rate closer to 4.0 mm/yr if the 700-800 year recurrence interval is applied. However, that 3 m estimate for slip in the most recent event was based on an offset channel at Rose Creek that may have been offset by two or more events, so it represents a maximum displacement. An alternative estimate is resolved by using the 700-800 year recurrence interval determined from the early and late Holocene record and applying the 1.5-2 mm/yr slip rate to arrive at an average displacement of 1.2-1.4 m for the larger events and less than a meter for the smaller events. This estimated average displacement is consistent with earthquakes in the M6.7-M7 range.

2.8.2 Effect of Fault Structure on Earthquake Occurrence

The location of Old Town north of the extensional structures that make up the step-over through San Diego Bay may help explain some features of earthquake occurrence at Old Town.

The structural setting of San Diego Bay and Old Town is similar to fault structures east of the Peninsula Ranges, where a large releasing step-over is formed by the faults of the Imperial Valley (Elders et al., 1972). A large number of studies have documented triggered slip on faults in the southern San Andreas fault system in the Imperial Valley in response to ruptures on nearby faults (e.g. Wei et al., 2011; Fuis, 1982). This similarity in fault structure and orientation may explain a mechanism for the interpretation that event E0 is potentially the result of either triggered slip or possibly shallow creep; however, a non-tectonic origin should not be ruled out.

If E0 represents a triggered slip event, its event horizon, well within the historically-aged sand strata but prior to construction of the golf course, suggests an event age sometime around the turn of the 20th century. Faults of coastal northern Baja and offshore of San Diego (e.g., the San Miguel-Vallecitos fault and the Agua Blanca fault system) exhibit a spatial distribution and orientation with respect to the RCF similar to that of the Imperial Valley, and so would be the most likely triggering mechanisms for event E0. Alternatively, the February 1892 AD earthquake on the Laguna Salada fault in northern Baja California was the last earthquake to have produced intensity VII damage in San Diego (Agnew et al., 1979) and is also a plausible triggering mechanism. Further, the area's historical record of seismicity has numerous accounts of earthquakes during this time period that likely occurred on the faults of coastal northern Baja California, but without precise dating of the event E0 horizon we do not attempt to identify a causative earthquake (Agnew et al., 1979).

For at least two occurrences at Old Town, small magnitude events inferred from minimal displacement on a limited number of fault strands were observed to occur shortly after larger magnitude events that shattered the full width of the fault zone. The event E4 horizon is

dated approximately 150 years after that of event E5, while event E1 appears to follow event E2 by about 100 years. Similar behavior has been observed on other faults in southern California, and has been modeled as a combination of reduced normal stress on extensional structures following large earthquakes as well as localized stress increase on well oriented faults (Stein et al., 1992; Nielsen and Knopoff, 1998). Thus, this pattern is possibly also a result of Old Town's proximity to the large extensional step in the RCF across San Diego Bay, which may allow for the preservation of some "tension aftershocks" described by Nielsen and Knopoff (1998).

Therefore it appears that the paleoseismic record at Old Town has captured at least twice, but possibly more given the limitations in stratigraphic resolution of T2, the occurrence of a relatively larger magnitude earthquake on the RCF, which is then followed by slip that is possibly transferred to the Old Town section of the RCF by one of the linking oblique-slip structures that splay across San Diego Bay. It is our interpretation that this scenario likely described the penultimate event E2, which is interpreted as a larger magnitude event that would have relieved the regional stresses in San Diego Bay allowing the initiation of earthquakes on nearby faults, such as the Spanish Bight fault, at a lower shear stress, resulting in rupture and slip related to event E1.

2.8.3 Cascading Seismicity of the Newport-Inglewood-Rose Canyon Fault System

With the RCF interpreted to represent the southern onshore extension of the NIRC, the increased activity in the late Holocene seen at Old Town has important implications for the seismic behavior of the longer NIRC. It has been suggested that the close spacing, in time, of the most recent paleoseismic events along the Agua Blanca fault, RCF, and Newport Beach segment of the NIF, represents a northward cascading sequence of earthquakes (Grant and

Rockwell, 2002). The proposed cascade includes the MRE seen at both Rose Creek and La Jolla, and now Old Town with event E2 occurring sometime in the mid-1700s AD (Grant and Rockwell, 2002). Recently, new work at Seal Beach has found evidence for three late Holocene earthquakes that are interpreted based on rapid subsidence of a fault-bounded marsh along the southern, onshore segment of the NIF (Leeper et al., 2017). The NIF rupture events at Seal Beach appear to correlate well with the events determined at Old Town (Figure 9b). Additionally, researchers working at other sites on the NIF and the Compton-Los Alamitos blind thrust (CPT-LA), which may be kinematically linked with the NIF at depth, further correlate with the results at Seal Beach, La Jolla, Rose Creek, and Old Town (Grant et al., 2002; Grant et al., 1997; Leeper et al., 2017; Leon et al., 2009; Wright, 1991). The close correlation in time, through multiple earthquake cycles of dated paleoearthquakes along the various segments of the NIRC suggests that this fault system does indeed communicate stress between fault segments in either very large earthquakes or a cascading sequence of earthquakes. The large earthquake hypothesis is problematic considering the slip rates of the faults involved when combined with the recurrence intervals. A 700-800 year recurrence of an earthquake rupturing the entire NIRC would require a much higher slip rate than is observed, as displacement per event would be larger based on scaling relationships (Wells and Coppersmith, 1994; Leonard, 2010). In contrast, similar patterns of sequential ruptures have been observed on continental strike-slip faults around the world, including the North Anatolian fault of Turkey (Stein et al., 1997; Rockwell, 2011) and the Velino-Magnola fault of central Italy (Schlagenhauf et al., 2011).

The apparent temporal pattern in earthquake occurrence (Figure 9b) raises important questions regarding the spatial extent of earthquake ruptures on the NIRC fault system. Models

of static Coulomb stress change on the offshore faults of the NIRC system found a ~30-40% likelihood for a full-length rupture of those segments (Sahakian et al., 2017). The most beneficial situation that would promote a through-going rupture of the offshore segments is one in which rupture is initiated on the Carlsbad segment, which would result in a southward-directed rupture into San Diego (Sahakian et al., 2017). Several geomorphic indicators of reversed polarity effects associated with unidirectional ruptures in San Diego indicate that the RCF may experience unidirectional southward-directed ruptures (Ben-Zion et al., 2012; Sahakian et al., 2017). However, high resolution CHIRP seismic data on the offshore NIRC segments reveal that the subsurface depth of deformation, and therefore recency of faulting, is variable along strike with the most recent faulting seen at the southern and northern ends of the offshore segments (Maloney; 2013; Klotsko et al., 2015; Sahakian et al., 2017). While the possibility exists that if those offshore segments with a lack of deformation experience pure horizontal displacement it may be below the resolution of current seismic profiles, we speculate that these offshore segments have not experienced an end to end rupture during the late Holocene (Klotsko et al., 2015; Sahakian et al., 2017). This observation is consistent with a sequential rupture model rather than the "wall-to-wall" rupture inferred to be possible by Sahakian et al. (2017). Therefore, our preferred interpretation is one where the southern portion of NIRC; made up of the onshore RCF from San Diego Bay to offshore La Jolla, and possibly the Torrey Pines segment of Sahakian et al., (2017), rupture together in moderately large earthquakes. North of the Carlsbad segment, which apparently has not ruptured to the surface in the past ~8,000 years and may act as a barrier to through going ruptures, the Camp Pendleton strands and the onshore NIF segments from at least Newport Beach to the Compton area, may rupture together (Sahakian et al., 2017; Klotsko et al. 2015).

The lack of large magnitude earthquakes in the paleoseismic record for the northernmost segments of the NIRC fault suggest that these segments may be closer to failure (Figure 9b). Indeed, the northern NIF zone has previously been identified as a possible seismic gap, with no known date for a last rupture (Grant and Rockwell, 2002; Byrant, 1988). Historical seismicity, such as the 1933 AD M_w 6.4 Long Beach earthquake and several smaller, deeper events beneath the oil fields north of Long Beach, confirm that these strands are active (Hauksson and Gross, 1991; Toppozada et al., 1989). However, it may also be the case that the northernmost segments of the NIRC behave in a similar fashion to the Carlsbad segment offshore, perhaps rupturing only in rare events.

2.9 Conclusions

The results from our paleoseismic study at Old Town show that the RCF has sustained seismic activity with ground rupturing earthquakes throughout the late Holocene and into the Historical period. The last relatively larger magnitude earthquake on the RCF at Old Town was apparently sometime in the mid-1700s likely just prior to the Spanish colonization of southern California. Additionally, the Old Town site contained evidence for a historical rupture on the RCF, which records of seismicity suggest is the May 27th 1862 AD earthquake. Furthermore, these results suggest that the RCF has a ~700-800 year recurrence interval for relatively larger magnitude earthquakes (M 6.7-7) that likely rupture the entire onshore portion of the RCF in San Diego. This recurrence interval is several hundred years shorter than previous estimates and suggests a smaller slip per event as discussed above. The close correlation in time of dated earthquakes at paleoseismic sites along strike of the NIRC suggests that the various fault segments communicate stress in either very large magnitude earthquakes or a cascading

sequence of earthquakes. Given the low reported slip rates of the faults involved, the relatively short ~700-800 year recurrence interval, as well as the apparent lack of deformation on some of the offshore fault segments our preferred interpretation is one which favors a cascading sequence of earthquakes along the NIRC.

2.10 Data and Resources

Paleoearthquakes dates presented in this paper have been taken from published works listed in the reference section below. Active fault traces in this paper are from the USGS Fold and Faults Database of the U.S. Geological Survey (http://earthquake.usgs.gov/hazards/qfaults/). Some plots were made using Generic Mapping Tools (GMT) version 5.4.3 (Wessel et al., 2013). Coastal Relief model acquired from the National Geophysical Database (National Geophysical Data Center, 2003). Radiocarbon dates were calibrated and age model constructed by OxCal v4.3.2 with Intcal13 radiocarbon calibration curve (Bronk Ramsey, 2009; Reimer et al., 2013).

2.11 Acknowledgements

We thank the City of San Diego for granting access to the Presidio Hills Golf Course in Old Town, and to Mr. Lee, the Golf Course leasee, for facilitating access. We also thank Rob Hawk for his assistance at the trench site, and the many folks from the California Geological Society and other institutions that dropped by for discussions on interpretations in the trenches, and Alexandra Sarmiento and Justin Zumbro from Geopentech for assistance in permitting and in the field, as well as the San Diego State University and University of California San Diego geo-students who stopped by the trench for a day or two (or three) to help wherever needed.

We thank the reviewers (Lisa Grant Ludwig, Robert Langridge, and an anonymous reviewer) for improving the presentation of this manuscript. This work was funded by US Geological Survey Award No. G16-AP00015, with additional support by Southern California Edison. The Southern California Earthquake Center provided support through loan of the trench shores. This research was supported by the Southern California Earthquake Center (Contribution No. 8057). Southern California Earthquake Center is funded by National Science Foundation Cooperative Agreement EAR-1033462 & US Geological Survey Cooperative Agreement G12AC20038.

Chapter 2, in full, is a reformatted reprint of the material as it appears in: Singleton, D.M., Rockwell, T.K., Murbach, D., Murbach, M., Maloney, J.M., Freeman, T. and Levy, Y., 2019. Late-Holocene rupture history of the Rose Canyon fault in Old Town, San Diego: Implications for cascading earthquakes on the Newport–Inglewood–Rose Canyon fault system. *Bulletin of the Seismological Society of America*, *109*(3), pp.855-874. The dissertation author was the primary investigator and author of this paper.

2.12 References

Abbott, P. L. 1991. "Flood Control in the Lower Reaches of the San Diego River." In *Environmental Perils, San Diego Region*, edited by Patrick Abbott and William Elliott, 189–94. San Diego, CA: San Diego Association of Geologist for the Geological Society of America Annual Meeting.

Agnew, D. C., M. Legg, and C. Strand. 1979. "Earthquake History of San Diego." In *Earthquake and Other Perils: San Diego Region*, edited by Pattrick L. Abbott and WJ. Elliott, 123–38. San Deigo, CA: San Diego Association of Geologist.

Anderson, J G., T. K. Rockwell, and D. C. Agnew. 1989. "Past and Possible Future Earthquakes of Significance to the San Diego Region." *Earthquake Spectra* 5 (2): 299–335.

Ben-Zion, Y., T. K. Rockwell, Z. Shi, and S. Xu. 2012. "Reversed-Polarity Secondary

Deformation Structures Near Fault Stepovers." *Journal of Applied Mechanics* 79 (3): 031025. https://doi.org/10.1115/1.4006154.

Biasi, G. P., R. J. Weldon, T. E. Fumal, and G. G. Seitz. 2002. "Paleoseismic Event Dating and the Conditional Probability of Large Earthquakes on the Southern San Andreas Fault, California." *Bulletin of the Seismological Society of America* 92 (7): 2761–81. https://doi.org/10.1785/0120000605.

Bronk Ramsey, C. 2009. "Bayesian Analysis of Radiocarbon Dates." *Radiocarbon* 51 (1): 337–60.

Byrant, W. A. 1988. "Recently Active Traces of the Newport-Inglewood Fault Zone, Los Angeles and Orange Counties, California." Sacramento. https://doi.org/DMG OFR 88-14.

Elders, W. A., R. W. Rex, P. T. Robinson, S. Biehler, and T. Meidav. 1972. "Crustal Spreading in Southern California." *Science1* 178 (4056): 15–24.

Fischer, P. J., G. I. Mills. 1991. "The offshore Newport-Inglewood-Rose Canyon fault zone, California: Structure, segmentation and tectonics." *In* Abbott, P.L., W. J., Elliott, (Editors). *Environmental Perils of the San Diego Region:* San Diego Association of Geologist, San Diego, California. p. 17-36.

Fuis, G. S. 1982. "Displacement on the Superstition Hills Fault Triggered by the Earthquake." *USGS Report: The Imperial Valley, California, Earthquake of October 15, 1979*.

Grant, L. B., L. J. Ballenger, and E. E. Runnerstrom. 2002. "Coastal Uplift of the San Joaquin Hills, Southern Los Angeles Basin, California, by a Large Earthquake since A.D. 1635." *Bulletin of the Seismological Society of America* 92 (2): 590–99. https://doi.org/10.1785/0120010119.

Grant, L. B., J. T. Waggoner, T. K. Rockwell, and C. Von Stein. 1997. "Paleoseismicity of the North Branch of the Newport-Inglewood Fault Zone in Huntington Beach, California, from Cone Penetrometer Test Data." *Bulletin of the Seismological Society of America* 87 (2): 277–93.

Grant, L. B., and T. K. Rockwell. 2002. "A Northward-Propagating Earthquake Sequence in Coastal Southern California." *Seismological Research Letters2* 73 (4): 461–69.

Hauksson, E., and S. Gross. 1991. "Source Parameters of the 1933 Long-Beach Earthquake." *Bulletin of the Seismological Society of America* 81 (1): 81–98.

Heusser, L. 1978. "Pollen in Santa Barbara Basin, California: A 12,000-Yr Record." *Geological Society of American Bulleting* 89: 673–78.

Hough, S. E., and A. Elliot. 2004. "Revisiting the 23 February 1892 Laguna Salada Earthquake." *Bulletin of the Seismological Society of America* 94 (4): 1571-1578.

Kennedy, M. P. 1975. “Geology of the San Diego Metropolitan Area, California.” *California Division of Mines and Geology Bulletin* 200: 9–39.

Kennedy, M.P. and E.E. Welday. 1980. Recency and character of faulting offshore metropolitan San Diego, California. *Calif. Div. Mines and Geol. Map Sheet 40.*

Kennedy M.P. and S.H. Clarke. 1999, Age of faulting in San Diego Bay in the vicinity of the Coronado Bridge; Addendum to analysis of late Quaternary faulting in San Diego Bay and hazard to Coronado Bridge. *Calif. Div. Mines and Geol., Open File Report* 97-10B, 12 p plus seismic lines.

Kern, J. P., and T. K. Rockwell. 1992. “Chronology and Deformation of Quaternary Marine Shorelines, San Diego County, California.” *Quaternary Coasts of the United States*, no. 48: 377–82.

Klotsko, S., N. Driscoll, G. Kent, and D. Brothers. 2015. “Continental Shelf Morphology and Stratigraphy Offshore San Onofre, California: The Interplay between Rates of Eustatic Change and Sediment Supply.” *Marine Geology* 369. Elsevier B.V.: 116–26. https://doi.org/10.1016/j.margeo.2015.08.003.

Leeper, R., B. Rhodes, M. Kirby, K. Scharer, J. Carlin, E. Hemphill-Haley, S. Avnaim-Katav, G. Macdonald, S. Starratt, and A. Aranda. 2017. “Evidence for Coseismic Subsidence Events in a Southern California Coastal Saltmarsh.” *Scientific Reports* 7 (March). Nature Publishing Group: 1–11. https://doi.org/10.1038/srep44615.

Legg, M., and D. C. Agnew. 1979. “The 1862 Earthquake in San Diego.” In *Earthquake and Other Perils: San Diego Region*, edited by Pattrick L. Abbott and W.J. Elliot, 139–41. San Deigo, CA: San Diego Association of Geologist.

Leon, L. A., J. F. Dolan, J. H. Shaw, and T. L. Pratt. 2009. “Evidence for Large Holocene Earthquakes on the Compton Thrust Fault, Los Angeles, California.” *Journal of Geophysical Research: Solid Earth* 114 (12): 1–14. https://doi.org/10.1029/2008JB006129.

Leonard, M. 2010. “Earthquake Fault Scaling: Self-Consistent Relating of Rupture Length, Width, Average Displacement, and Moment Release.” *Bulletin of the Seismological Society of America* 100 (5 A): 1971–88. https://doi.org/10.1785/0120090189.

Lindvall, S., and T. K. Rockwell. 1995. “Holocene Activity of the Rose Canyon Fault Zone in San Diego, California.” *Journal of Geophysical Research* 100 (B12): 24121–32.

Maloney, J. M. 2013. "Fault Segments and Step-overs: Implications for Geohazards and Biohabitats". Doctoral Dissertation. Scripps Institution of Oceanography-University of California San Diego.

Moore, G. W. 1972. “Offshore Extension of the Rose Canyon Fault, San Diego, California.”

Geological Survey Professional Paper 800–2: 113–16.

Moore, G. W., and M. P. Kennedy. 1975. "Quaternary Faults at San Diego Bay, California." *J. Res. US Geol. Surv*. Vol. 3.

National Geophysical Data Center, 2003. U.S. Coastal Relief Model - Southern California. National Geophysical Data Center, NOAA. doi:10.7289/V500001J [April 17, 2018].

Nielsen, S. B., and L. Knopoff., 1998. "The Equivalent Strength of Geometrical Barriers to Earthquakes." *Journal of Geophysical Research* 103 (B5): 9953–65.

Reimer, P. J., E. Bard, A. Bayliss, J. W. Beck, G. P. Blackwell, and C. Bronk Ramsey. 2013. "Intcal13 and Marine13 Radiocarbon Age Calibration Curves 0–50,000 Years Cal Bp." *Radiocarbon* 55 (4): 1869–87. www.radiocarbon.org.%0Awww.radiocarbon.org.

Rockwell, T. K. 2010a. "The Rose Canyon Fault Zone in San Diego." *Fifth International Conference on Recent Advances in Geotechnical Earthquake Engineering and Soil Dynamics and Symposium in Honor of Professor I.M. Idriss*, no. 7.06c: 1–9.

Rockwell, T. K. 2010b. "Seismic Source Characteristics of Onshore Rose Canyon Fault." *San Onofre Nuclear Generating Station Seismic Hazard Assessment Program 2010 Seismic Hazard Analysis Report; Appendix A, Attachment A-2*.

Rockwell, T. K. 2011. "The North Anatolian Fault." In *Encyclopedia of Natural Hazards*, edited by Peter T. Bobrowsky. Springer Science+Business Media. https://doi.org/10.1007/978-1-4020-4399-4.

Rockwell, T.K., J. M. Fletcher, O. J. Teran, A. P. Hernandez, K. J. Mueller, J. B. Salisbury, S. O. Akciz, and P. Štěpančíková. 2015. "Reassessment of the 1892 Laguan Salada Earthquake: Fault Kinematics and Rupture Patterns. " *Bulletin of the Seismological Society of America* 105 (6): 2885-2893.

Rockwell, T. K., S. Lindvall, C. C. Haraden, K. C. Hirabayashi, and E. Baker. 1991. "Minimum Holocene Slip Rate for the Rose Canyon Fault in San Diego, California." In *Environmental Perils: San Diego Region*, edited by Patrick L. Abbott and William J. Elliott, 37–46. San Diego, CA: San Diego Association of Geologist for the Geological Society of America Annual Meeting.

Rockwell, T. K., and M. Murbach. 1999. "Holocene Earthquake History of the Rose Canyon Fault Zone." U.S. Geological Survey Final Technical Report for Grant No. 1434-95-26133

Rockwell, T. K., K. M. Scharer, and T. E. Dawson. 2016. Earthquake Geology and Paleoseismology of Major Strands of the San Andreas Fault System: Chapter 38. *Applied Geology in California* 26: 721–56. http://pubs.er.usgs.gov/publication/70177065.

Rugg, S., R. Torres, and T. K. Rockwell. 2013. "TDY Fault Study: San Diego International

Airport." Kleinfelder Final Report for the San Diego County Regional Airport Authority, San Diego, CA, Kleinfelder Project No. 125800.

Sahakian, V., J. Bormann, N. Driscoll, A. Harding, G. Kent, and S. Wesnousky. 2017. "Seismic Constraints on the Architecture of the Newport-Inglewood/Rose Canyon Fault: Implications for the Length and Magnitude of Future Earthquake Ruptures." *Journal of Geophysical Research: Solid Earth* 122 (3): 2085–2105. https://doi.org/10.1002/2016JB013467.

Schlagenhauf, A., I. Manighetti, L. Benedetti, Y. Gaudemer, R. Finkel, J. Malavieille, and K. Pou. 2011. "Earthquake Supercycles in Central Italy, Inferred From 36Cl Exposure Dating." *Earth and Planetary Science Letters* 307 (3–4). Elsevier B.V.: 487–500. https://doi.org/10.1016/j.epsl.2011.05.022.

Stein, R. S., A. A. Barka, and J. H. Dieterich. 1997. "Progressive Failure of the North Anatolian Fault since 1939 by Earthquake Stress Triggering." *Geophysical Journal International* 128: 594–604.

Stein, R. S., G. C. P. King, and J. Lin. 1992. "Change in Failure Stress on the Southern San Andreas Fault System Caused by the 1992 Magnitude = 7.4 Landers Earthquake." *Science* 258 (5086): 1328–32.

The Los Angeles Star. June 21, 1862. "San Diego Items-Earthquakes," p.2 col. 2.

Toppozada, T., J. H. Bennett, G. Borchardt, R. Saul, and J. F. Davis. 1989. "Earthquake Planning Scenario for a Major Earthquake on the Newport-Inglewood Fault Zone." *Division of Mines and Geology: California Geology* 42 (4).

Wei, M., D. Sandwell, Y. Fialko, and R. Bilham. 2011. "Slip on Faults in the Imperial Valley Triggered by the 4 April 2010 Mw 7.2 El Mayor-Cucapah Earthquake Revealed by InSAR." *Geophysical Research Letters* 38 (1): 1–6. https://doi.org/10.1029/2010GL045235.

Wells, D. L., and K. J. Coppersmith. 1994. "New Empirical Relationships among Magnitude, Rupture Length, Rupture Width, Rupture Area, and Surface Displacement." *Bulletin of the Seismological Society of America* 84 (4): 974–1002.

Wessel, P., W. H. F. Smith, R. Scharroo, J. F. Luis, and F. Wobbe, Generic Mapping Tools: Improved version released, EOS Trans. AGU, 94, 409-410, 2013

Woodward and Clyde. 1985. Geologic and fault investigation, San Diego police administration and technical center, San Diego, CA. Technical report for Starboard Development Company,

Woodward and Clyde. 1994. Report of fault hazard investigation for the entertainment and sports center, San Diego, California. Geotechnical report for Centre City Development Corporation.

Wright, T. L. 1991. “Structural Geology and Tectonic Evolution of the Los Angeles Basin, California.” In *Active Margin Basins*, edited by Kevin T. Biddle, AAPG Memoi, 35–79. Tulsa, OK: The American Association of Petroleum Geologist.

Table 2.1. List of radiocarbon samples collected at Old Town-San Diego, CA. Sample names with X in front were excluded from age model based on inheritance discussed in text.

Rose Canyon Fault-Old Town- Trench 1 (T1) & Trench 2 (T2)				
Sample #	Face (Trench)	Unit	14C age (Yrs BP)	±
C74N	North (T2)	100	135	15
C72N	North (T2)	102	150	15
C73N	North (T2)	102	110	20
C43S	South (T2)	105/110	135	15
C55N	North (T2)	105/110	105	25
C40S	South (T2)	110	180	15
C41S	South (T2)	110	180	25
19	South (T1)	3a (~110)	195	15
C39S	South (T2)	110	305	25
C19S	South (T2)	115	950	20
C38S	South (T2)	120	1190	15
27	South (T1)	3c (~120)	1005	15
29	South (T1)	3c (~120)	1165	15
45	South (T1)	3c (~120)	1165	15
C53S	South (T2)	125/130	1510	25
C34N	North (T2)	125/130	1305	15
8	South (T1)	4a (~130)	1400	70
C70N	North (T2)	130	1490	15
C71N	North (T2)	130	1505	20
C15N	North (T2)	140	1610	70
C52S	South (T2)	140	1595	20
C37N	North (T2)	140	1645	20
12	North (T1)	4b (~140)	1510	15
35	North (T1)	4c (~150)	1725	30
13	North (T1)	4c (~150)	1815	15
C17S	South (T2)	160	1915	15
C18S	South (T2)	160	2085	15
C1S	South (T2)	160	2035	20
C56S	South (T2)	200/205	1995	30
C45S	South (T2)	200/205	2175	15
C28N	North (T2)	210/215	2265	20
5	South (T1)	4d (~215/220)	2265	15
C26S	South (T2)	220	2365	20
C59N	North (T2)	220	2520	15
C16S	South (T2)	225	2760	20
C65N	North (T2)	300	2985	35

Table 2.1. Continued. List of radiocarbon samples collected at Old Town-San Diego, CA. Sample names with X in front were excluded from age model based on inheritance discussed in text.

Rose Canyon Fault-Old Town- Trench 1 (T1) & Trench 2 (T2)				
Sample #	Face (Trench)	Unit	14C age (Yrs BP)	±
X C22S	South (T2)	140	165	20
X C21N	North (T2)	145	3940	20
X C8N	North (T2)	150	2125	15
X C29N	North (T2)	160/200	2475	20
X C3S	South (T2)	200	3785	20
X C57N	North (T2)	200	2845	15
X C63S	South (T2)	300	4195	15

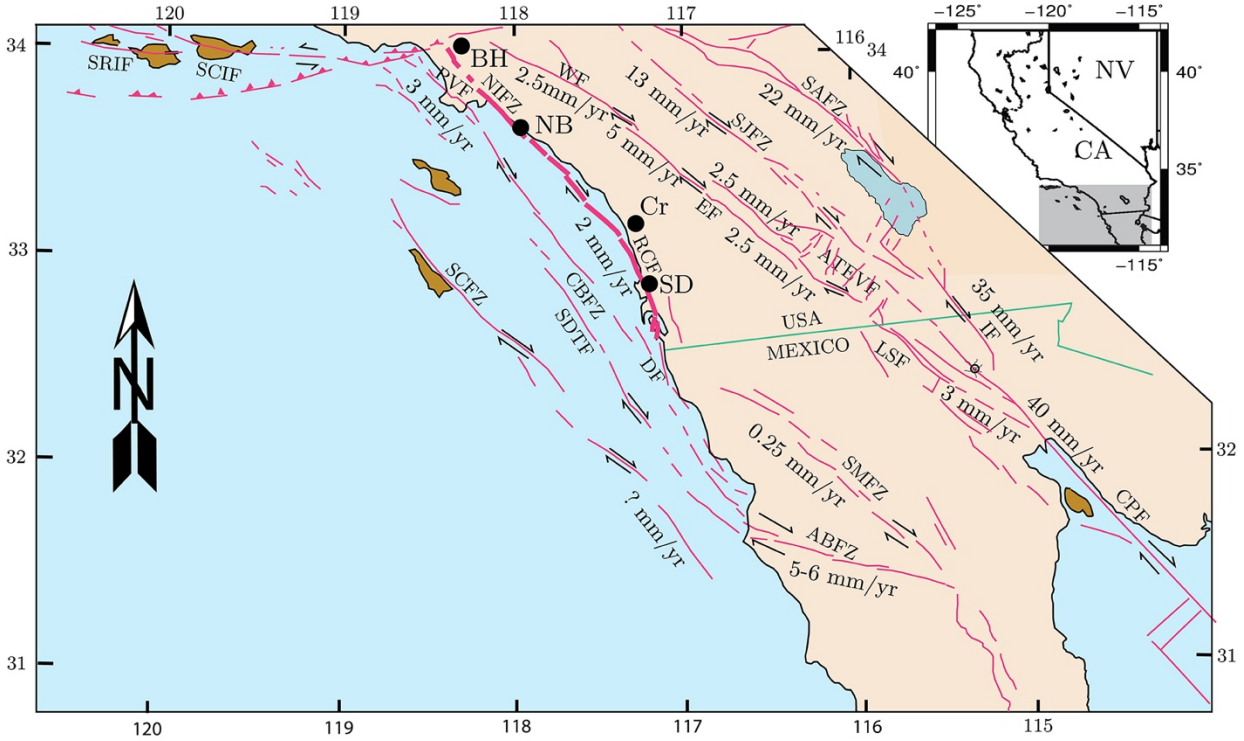

Figure 2.1. Active faults of southern California with their corresponding slip rates. Shaded box in inset shows location in California. The trace of the Newport-Inglewood-Rose Canyon fault system is bolded. Circles are location of urban centers mentioned in the text. SAFZ=San Andreas fault zone, IF=Imperial fault, SJFZ=San Jacinto fault zone, EF=Elsinore fault zone, CPF=Cerro Prieto fault, LSF=Laguna Salada fault zone, SMFZ=San Miguel fault zone, ABFZ=Agua Blanca fault zone, DF=Descanso Fault, RCF=Rose Canyon fault zone, NIFZ=Newport Inglewood fault zone, PVF=Palos Verde fault zone, CBFZ=Coronado Bank fault zone, SDTF=San Diego Trough fault, SCFZ=San Clemente fault zone, WF=Whittier fault zone, SCIF=Santa Cruz Island fault, SRIF=Santa Rosa Island fault. BH=Beverly Hills, NB=Newport Beach, Cr=Carlsbad, SD=San Diego.

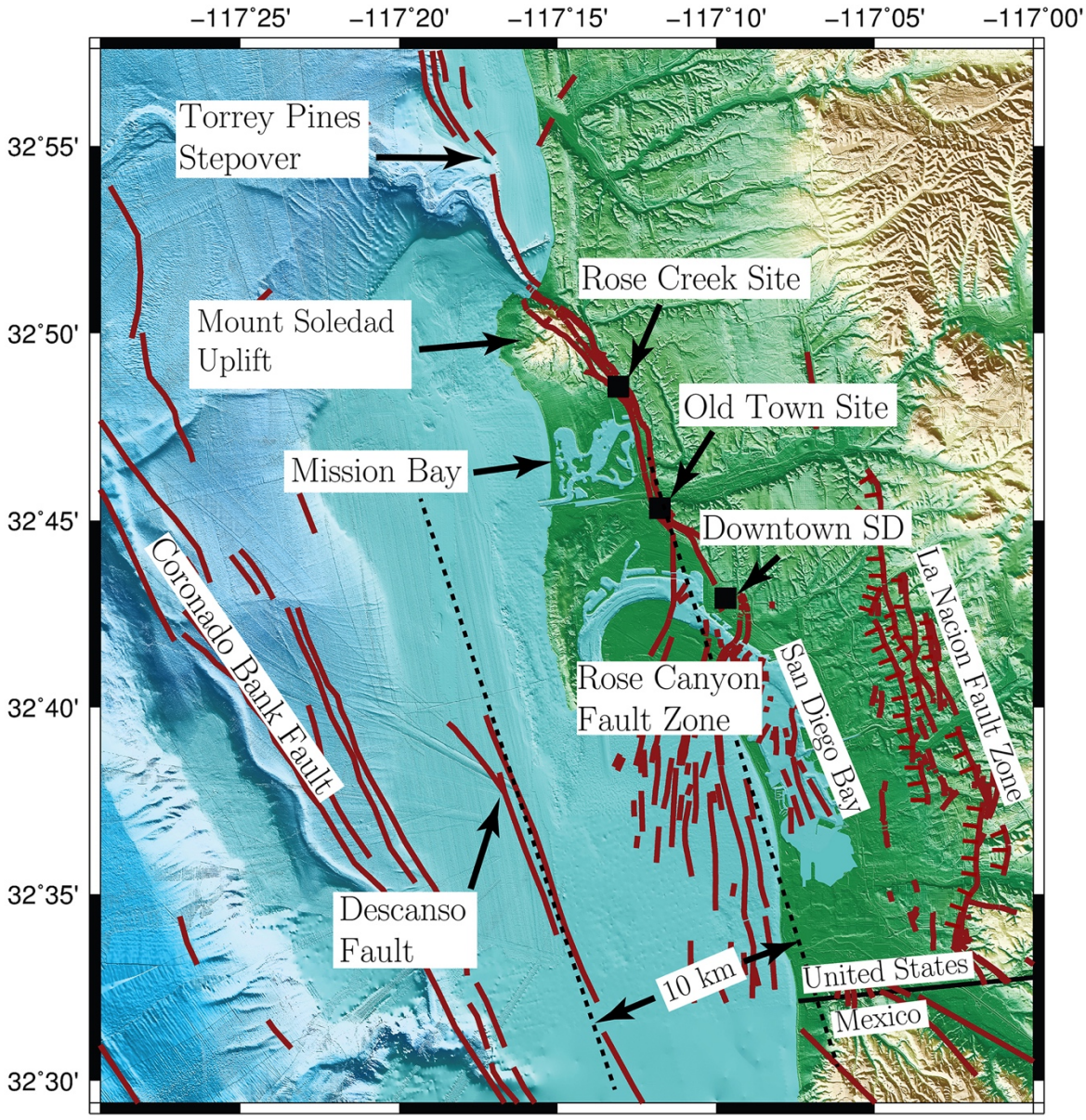

Figure 2.2. The Rose Canyon fault zone through San Diego with associated geomorphic expression. From the south, the Rose Canyon fault zone steps onshore, through San Diego Bay, likely as part of a 10 km stepover from the Descanso fault. Also shown is the La Nacion fault zone, which accommodates minor extension across San Diego Bay (Rockwell, 2010a). Locations of the Rose Creek and Old Town paleoseismic sites as well as downtown San Diego are shown as black squares.

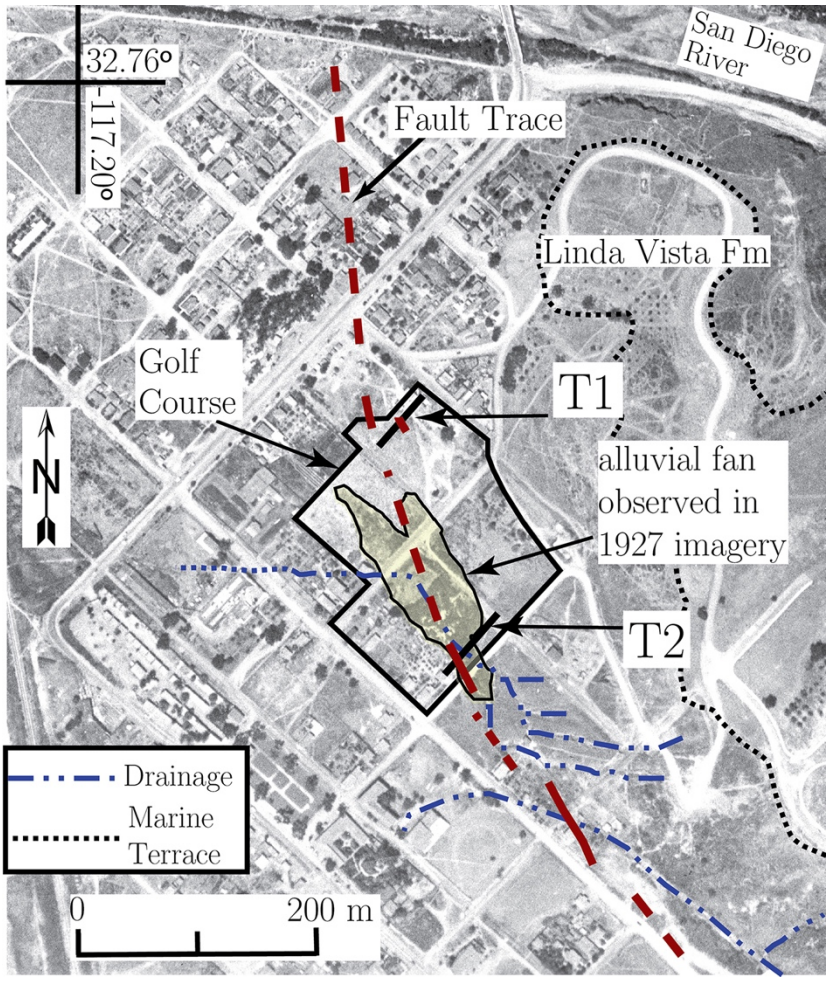

Figure 2.3. Aerial photograph from 1927 showing the trace of the Rose Canyon fault through the Old Town area. The location of the future Presidio Hills Golf Course is outlined in solid black along with the two trench locations (T1 and T2). The alluvial drainages and alluvial fan seen in the exposures of trench T2 and in the 1927 aerial photograph are also shown. Note the right-lateral deflection of the drainages indicating active motion of the Rose Canyon fault through Old Town. The outline (dotted area) of a marine terrace topped with Linda Vista Formation is also mapped (modified from Rockwell 2010a).

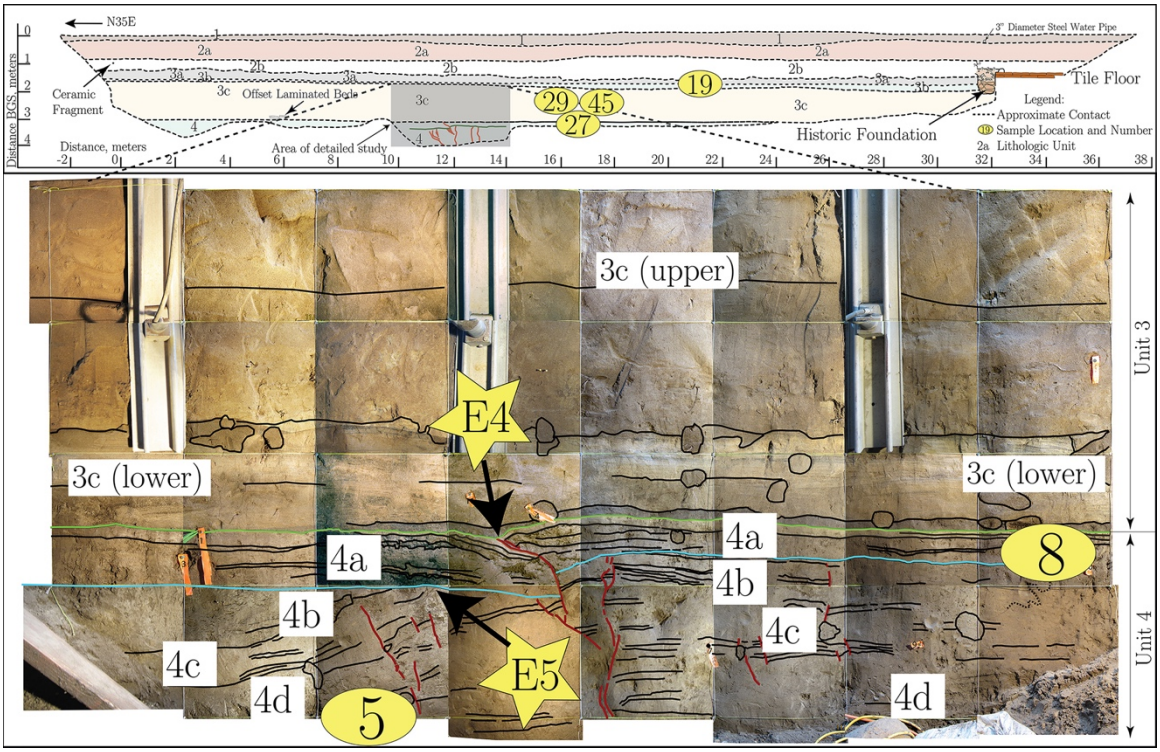

Figure 2.4. Log of the south face of trench T1 with a photomosaic of the hand excavated section showing faulted stratigraphy. Locations of interpreted event horizons are marked as stars. Locations where detrital charcoal was sampled for radiocarbon dating are marked as ovals. Stratigraphic units are marked with boxes. BGS=below ground surface.

Figure 2.5. 5a) A log of trench T2 south face across the fault zone. Locations of interpreted event horizons are marked as stars. Locations where detrital charcoal was sampled for radiocarbon dating are marked as ovals. Stratigraphic units are marked with white boxes. Shaded areas correspond to detailed close ups shown in Figures 7b and 7c. BGS=below ground surface; K=Krotovina; ff=Fissure-fill. Unannotated photomosaic of south face of T2 available in electronic supplement to this article, see Figure S1. 5b) Bottom figure shows log of full south face of T2. Shaded area is the location of Figure 5a.

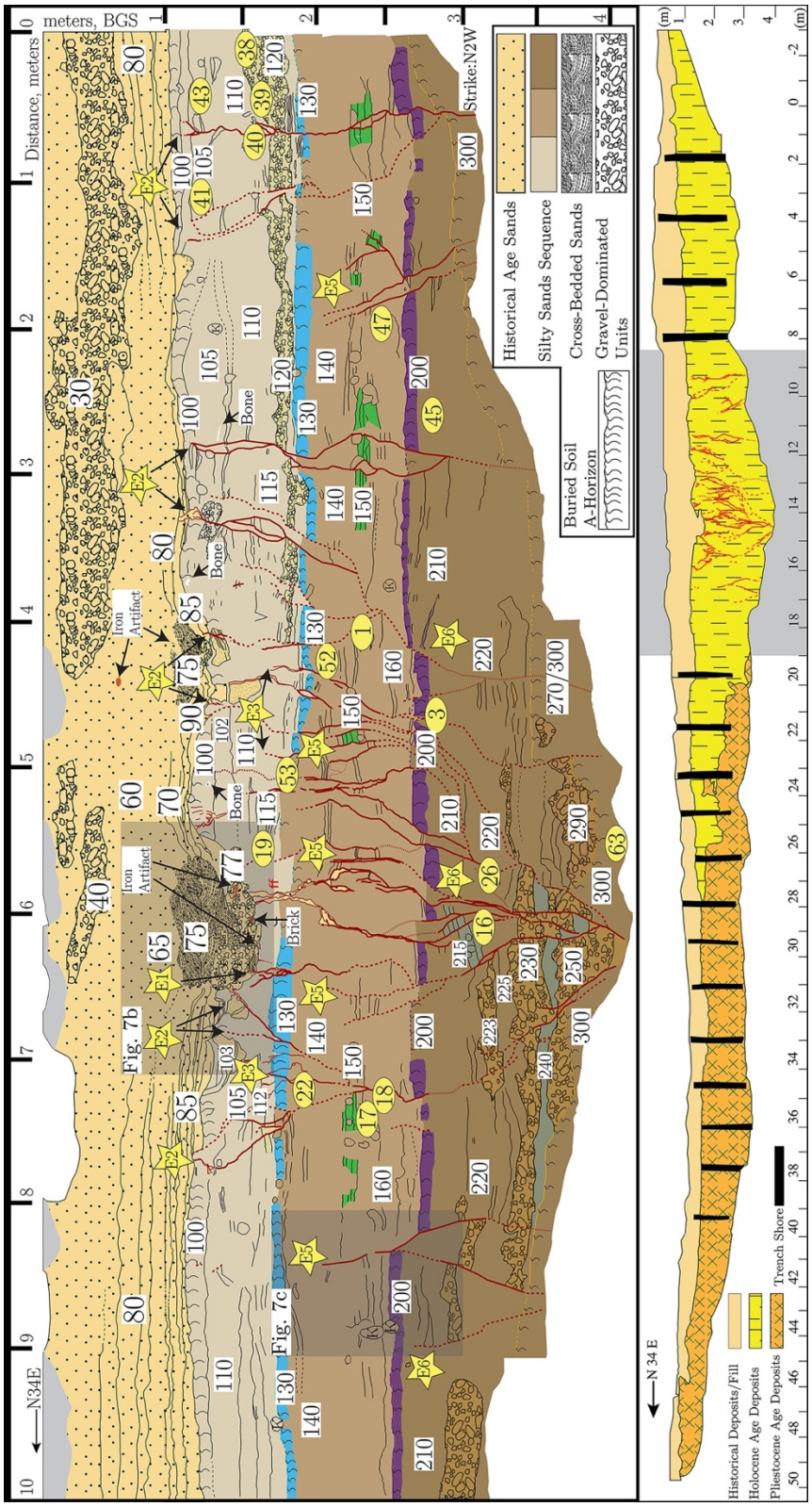
Distance, meters
meters, BGS
N34E
N 34 E
Strike:N2W
Fig. 7b
Fig. 7c
Iron Artifact
Brick
Bone
Historical Age Sands
Silty Sands Sequence
Cross-Bedded Sands
Gravel-Dominated Units
Buried Soil A-Horizon
Historical Deposits/Fill
Holocene Age Deposits
Pleistocene Age Deposits
Trench Shore

Figure 2.6. Log of main fault zone observed in trench T2 north face. Locations of interpreted event horizons are marked as stars. Locations where detrital charcoal was sampled for radiocarbon dating are marked as ovals. Stratigraphic units are marked with white boxes. Shaded area corresponds to detailed close up shown in Figure 7a. Symbols follow same legend as Figure 5a. BGS=below ground surface; K=Krotovina; ff=Fissure-fill. Unannotated photomosaic of the north face of T2 available in electronic supplement to this article, see Figure S2.

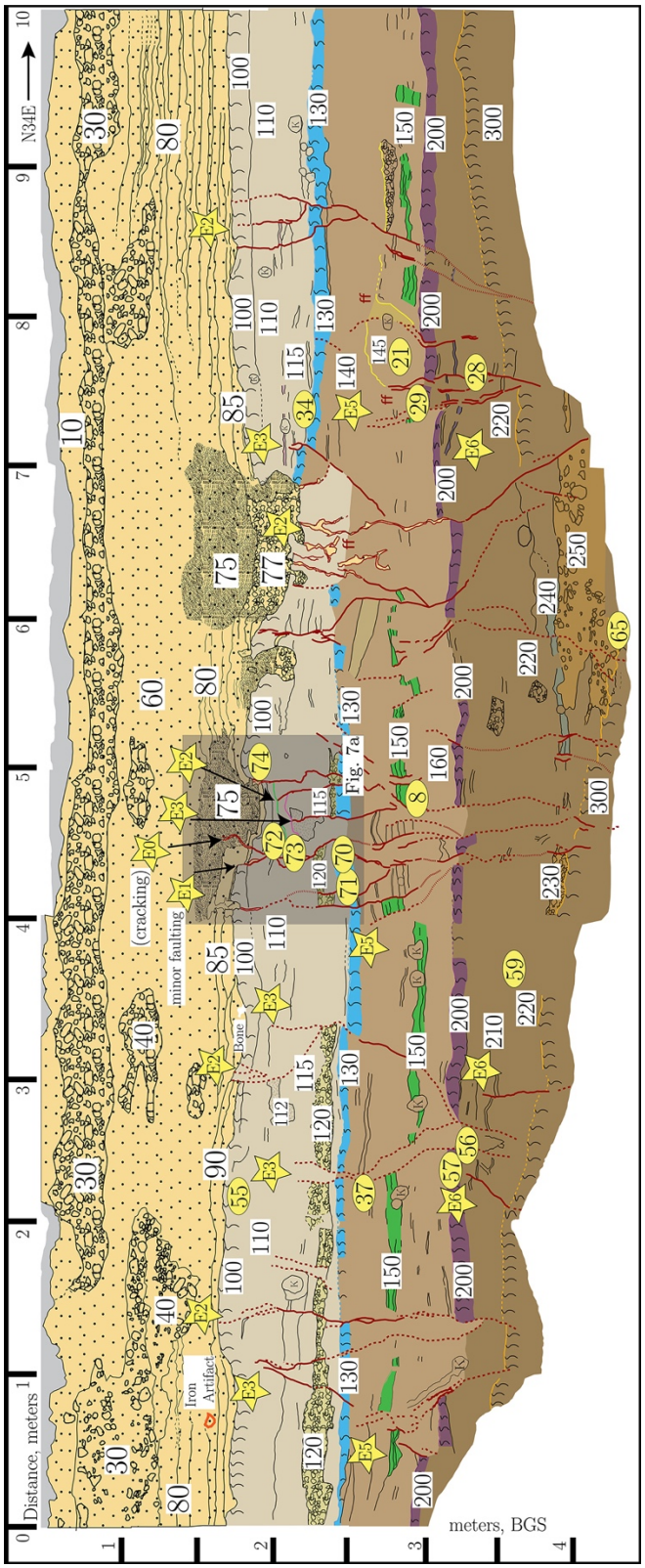
Distance, meters
N34E
meters, BGS
Iron Artifact
Bone
(cracking)
minor faulting
Fig. 7a

Figure 2.7. a) From the north face of trench T2 (location marked as shaded box in Figure 6), the figure shows the faulted soil A horizon (unit 100 and historical living surface at time of California's settlement by the Spanish), buried soil horizon (unit 105), and fluvial deposits (unit 112). The panel shows evidence for three separate surface rupturing events as well as minor cracking. Event E3 is seen as faulting to unit 112, event E2 is seen as faulting and fissure infilling of units 105 -100, event E1 is seen as displacement, ~3-5 cm, of historical age alluvial sands. Also shown is fissure infilling of young sediments possibly from triggered slip or creep event (E0). b) Evidence for events E1 and E2 on the south face of trench T2 (location marked as shaded box in Figure 5a). Event E2 is seen rupturing to unit 100 with tilting of unit 103, a channel pipe composed of medium- to coarse-grained sands. Event E1, interpreted to be the 1862 AD San Diego earthquake, is seen as infilling of fissure from historical era sands, which contain iron bar and brick. c) Evidence for events E5 and E6 from the south face of trench T2 (location marked as shaded box in Figure 5a). Evidence for event E6 is seen as upward terminating fault strands capped by unit 200. Evidence for event E5 is seen as vertical displacement (~20 cm) of unit 200 that is then capped by units 140-130.

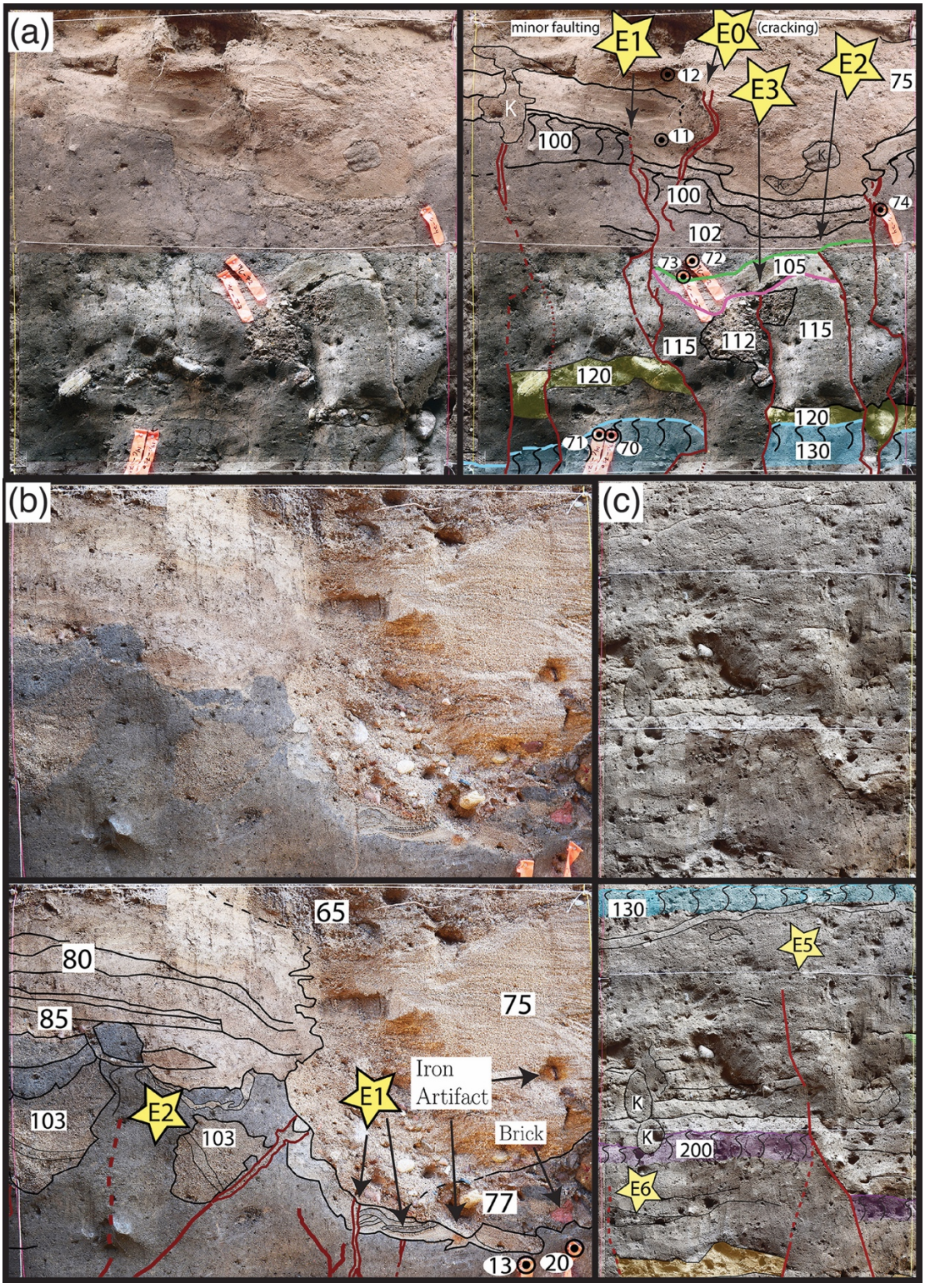
(a)
minor faulting
E1
E0
(cracking)
E2
E3
75
12
K
100
11
100
74
102
73
72
105
115
112
115
120
120
130
71
70
(b)
(c)
65
80
85
75
103
E2
103
E1
Iron
Artifact
Brick
77
13
20
130
E5
K
K
200
E6

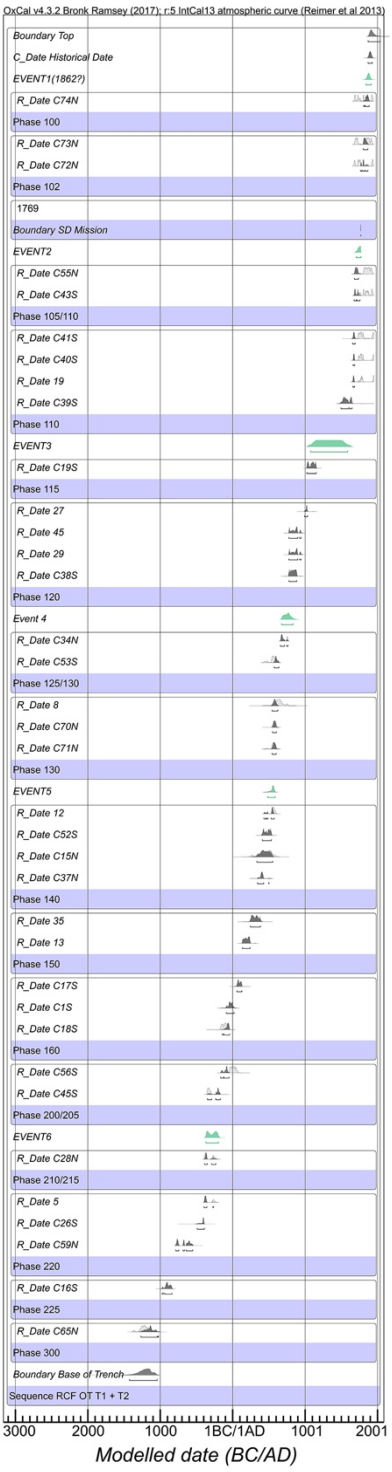

Figure 2.8. Age model for Old Town developed with dates listed in Table T1. Shown are the probability density functions (PDF) for each sample collected in Old Town. Also shown are the event PDF's determined by OxCal. Age model developed through OxCal v 4.3.2 (Bronk Ramsey 2009).

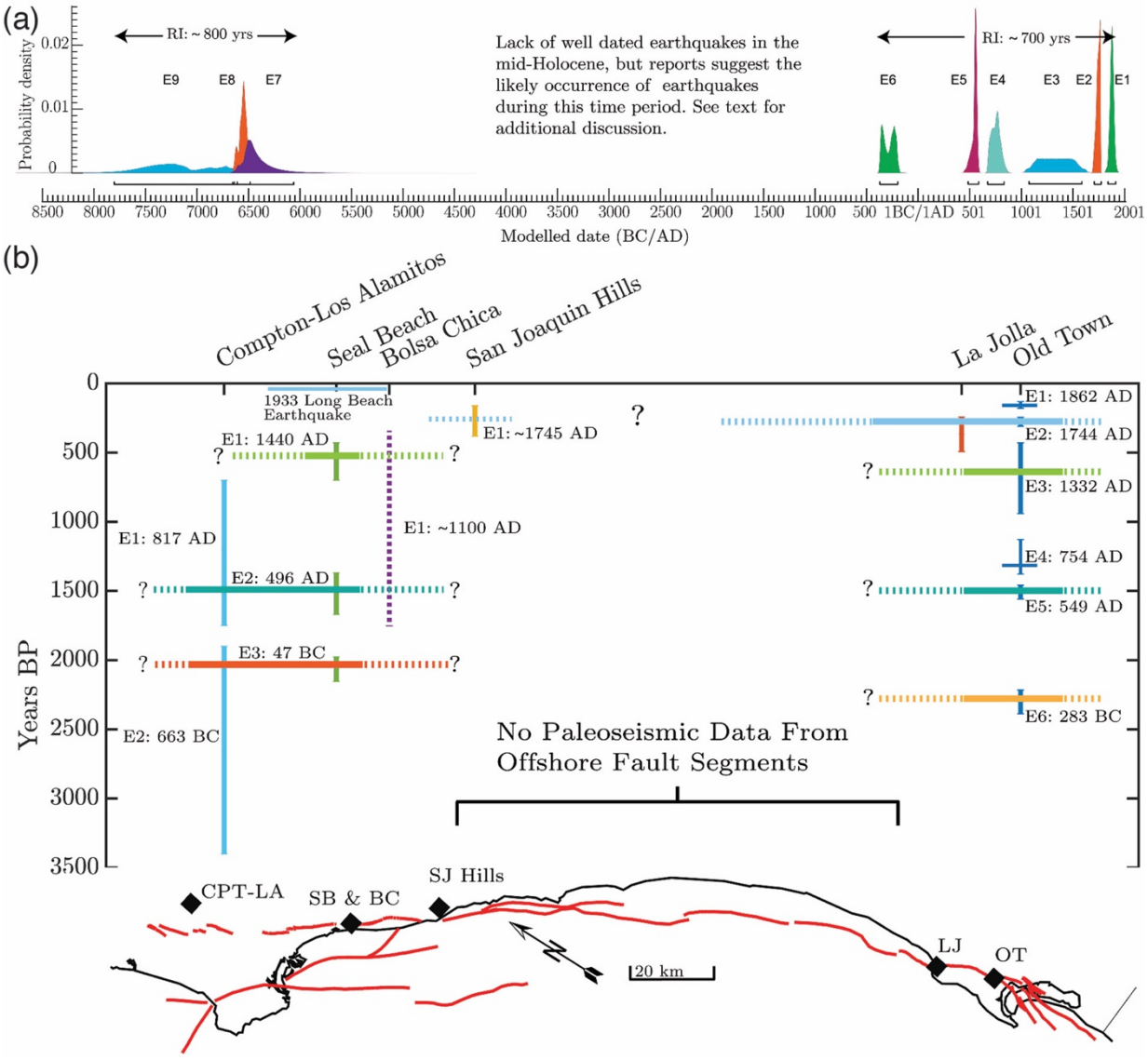

Figure 2.9. a) Probability density functions of event horizons determined via the OxCal age model for the Old Town and Rose Creek paleoseismic sites. b) Earthquake occurrence along the NIRC, which shows the reported occurrence of earthquakes at several paleoseismic sites along strike of the NIRC system. The map at the bottom shows the trace of the NIRC, as well as locations of paleoseismic sites (black squares). Vertical error bars are 95% confidence interval. Paleoseismic data from Grant et al., (1997), Grant et al. (2002), Leon et al., (2009), Leeper et al., (2017), Rockwell and Murbach (1996).

3. Slip rate for the Rose Canyon fault through San Diego, CA based on analysis of new GPS data: Evidence of a potential Rose Canyon – San Miguel-Vallecitos fault connection?

3.1 Abstract

The Rose Canyon fault is the southern extension of the larger Newport-Inglewood-Rose Canyon fault system, which represents a major structural boundary in the Inner Continental Borderland (ICB) offshore southern California. 10-15% of the total plate boundary motion is thought to be accommodated by the faults of the ICB, but the exact distribution of slip is uncertain. Slip is fed into the ICB by the transpeninsula faults that cut across Baja California, and a portion of this slip is potentially transferred into the Rose Canyon fault by the offshore Descanso fault or by the San Miguel-Vallecitos fault system. With an onshore segment, the Rose Canyon fault is unique among ICB faults, and offers an opportunity to constrain the slip rate using traditional geodetic methods. GPS surface velocities from a combined campaign and continuous GPS network are used to constrain elastic rheological models of the Rose Canyon fault. Reprocessed legacy multi-channel seismic data are then employed to investigate potential fault structures that might facilitate the transfer of slip into the Rose Canyon fault. Results of the elastic half space models suggest that the Rose Canyon Fault may be slipping towards the higher end of geologic estimates, with the preferred model indicating a slip rate of ~2.4 mm/yr and the optimally oriented transect for this model suggesting a higher rate of 2.9 mm/yr. Results from an asymmetrical elastic half space model indicate a rheological contrast across the Rose Canyon fault, similar to observations from the northern Newport-Inglewood fault segments. Observed GPS surface velocities south of San Diego Bay, point towards a more easterly trace of the Rose Canyon fault and suggest a possible connection with the San Miguel-Vallecitos fault system. Such a connection would have important consequences for regional seismic hazard.

3.2 Introduction

The Inner Continental Borderland (ICB) offshore southern California is a tectonically complex region composed of several active sub-parallel north-northwest trending faults that together makeup the offshore component of the Big Bend Domain (Figure 1) (Maloney et al., 2016, Wetmore et al., 2018). While faults east of the ICB (i.e., the Southern San Andreas system) accommodate the majority of the plate boundary budget, roughly 10-15% of total plate motion is thought to be accommodated by the faults of the ICB (Bennett et al., 1996; Platt and Becker, 2010). The total motion across the ICB is reasonably well-constrained, but the offshore location makes determining individual rates on ICB faults difficult, with only a handful of studies successfully resolving a geologic slip rate on a few fault strands (e.g., Ryan et al., 2009; Brothers et al., 2015; McNeilan et al., 1996; Lindvall and Rockwell, 1996). The faults that make up the ICB transfer slip around the Big Bend, feeding it northward into the faults of the Western Transverse Ranges (Platt and Becker, 2010; Humphreys and Weldon, 1991). In northern Baja California, faults of the Transpeninsula Fault system take up the excess deformation that bleeds off the transform-rift interactions in the Gulf of Mexico, and feed it into the offshore ICB (Dixon et al, 2002, Suraez-Vidal et al., 1991; Humphreys and Weldon, 1991). Among these faults are the San Miguel-Vallecitos and the Agua Blanca faults, which together transfer 6-8 mm/yr of slip into the ICB (Figure 1) (Bennett et al., 1996; Dixon et al., 2002).

The San Miguel-Vallecitos and Agua Blanca faults exhibit contrasting seismic characteristics and geomorphic expressions, which may be a consequence of the different roles these two faults play in distributing tectonic deformation across the peninsula. The Agua Blanca Fault cuts west-northwest across the Baja Peninsula and trends oblique to the plate

boundary vector by as much as 25 degrees (Dixon et al., 2002). Despite this misalignment, the Agua Blanca fault has as much as 15 km of total offset and is well expressed in the landscape (Allen et al., 1960; Gold et al., 2020 in review; Wetmore et al., 2018). The range of slip rate estimates on the Agua Blanca fault is broad, with geologic rates indicating anywhere from 2-10 mm/yr of motion across the fault (Hatch, 1987, Schug, 1987; Rockwell et al., 1993; Gold et al., 2020 in review); while rheological models constrained by GPS surface velocities indicate that the fault may be accommodating 2-6 mm/yr (Dixon et al., 2002). Historical seismicity on the Agua Blanca has been relatively sparse with no historical surface ruptures and very low levels of microseismicity (Rockwell et al., 1987, 1993; Vidal-Villegas et al., 2018).

Contrasting with the Agua Blanca fault is the San Miguel-Vallecitos fault, which trends north-northwest and is better aligned to the plate boundary vector (Dixon et al., 2002). However, this favorable orientation does not translate into obvious indicators of faulting. Instead, the San Miguel-Vallecitos fault exhibits a subtler geomorphic expression and a small ~600-1000 m total offset, which is suggestive of a young fault (Dixon et al., 2002; Hirabayashi et al., 1996; Wetmore et al., 2011). A single geologic slip rate estimate based on the soil chronology of an offset ridge suggests a 0.33-0.55 mm/yr late-Pleistocene rate for the San Miguel-Vallecitos Fault; interestingly, rheological models indicate a faster GPS rate of 2-4 mm/yr (Hirabayashi et al., 1996; Dixon et al., 2002). Despite the small total offset and potentially low slip rate, the San Miguel-Vallecitos fault has hosted seven M 6.0+ earthquakes in the past century, culminating in the Mw 6.8 San Miguel earthquake which produced over a meter of surface displacement, accompanied by a much higher rate of microseismicity, hinting at the potential of a more nuanced situation than a slow slip rate fault in Baja California (Reyes et al., 1975; Hirabayashi et al., 1996).

The role these two faults play in partitioning slip into the ICB is important because of their ability to feed slip into different fault systems. The Agua Blanca fault trends offshore south of Ensenada, Mexico where the fault diverges into several strands that likely interact with several faults systems in the ICB (Figure 1) (Legg, 1985; Legg et al., 1991). The north-northwest trend of the San Miguel-Vallecitos fault means that any motion occurring on this fault is most likely fed directly into the Rose Canyon fault, although the exact mechanics of this connection remain uncertain (Figure 1) (Hirabayashi et al., 1996; Treiman, 1993; Suarez-Vidal et al., 199l). Therefore, the amount of slip accommodated individually by these two transpeninsula faults could have a direct effect on the individual slip rates of faults in the ICB.

The Newport Inglewood-Rose Canyon fault marks the eastern boundary of the ICB and is a major structural element separating subduction related metamorphic complexes to the west, from the Peninsular Range provinces to the east (Figure 1) (Yeats, 1974; Wright, 1991; Boles et al., 2015). As the name suggests, the Rose Canyon fault is the southern segment of the larger Newport-Inglewood-Rose Canyon fault system, and directly underlies the city of San Diego, CA (Moore, 1972; Lindvall and Rockwell, 1995; Sahakian et al., 2017). The Rose Canyon fault is unique among faults of the ICB because of its significant onshore segment, offering an opportunity to use traditional terrestrial techniques to quantify the fault's slip rate. Unfortunately, this coastal onshore section coincides with a dense urban environment along the fault trace, obscuring or removing geomorphic features typically used as piercing points. Nevertheless, an early slip rate estimate for the Rose Canyon fault comes from 3-D trenching at Rose Creek, where an offset small gravel-filled channel was traced across the Mt. Soledad strand of the Rose Canyon fault to determine a minimum slip rate of 1.1 mm/yr (Lindvall and Rockwell, 1995). However, limited resolution of the underlying age model and the removal by

mechanical grading of the stratigraphic horizon containing the offset drainage on the western side of the fault, in combination with geomorphic evidence of other active fault strands at this latitude, argues for a higher slip rate (Lindvall and Rockwell, 1995). Using historical aerial photography, a later study determined a ~2 mm/yr slip rate for the Rose Canyon fault by mapping deflected drainages incised into a fluvial terrace overlying the last interglacial marine terrace; however, the timing of this incision and therefore the age of offset is uncertain (Rockwell, 2010).

The uncertainties associated with these slip rate estimates translate to an unknown upper bound for the amount of motion occurring on the Rose Canyon fault (Rockwell, 2010). Recently, new paleoseismic evidence on the Rose Canyon fault supports the occurrence of several surface rupturing earthquakes over the past ~3,300 years and a recurrence interval that is shorter than previous estimates by a few hundred years (Singleton et al., 2019). This shorter recurrence interval may be an indication that the Rose Canyon fault is accommodating slip towards the higher end of geologic estimates. If true, a faster slip rate for the Rose Canyon fault would have important implications for the seismic hazard of the highly urban environment (Field et al., 2014). Furthermore, a well constrained slip rate on the Rose Canyon fault would give a better idea of the slip available for other fault systems in the ICB, and therefore a better characterization of the seismic hazard of the region. Lastly, because of the possible connection between the Rose Canyon fault and the San Miguel-Vallecitos fault, by determining the amount of slip occurring on the Rose Canyon fault we may be able to better resolve the distribution of slip occurring across the Baja Peninsula. If the slip rate currently being accommodated by the Rose Canyon fault is significantly higher than geologic estimates, this could signal that the San Miguel-Vallecitos has experienced a shift in stress accumulation.

An alternative to traditional slip rate estimates from geologic features is the widespread use of space geodetic techniques for measuring surface deformation (e.g., Fialko, 2006; Segall, 2010; Materna and Burgmann, 2016). Daily position estimates from Global Positioning System (GPS) data have been used successfully to constrain deformation models of faults across all types of plate boundary environments. For fault studies in urban areas, using GPS data to determine a slip rate can be advantageous because the technique does not rely on the preservation of geologic piercing points, is sensitive to crustal deformation over short time scales, and requires a relatively small spatial footprint. For these reasons, slip rate models constrained by GPS surface velocities are a convenient alternative to labor intensive methods such as 3-D trenching. With a terrestrial area to the east and west, the Rose Canyon fault offers a unique opportunity to quantify the slip rate via terrestrial geodetic methods for a fault within the mostly submerged ICB.

South of Downtown San Diego, the Rose Canyon fault splays out into a complex network of faults to form a stepover with either an offshore branch of the Agua Blanca system or a connection with the San Miguel-Vallecitos fault (Legg et al., 1991; Treiman, 1993). This stepover is responsible for the subsidence of San Diego Bay, and allows for marine seismic reflection techniques to image fault structures more effectively than is possible onshore beneath the city of San Diego. The faults of San Diego Bay accommodate the transfer of motion from regional faults to the south into the Rose Canyon fault, but the exact mechanisms of this connection are not well known (Treiman, 1993). Legacy multi-channel seismic (MCS) data collected in San Diego Bay show numerous faults that may provide a fault structure to accommodate the transfer of slip from regional faults.

In this study, we combine ~20 years of campaign GPS data from a clustered-benchmark network that spans the Rose Canyon fault with data from continuous GPS stations, to determine the surface velocity across the San Diego region. This surface velocity is used to constrain elastic half-space models of deformation on the Rose Canyon fault in order to investigate the effect of varying slip rates and rheological contrasts on how well data fit a given model. We also examine legacy MCS seismic data reprocessed to improve resolution, to search for fault structures beneath San Diego Bay that may provide a mechanism for slip to be transferred into the Rose Canyon fault.

3.3 Methods

3.3.1 GPS data collection and processing

In 1998, a network of campaign GPS sites was constructed across the San Diego Region with the goal of determining a slip rate on the Rose Canyon fault (Figures 2 and 3) (Agnew, 2007). This network consists of four sites that span the fault trace, and at each site a cluster of benchmarks (2-4) was constructed ~100 m apart (Figure 3). We take advantage of the high accuracy of GPS signal over short baselines to check monument stability of the closely spaced benchmarks. Each benchmark is surveyed with a specially designed fixed-height antenna post, which kinematically mates with the benchmark and is vertically centered with ultra-high precision bubble levels that place the GPS antenna phase center over the benchmark with sub-millimeter repeatability (Agnew, 2007). The network was surveyed in three campaigns, during the initial construction from 1998-1999, a second phase from 2003-2006, and finally in 2016-2017. For each campaign, the benchmarks were surveyed with Ashtech Z-XII receivers and Ashtech choke ring antennas.

At three of the survey sites (COW1-4, SWT1-4, TJE1-3) the GPS equipment could not be left unattended overnight, so each benchmark was observed for a minimum of 6 hours for at least three days, typically consecutive days. Sites STG1-2 and WDW1-2 are located on secure Naval property and GPS equipment was left to record 24-hour sessions for several consecutive days. Beginning in the early 2000s, the number of continuous GPS stations in the San Diego area began to densify. Thus, many of the continuous stations used in this study overlap with at least two occupations of the campaign GPS sites. Continuous GPS data were downloaded from external processing centers at UNAVCO and NASA-JPL.

Daily position estimates from phase observations and time series of the GPS data were processed using the GAMIT/GLOBK software package, version 10.7 (Herrring et al., 2018). To improve the stability of the network, continuous GPS data were processed jointly with the campaign data. Initially 12-15 sites across North America were combined with the early campaign data, with Plate Boundary Observatory (PBO) sites in southern California added as they came online. GPS processing software, such as GAMIT/GLOBK will typically produce velocity uncertainties that are underestimated (<0.5 mm/yr) (e.g., Herring et al., 2018; Feigl et al., 1993; Langbein and Johnson, 1997). This can be corrected for by adding an appropriate amount of noise in the form of two end member models; a white noise (random) error model that accounts for uncertainty in daily position estimates, and a long term correlated random walk component that accounts for instability in station monumentation (Herring et al., 2018; Johnson and Agnew, 1995). The daily time series of GPS data were examined for outliers or noisy segments of data, and appropriate weights were added so that the normalized RMS scatter was stable at ~1; the amount of random walk noise was determined from the continuous GPS time series.

Velocities for all stations were calculated using the ITRF14 reference frame. A local reference frame was realized by referencing site velocities to one of three stations in the San Diego region. Reference stations were chosen for central locations and distance relative to regional faults. The impact of seasonal transient deformation in the campaign data should be minimal as many of the occupations occurred during the fall and winter of each surveying effort. However, during 2003-2006, and 2016 some of the campaign sites where occupied in the spring and summer, but the potential scatter introduced by the seasonality should have a minimal effect on the overall velocity, which is sensitive to scatter at the beginning and end of the timeseries (Dixon et al., 2002).

3.3.2 Deformation models

To model the velocity field across the San Diego region, we use two models of elastic deformation. For comparison with deformation models, the GPS surface velocities were projected onto the average strike of the Rose Canyon fault through San Diego (N27°W) (Fig. 2) and collapsed into a perpendicular transect. The main plate boundary faults in Southern California are located 100-150 km east of the Rose Canyon fault, in an area of high heat flow that results in moderately shallow locking depths (Lindsey and Fialko, 2013). The distance and heat flow translate into a minimal strain signal from those faults extending into the San Diego region (Lindsey and Fialko, 2013). Across the study area (~80 km), we calculate a gradient of less than 1.0 mm/yr as a result of these plate boundary faults, and within 30 km of the Rose Canyon Fault their effect is less than 0.5 mm/yr. Nevertheless, a few of the eastern-most stations used in this study are likely within the strain field from the Elsinore Fault, and so its impact on the model is assessed.

3.3.2.1 Deformation models - homogeneous elastic half-space

Although relatively simple, buried dislocation models in an elastic half space have been shown to be effective as first order models to describe the result of motion occurring at depth along a fault (e.g., Savage and Burford, 1973; Segall, 2010; Materna and Burgmann, 2016). We model the effect of fault motion on surface velocity as a simple elastic half-space dislocation with one or two parallel faults. For two infinitely long parallel faults, the fault perpendicular velocity (*V(x)*) can be approximated by:

$$V(x) = \frac{\dot{s_a}}{\pi} tan^{-1}\left(\frac{x}{D}\right) + \frac{\dot{s_b}}{\pi} tan^{-1}\left(\frac{x - S_b}{D}\right)$$

where the fault's slip rate ($\dot{s}$) controls the amplitude of the arctangent profile, while the curvature of the profile is inversely related to the locking depth (*D*). The horizontal distance perpendicular to the fault is given by *x,* with a single fault centered at *x=0.* The effect of the secondary fault is described with $x\text{-}S_b$, where S_b represents the perpendicular distance of the second fault relative to the first. Parameter subscripts *a* and *b* in the above equation are used to describe the effect of multiple parallel faults.

3.3.2.2 Deformation models – asymmetric elastic half-space

The asymmetric elastic half space model describes the effect of contrasting shear modulus on either side of a fault (Le Pichon et al., 2005; Segall, 2010). Similar to the homogeneous elastic half space model, the arctangent profile is described by the fault slip rate ($\dot{S}$) and locking depth (*D*) as well as an asymmetry parameter (*A*). *A*, describes the effect of contrasting shear modulus ($\mu_1$andμ_2) where $A = \frac{\mu_1}{\mu_2 + \mu_1}$. With *A=0.5,* the asymmetric elastic half space model is equivalent to the homogeneous elastic half space model. The asymmetry parameter results in deformation being concentrated on the side of fault with a higher shear modulus. The perpendicular velocity field is described by:

$$For\ x < 0\ :\ V(x) = \frac{2A\dot{s_a}}{\pi} tan^{-1}\left(\frac{x}{D}\right)$$
$$For\ x \geq 0\ :\ V(x) = \frac{2(1-A)\dot{s_a}}{\pi} tan^{-1}\left(\frac{x}{D}\right)$$

Following the methods of Dixon et al. (2002), we evaluate the fit of the elastic half-space models to the GPS data with the X^2 statistical test: $X^2 = \Sigma(O-E)^2/\sigma^2$ where O is the observed data, E is the expected value (taken from the elastic half-space model evaluated at the benchmark distances), σ is the error in the observations, and the sum is evaluated over the entire dataset. The minimum X^2 value is taken to indicate the best fitting model to the data. When the errors are appropriately estimated the $\widetilde{X^2}$ value, defined as X^2/d, where d is the number of degrees of freedom, will be close to 1 for well-fit models. A value of $\widetilde{X^2}$ <1 indicates that the errors are overestimated, while $\widetilde{X^2}$ >1 indicates a poorly fitting model or errors that are underestimated. Our dataset consists of a relatively small number of data points (N=23) so these rules will act as guidelines.

3.3.3 Reprocessing legacy MCS data

The MCS data used in this study are part of a seismic hazard assessment of the Coronado bridge in the mid-1990s (Kennedy and Clarke, 1996). The original survey collected 130 km lines of MCS data, originally stored on magnetic tape files (Kennedy and Clark, 1996; 1999). These lines were transferred to modern digital format and reprocessed through the Shearwater Reveal software package (Reveal, 2019). To increase the resolution of the data, we applied a processing scheme that included a linear moveout and f-k filtering, water bottom mute, common midpoint stacking and normal move-out correction with velocity semblance,

brute stacking, and time migration. Unfortunately, the original navigation files for the MCS lines were destroyed in a warehouse fire, so the locations were digitized from the paper figures included in the original report. To do this we georeferenced the figures and then digitized the individual MCS lines. The total length of the digitized line was divided into equally spaced 'shots' at 3.125 m spacing, which is the shot spacing of the original acquisition (Kennedy and Clarke, 1996). Due to uncertainties in the digitization of the original figure, the final locations likely carry a location error of ~20-100 m.

3.4 Results

3.4.1 Stability of campaign survey sites and GPS data quality

Results of the short intra-cluster baselines processed with the L1- and L2-independent carrier phase of the GPS signal, show that the campaign network has maintained sub-millimeter stability over the 20-year period of the survey (Figure 4). The weighted RMS scatter in the north, east, and up components of the intra-cluster baselines are below ~1 mm (Table 1). This level of stability indicates that the campaign stations should be reliable GPS benchmarks to estimate surface velocity. The quality of the data also demonstrates that fixed-height monumentation with ultra-high precision bubble levels, can be set up with high-accuracy by independent investigators with large gaps in time between surveys (years to decades).

The combined campaign and continuous GPS data define a velocity gradient perpendicular to plate motion of about 3.5 mm/yr across the San Diego region. In a local reference frame, the relative velocity data give a gradient of ~3 mm/yr near the Rose Canyon fault. In a reference frame relative to a site east-northeast of the Rose Canyon Fault, GPS benchmarks on the western side of the fault move north-northwest, consistent with right lateral

motion. Components of horizontal velocities for sites used in this study relative to ITRF14 are listed in Table 2.

3.4.2 Single and double fault homogeneous elastic half-space model

When the relative position estimates across the San Diego region were compared to a single fault model in homogeneous elastic half-space, the resultant $\widetilde{X^2}$< 1 (Table 3). Following the methodology of Dixon et al. (2002), we interpret a $\widetilde{X^2}$ < 1 to indicate errors that are overestimated. In order to compare results between different reference stations, the errors for the relative position data were adjusted so that the $\widetilde{X^2}$ ~1, resulting in a factor ~1.5 reduction in the GPS rate error. The fault parallel velocities and adjusted errors across the Rose Canyon fault relative to three reference stations are shown in Figure 5. Figure 5 also shows theoretical velocity profiles for a single fault in a homogenous elastic half space that describes the motion on the Rose Canyon fault for several potential slip rates. The transect with DESC as the reference station is the most centralized of three reference stations, so that the orthogonal projections of other GPS sites are minimized (average projection ~14 km) (Figure 2). The average orthogonal projections for the SIO5 and POTR transects are 21 km and 32 km. We therefore take DESC to be our preferred transect.

For the single fault model, the RMS misfit of nonreference stations for the optimally oriented DESC transect is 0.61 mm (by definition the reference station has a zero misfit). The RMS misfit for the SIO5 and POTR transect are 0.78 mm and 0.80 mm, respectively. The relatively small size of the data misfit (< 1 mm/yr) suggests that the velocity data fit the single fault homogeneous elastic half space model well. Table 3 contains the X^2 values of the fault models for the three transects. Included in Figure 5 are the X^2 values as a function of slip rate using the normalized errors described above. The weighted mean of the slip rate estimates and

their RMS scatter about the mean is 2.8 ± 0.5 mm/yr and is taken as the best slip rate estimate for the Rose Canyon fault in a single fault homogeneous elastic half-space model. However, for the optimally oriented DESC transect the data suggest a higher slip rate of 3.4 mm/yr (Table 3; Fig. 4b).

We also explored the effect of varying the locking depth with slip rate on the X^2 values. Unfortunately, with a lack of GPS sites within 10 km on the east side of the Rose Canyon fault, our data are relatively insensitive to changes in locking depth, with the data fitting a large range of locking depths (~1-25 km). Nevertheless, the DESC transect was best fit with a slip rate of 3.6 mm/yr and a locking depth of ~16 km ($X^2 = 3.899$). This locking depth is similar to the depth of seismicity (15 km) found by Magistrale (1993) for an earthquake swarm beneath San Diego Bay. Given this similarity, a locking depth of 15 km is chosen as representative for the remaining models.

For the two-fault model, the model parameters for the Elsinore fault were fixed based on independent data. For the southern section of the Elsinore fault, slip rate estimates range from 1.5-2.4 mm/yr based on geologic and geodetic evidence from which we selected a rate of 2.0 mm/yr; meanwhile microseismicity studies suggest a locking depth of 12 km (Bird, 2009; Fletcher et al., 2011; Rockwell, et al., 2019; Magistrale, 2002). Table 3 shows the best fit slip rate and associated X^2 values for the double fault model. X^2 misfits for the best fit model were calculated with the same error reduction criteria as the single fault model. With the addition of the Elsinore Fault there is a small worsening of the model fit, with X^2 values increasing slightly.

The RMS misfit of nonreference stations for the optimally oriented DESC transect is 0.63 mm, for the SIO5 and POTR transect the RMS misfit are 0.74 mm and 0.71 mm,

respectively. The weighted mean of the slip rate estimates and their RMS scatter about the mean is 2.4 ± 0.5 mm/yr and is taken as the best slip rate estimate for the Rose Canyon fault in a double fault homogeneous elastic half-space model. However, similar to the single fault model, the optimally oriented DESC transect suggests a higher slip rate of 2.9 mm/yr (Table 3, Fig. 5e). Figure 5d-f shows the results of the double fault elastic half space models, with inset that show X^2 values vs slip rate.

These results show that despite the distance of most GPS sites relative to the Elsinore fault (>50 km), there is still a small but noticeable effect of the fault's strain field on GPS surface velocities. With reference stations that are within 30-35 km of the Elsinore Fault (DESC and POTR), the effect of the Elsinore Fault is to overestimate the slip rate on the Rose Canyon Fault by ~0.4 mm/yr. Given the influence of the Elsinore Fault's strain field on the reference stations, the slip rate estimates from the double fault model are likely more realistic than the single fault models. However, because our data set is relatively sparse and has a variable spatial distribution, it may not capture completely the subtle characteristics of a more complicated double fault model.

3.4.3 Asymmetric elastic half-space model

For the asymmetric elastic half space model, the X^2 misfit supports a contrasting rheology across the fault zone, but with a higher slip rate than the homogenous elastic half-space model (Table 3). For the preferred DESC transect, Figure 6 shows the results of this model and Figure 7 shows contours of the X^2 misfit and the best fit model calculated using the same error reduction criteria described above. For the three transects, the RMS values for the model parameters are 4.5 mm/yr for slip rate ($\dot{S}$) and 0.244 for the asymmetry parameter (A), locking depth for asymmetry model was set at 15 km. The relatively high 4.5 mm/yr slip rate is

likely due in part to the SIO5 transect that also has a correspondingly large X^2 value. Additionally, the higher estimate for slip rate may be a result of the model attempting to fit the higher rates on the western side of the fault. The asymmetry model results show a better overall fit (lower X^2 value) to the data than the homogenous elastic half space models (Table 3). Using the RMS value for A of 0.244 this corresponds to a shear modulus ratio of μ_1/μ_2 = ~3.

Similar to the depth parameter determined with the single fault homogeneous elastic half space, our data misfits are relatively insensitive to changes in the model near the fault. The lack of sensitivity of our dataset to the asymmetry parameter *A* seen in Figures 6 and 7 is most likely a reflection of this lack of data close to the fault trace on the eastern side (within 10 km), as well as only two locations on the west side at ~2 km and ~7-8 km. It is this region that is most affected by changes to the asymmetry parameter and so our results here should be viewed as only rough estimates.

3.4.4. Legacy MCS profiles

The reprocessing of legacy MCS data with improved computational techniques dramatically increased the resolution at depth allowing for better characterization of fault geometry and stratigraphy. The reprocessed MCS data resulted in good-quality, usable data down to ~450 ms, and imaged many of the fault segments previously mapped in San Diego Bay. In the southern portion of San Diego Bay, a large fault is well expressed in MCS line T196-a792 that separates relatively flat-lying to gently east-dipping stratigraphy in the west, from steeply west-dipping stratigraphy in the east (Figure 8). The fault exhibits a down-to-the-east sense of displacement and develops into a negative flower structure towards the surface. The MCS data show progressively increasing offsets and stratigraphic dips with depth

associated with this fault in south San Diego Bay. Thus, this fault appears to exert a control on deposition and subsidence in the southern portion of San Diego Bay.

Using the reprocessed MCS data, we extend the mapped trace of this large fault in south San Diego Bay to connect with two previously mapped fault segments from the USGS/CGS fault database (Figure 8) (USGS, 2019). Similar to many of the smaller fault segments in the southern portion of San Diego Bay, the orientation of this fault is to the northwest, similar to that of the Rose Canyon and San Miguel Vallecitos faults. This fault appears to be a major structural element in the southern portion of San Diego Bay. Moving northward to the south-central portion of San Diego the MCS line T196-088 shows several distributed sub-parallel faults that are eastward dipping and show down-to-the-east sense of displacement (Figure 8).

3.5 Discussion

3.5.1. Slip rate on the Rose Canyon Fault

The results of the elastic half space models indicate that the slip rate on the Rose Canyon Fault may be toward the higher end of geologic estimates. The maximum slip rate estimate from the deflected drainages at Old Town is equal to the weighted mean slip rate from the double fault models of 2.4 mm/yr. While this value is within the uncertainties of geologic estimates, the preferred DESC transect suggests a higher rate (Table 3). If the poorly situated POTR transect is excluded, the weighted mean and RMS scatter about the mean for a Rose Canyon fault slip rate is 2.8 +/- 0.4 mm/yr. Considering the large orthogonal projections of GPS sites when using the POTR transect (13 sites greater than 30 km and a maximum projection of ~70 km), it may be reasonable to exclude the model results from this transect. Considering the effect of the Elsinore Fault on the eastern stations, the results of the double

fault homogeneous elastic half space models are likely more representative of the actual strain field in San Diego. Although simple, elastic half space models are likely sufficient representatives for the Rose Canyon Fault given that paleoseismic evidence from Old Town indicates that the Rose Canyon Fault is likely towards the middle of its seismic cycle. Therefore, the modeled effect of a viscoelastic response of the lower crust and upper mantle would produce a surface velocity profile that would closely mimic an elastic rheology (Dixon et al., 2002; Singleton et al., 2019).

Large geodetic studies across the entire plate boundary in southern California and northern Baja California, Mexico indicate that the ICB accommodates 6-8 mm/yr of plate motion (Bennett et al., 1996; Platt and Becker, 2010). With a limited number of studies able to estimate slip rates on the offshore faults of the ICB there are still large uncertainties regarding the exact distribution of slip on individual faults. Nevertheless, using high-resolution geophysical data in combination with ROV coring, offset submarine channel features have provided constraints on the slip rate of both the offshore Palos Verdes fault and San Diego Trough fault, ~1.7 mm/yr and ~1.5 mm/yr, respectively (Brothers et al., 2015; Ryan et al., 2012). With a slip rate of 2.4 mm/yr for the Rose Canyon fault suggested by the double fault models, there is a potential total of 5.6 mm/yr of slip being accommodated by the Palos Verdes, San Diego Trough, and Rose Canyon faults. While there is evidence for variable slip along strike of these faults, and the other slip rates estimates are from ~100 km north of San Diego, it appears there remains 0.4-2.2 mm/yr of slip unaccounted for that is potentially being accommodated by fault systems such as the San Clemente fault (McNeilan et al., 1996, Brothers et al., 2015; Fischer and Mills, 1992; Lindvall and Rockwell, 1995).

3.5.2. A Rose Canyon – San Miguel-Vallecitos fault connection?

From La Jolla where the Rose Canyon fault comes onshore, to just north of downtown San Diego the Rose Canyon fault has a well-defined relatively narrow surface trace. South of downtown, the Rose Canyon fault splays out into a complex fault network forming a stepover to either the offshore Descanso fault or connecting to the San Miguel-Vallecitos fault (Figure 2) (e.g., Treiman, 1993; Rockwell, 2010; Suarez-Vidal et al., 1993; Marshall, 1989). North-trending faults beneath the northern portion of San Diego Bay are well-imaged in high-resolution seismic data (Figure 2). Sections of these faults exhibit recent Holocene displacements and are potential linking faults to support a connection to the offshore Descanso Fault (Maloney, 2013; Marquez, 2017; Rockwell, 2010; Legg, 1991). To the east of these potential linking faults, northwest trending faults and seismic lineations in south San Diego and Tijuana, as well as gravity and crystalline basement profiles, are cited as evidence for an elongated basin between the Rose Canyon and San Miguel-Vallecitos faults that is centered beneath south San Diego Bay (Treiman, 1993; Marshall, 1989; Heaton and Jones, 1989).

Figure 9 shows the GPS surface velocities relative to site SIO5, which is located on the trace of the Rose Canyon fault. Sites east of the fault trace are seen moving south-southeast while sites to the west are seen to move north-northwest, consistent with right lateral motion across the Rose Canyon fault. Site TJE, composed of the intra-cluster benchmarks TJE1-3, is seen to move north-northeast in a similar direction and with a similar magnitude to sites located on the Point Loma peninsula (Figure 4 and 9). This similarity in surface velocity is a potential indication that site TJE lies within the same micro-crustal block as sites on Point Loma and argues for a more easterly trace of the Rose Canyon Fault (Figure 9). This proposed micro-block would be bounded on the east by a potential Rose Canyon–San Miguel-Vallecitos fault connection and to the west by offshore faults such as the Descanso or Coronado Bank faults.

However, site TJE is located in an area where hillslope instability is common, so the possibility exists that shallow subsurface movement could be influencing the station velocity, but given the stability of the intra-cluster baselines at site TJE over the 20-year study period this is likely not a significant issue (Table 1).

The northwest trending faults imaged by the reprocessed MCS data beneath the southern portion of San Diego Bay could be the result of a potential fault structure that connects the Rose Canyon fault with San Miguel-Vallecitos fault. The progressively increasing dips with depth show that this fault has controlled deposition in the southern portion of the bay with an east-side down sense of displacement, down-dropping sediment away from the linking faults imaged in the northern portion of the bay (Figure 8). This sense of displacement away from potential linking faults and the central part of the stepover is in contrast with modelling results of pull-apart basins (van Wijk et al., 2016). Faulting in south San Diego Bay occurs very close to the seafloor and samples from boreholes in the central portion of the Bay suggest that this deformation has likely been occurring since at least mid-Pleistocene and potentially into the Holocene (Kennedy and Clarke, 1999).

The northwest orientations of faults in south San Diego Bay are similar to the long axis of a gravity low beneath San Diego Bay (Marshall, 1989). It has been suggested that the orientation of the gravity and crystalline basement is evidence for a northwest oriented basin beneath San Diego Bay that extends into Tijuana, Mexico (Marshall, 1989; Elliot, 1970). Marshall (1989) further proposed that the gravity low beneath south San Diego Bay is the result of a rhombochasm-like nested graben that accommodates transtension from a stepover between the Rose Canyon and San Miguel-Vallecitos faults. If the style of deformation seen in Figure 8 continues into the southernmost portion of the bay and beneath the Tijuana estuary, it is well

oriented to connect with the Tijuana seismicity lineament of Heaton and Jones (1989), and provide a fault network that may be part of the rhombochasm nested graben model, potentially transferring slip between the San Miguel-Vallecitos and the Rose Canyon faults (Marshall, 1989; Kennedy et al., 1975).

If such a fault network extends beneath the Tijuana River estuary and the city of Tijuana, Mexico it may be in the early stages of development as no obvious indicators of faulting have been observed at the surface (Treiman, 1993). The major fault segments of the San Miguel-Vallecitos fault and to a smaller degree the faults of San Diego Bay, are oriented in an en echelon pattern separated by stepovers, typical of strike slip faults and pull apart basins early in their development (Figure 1 and 2) (van Wijk et al., 2016; Wesnousky, 1988). Additionally, the orientation of the San Miguel-Vallecitos fault is favorable for a connection with the Rose Canyon fault (Figure 1). Therefore, at least some amount of slip occurring on the Rose Canyon fault is likely transferred from the San Miguel-Vallecitos fault zone. From the results of the elastic half space models, the apparent slip rate on the Rose Canyon fault is towards the higher end of geologic estimates, and could be an indication that the San Miguel-Vallecitos fault is accommodating a higher slip rate than geologic estimates. With an orientation that is better aligned with the overall plate boundary vector, finite element modeling suggests that for similar frictional and rheological properties, the San Miguel-Vallecitos fault should be favored over the Agua Blanca fault to carry more of the plate motion across the Baja California Peninsula (Dixon et al., 2002). In combination with these model results, the higher rate of microseismicity and paleoseismic evidence that suggests at least two surface rupturing earthquakes in the past 600 years, in addition to the higher rate on the Rose Canyon fault, could

be arguments for a faster late-Holocene rate on the San Miguel-Vallecitos fault zone (Hirabayashi et al., 1996).

3.5.3. Rheological contrasts across the southern Newport-Inglewood-Rose Canyon fault

The Newport-Inglewood-Rose Canyon fault system has long been recognized as a major structural boundary separating thinner metamorphosed oceanic lithosphere from a thicker continental rheology (Hill, 1971; ten Brink et al., 2000; Nazareth and Clayton, 2003; Lekic et al., 2011). Analysis of gas concentrations from oil wells in the Los Angeles basin confirm that the Newport-Inglewood fault is a deeply-seated fault with a direct connection to mantle sources of Helium that are not observed along other faults in the Los Angeles Basin or ICB (Boles et al., 2015). South of the Los Angeles Basin, MCS reflection data suggest the boundary between the metamorphic oceanic lithosphere and Peninsular province also lies below the trace of the Newport-Inglewood-Rose Canyon fault (Bohannon and Geist, 1998).

The results from the asymmetric half space models indicate that the boundary between compliant Peninsula Range batholith and metamorphosed oceanic lithosphere may exist as far south as San Diego Bay. Using the mean value for the asymmetry parameter (*A=0.244)* and a reasonable value for the shear modulus of granite ($\mu_1 = 24\ GPa$) for the Peninsular ranges, a shear modulus for the ICB province of ~8 GPa is indicated. With the addition of an asymmetric elastic rheology across the Rose Canyon fault a higher slip rate is able to fit the data (Table 3). The 5 mm/yr of slip indicated when using the POTR transect is almost certainly an overestimation that results from the transect's poor orientation as discussed above. Excluding the results of the POTR transect, the mean slip rate estimate is 4.2 mm/yr, which would indicate that the Rose Canyon fault is accommodating a large majority of the ICB slip budget. However, given the spatial limitations of our dataset close to the fault these results are also

likely an overestimation. Nevertheless, the improved fit in the data suggested by the smaller χ^2 values may indicate that a similar rheological contrast that is present along the northern segments of the Newport-Inglewood fault segment, also exists across the southern Rose Canyon segment. This contrast would argue for a higher slip rate than indicated with the homogenous double fault model.

3.5.4. Seismic hazard for San Diego-Tijuana region

The higher slip rate on the Rose Canyon fault indicated by the results of the elastic half space models has important implications for the seismic hazard of coastal San Diego and Tijuana, Mexico. A fault's slip rate has a direct effect on the frequency of expected earthquakes and so is considered a key parameter in the construction of seismic hazard models (Field et al., 2014). If the results of our study are representative of the actual slip rate being accommodated by the Rose Canyon fault, it could indicate that the fault may host more frequent earthquakes than suggested by previous slip rate estimates (Field et al., 2014). Indeed, recent paleoseismic evidence suggests that the recurrence interval for the Rose Canyon fault is shorter than previous estimates by ~300-600 years (Lindvall and Rockwell, 1995; Singleton et al., 2019).

The potential connection of the Rose Canyon Fault to the San Miguel-Vallecitos fault would have important consequences for the seismic hazard of Tijuana, Mexico. Not only could the city be underlain by a potentially active fault system, but the expected magnitude of future earthquakes could be higher. A stepover from the Rose Canyon fault to the offshore Descanso fault is ~10 km so that a through-going rupture is not predicted (Wesnousky, 2006). However, a potential stepover from the Rose Canyon fault to the San Miguel-Vallecitos fault through San Diego Bay is on the order of ~4 km, so that a through-going rupture is possible (Wesnousky, 2006). If an earthquake rupture initiated on the offshore Torrey Pines segment of Sahakian et

al., (2017), and ruptured south through the San Diego Bay pull-apart connection with the San Miguel-Vallecitos, continuing until the large bend south of Tijuana, Mexico mapped in Fletcher et al. (2014) (located just south of Rodriguez Dam), the total rupture length would be ~77 km. Earthquake scaling relationships suggest the magnitude of such an earthquake could be as high as M_w 7.3, which would cause a large amount of destruction in the region (Leonard, 2010). However, several studies have found conflicting evidence regarding the nature of faulting in the Tijuana River valley, so such a fault structure beneath Tijuana, Mexico remains speculative (Treiman, 1993; Gastil et al., 1979; Espinoza-Cardena, 1983).

3.6 Conclusions

The aim of this study was to utilize the Rose Canyon fault's onshore segment to determine a slip rate using traditional terrestrial geodetic techniques. The results of our study show that the network of fixed-height short-baseline intra-clustered GPS benchmarks has maintained monument stability over the 20-year study period, and can be used as reliable GPS sites. The combined campaign and continuous GPS surface velocities indicate a ~3.5 mm/yr gradient across the San Diego Region. The results of constraining single and double fault homogeneous elastic half-space models, with GPS surface velocities indicate that the Rose Canyon Fault may be slipping at 2.8 ± 0.5 mm/yr or 2.4 ± 0.5 mm/yr, respectively. Given the effect of the neighboring Elsinore fault, the results of the double fault homogeneous elastic half space model are preferred. The double fault model for the optimally oriented DESC transect indicates a rate of 2.9 mm/yr. The asymmetric elastic half space model results suggest the oceanic-continental lithospheric boundary present along the northern Newport-Inglewood segment continues at least as far south as San Diego. The model results suggest a value of

A=0.244 and a slip rate of ~4 mm/yr. Surface velocities relative to site SIO5 located on the trace of the Rose Canyon fault provide evidence for a more easterly trend of the Rose Canyon fault through southern San Diego. Suggesting a possible connection with the southerly San Miguel-Vallecitos fault system. Reprocessed MCS data from south San Diego Bay image several northwest oriented faults that are well aligned to provide a fault structure to accommodate motion between these two regional fault systems.

3.7 Acknowledgements

We thank Mike Floyd and Tom Herring for their assistance with the GAMIT/GLOBK software package. We also thank Andy Yatsko for facilitating access to Navy property and Susheel Adusumilli for his help in the field.

Chapter 3, in part is currently being prepared for submission for publication of the material. Singleton, D. M., Maloney, J. M., Agnew., D., C., Rockwell, T. K., Brothers., D., Slip rate for the Rose Canyon fault through San Diego, CA based on analysis of new GPS data: Evidence of a potential Rose Canyon – San Miguel-Vallecitos fault connection? The dissertation author was the primary investigator and author of this material.

3.8 References

Agnew, D. C. 2007. *Geodetic Measurements for Urban Earthquake Hazard in San Diego, California: The Rose Canyon Fault Zone*. Final Report, USGS Award Number: 04HQGR0008.

Allen, C. R., Silver, L. T., & Stehli, F. G. 1960. Agua Blanca fault—a major transverse structure of northern Baja California, Mexico. *Geological Society of America Bulletin*, *71*(4), 467-482.

Bird, P. 2009. Long-term fault slip rates, distributed deformation rates, and forecast of seismicity in the western United States from joint fitting of community geologic, geodetic, and stress direction data sets. *Journal of Geophysical Research: Solid Earth*, *114*(B11).

Bennett, R. A., Rodi, W., & Reilinger, R. E. 1996. Global Positioning System constraints on fault slip rates in southern California and northern Baja, Mexico. *Journal of Geophysical Research: Solid Earth*, *101*(B10), 21943-21960.

Brothers, D. S., Conrad, J. E., Maier, K. L., Paull, C. K., McGann, M., & Caress, D. W. 2015. The Palos Verdes Fault offshore Southern California: Late Pleistocene to present tectonic geomorphology, seascape evolution, and slip rate estimate based on AUV and ROV surveys. *Journal of Geophysical Research: Solid Earth*, *120*(7), 4734-4758.

Boles, J. R., Garven, G., Camacho, H., & Lupton, J. E. 2015. Mantle helium along the Newport-Inglewood fault zone, Los Angeles basin, California: A leaking paleo-subduction zone. *Geochemistry, Geophysics, Geosystems*, *16*(7), 2364-2381.

Bohannon, R. G., & Geist, E. 1998. Upper crustal structure and Neogene tectonic development of the California continental borderland. *Geological Society of America Bulletin*, *110*(6), 779-800.

Dixon, T., Decaix, J., Farina, F., Furlong, K., Malservisi, R., Bennett, R., & Lee, J. 2002. Seismic cycle and rheological effects on estimation of present-day slip rates for the Agua Blanca and San Miguel-Vallecitos faults, northern Baja California, Mexico. *Journal of Geophysical Research: Solid Earth*, *107*(B10), ETG-5.

Espinoza-Cardena, J., 1983, Gravedad y magnetismo en la parte norte del sistema de fallas San Miguel (Tramo Tijuana-Valle de las Palmas): M.S. thesis, Centro de Investigacion Cientifica y Education Superior de Ensenada, Ensenada, Baja California, México, 78 p.

Feigl, K.L., Agnew, D.C., Bock, Y., Dong, D., Donnellan, A., Hager, B.H., Herring, T.A., Jackson, D.D., Jordan, T.H., King, R.W. and Larsen, S., 1993. Space geodetic measurement of crustal deformation in central and southern California, 1984–1992. *Journal of Geophysical Research: Solid Earth*, *98*(B12), pp.21677-21712.

Field, E.H., Arrowsmith, R.J., Biasi, G.P., Bird, P., Dawson, T.E., Felzer, K.R., Jackson, D.D., Johnson, K.M., Jordan, T.H., Madden, C. and Michael, A.J., 2014. Uniform California earthquake rupture forecast, version 3 (UCERF3)—The time-independent model. Bulletin of the Seismological Society of America, 104(3), pp.1122-1180.

Fialko, Y., 2006. Interseismic strain accumulation and the earthquake potential on the southern San Andreas fault system. *Nature*, *441*(7096), pp.968-971.

Fischer, P.J., and Mills, G.I. 1991, October. The offshore Newport±Inglewood±Rose canyon fault zone, California: Structure, segmentation, and tectonics. In *Environmental Perils, San*

Diego Region. San Diego Association of Geologists for Geologic Society of America Meeting (pp. 17-36).

Fletcher, K.E., Rockwell, T.K. and Sharp, W.D., 2011. Late Quaternary slip rate of the southern Elsinore fault, Southern California: Dating offset alluvial fans via 230Th/U on pedogenic carbonate. *Journal of Geophysical Research: Earth Surface*, *116*(F2).

Fletcher, J.M., Teran, O.J., Rockwell, T.K., Oskin, M.E., Hudnut, K.W., Mueller, K.J., Spelz, R.M., Akciz, S.O., Masana, E., Faneros, G. and Fielding, E.J., 2014. Assembly of a large earthquake from a complex fault system: Surface rupture kinematics of the 4 April 2010 El Mayor–Cucapah (Mexico) Mw 7.2 earthquake. *Geosphere*, *10*(4), pp.797-827.

Gastil, R.G., Patterson, D.L., and Abbott, P.L., 1979. The Valle Formation-physical stratigraphy and depositional model, southern Vizcaino Peninsula, Baja California Sur. In *Baja California Geology, Field Guides and Papers. Geological Society of America Annual Meeting Guidebook, San Diego, California* (pp. 73-76).

Gold, P.O., Behr, W.M., Fletcher, J.M., Rockwell, T.K., and Figueiredo, P.M., 2020. Time-Invariant Lat Quaternary Slip Rates Along the Agua Blanca Fault, northern Baja California, Mexico. *Tectonics in review*

Hatch, M.E., 1987. *Neotectonics of the Agua Blanca Fault, Valle Agua Blanca, Baja California, Mexico* (Master thesis, San Diego State University, Department of Geological Sciences).

Herring, T.A., King, R.W. and McClusky, S.C., 2018. Introduction to Gamit/Globk. *Massachusetts Institute of Technology, Cambridge, Massachusetts*.

Heaton, T.H. and Jones, L.M., 1989. Seismological research issues in the San Diego region. n *The Seismic Risk in the San Diego Region: Special Focus on the Rose Canyon Fault Systems: Workshop Proceedings* (pp. 42-49).

Hill, M.L., 1971. Newport-Inglewood zone and Mesozoic subduction, California. *Geological Society of America Bulletin*, *82*(10), pp.2957-2962.

Hirabayashi, C.K., Rockwell, T.K., Wesnousky, S.G., Stirling, M.W. and Suarez-Vidal, F., 1996. A neotectonic study of the San Miguel-Vallecitos fault, Baja California, Mexico. *Bulletin of the Seismological Society of America*, *86*(6), pp.1770-1783.

Humphreys, E.D. and Weldon II, R.J., 1991. Kinematic Constraints on the Rifting of Baja California: Chapter 12: Part III. Regional Geophysics and Geology. *The Gulf and Peninsular Province of the Californias*, pp. 217-229

Johnson, H.O. and Agnew, D.C., 1995. Monument motion and measurements of crustal velocities. *Geophysical Research Letters*, *22*(21), pp.2905-2908.

Kennedy, M.P. and Clarke, S.H., 1996. *Analysis of late Quaternary faulting in San Diego Bay and Hazard to the Coronado Bridge* (Vol. 97). California Department of Conservation, Division of Mines and Geology.

Kennedy, M.P. and Clarke, S.H., 1999. *Age of Faulting in San Diego Bay in the Vicinity of the Coronado Bridge, An Addendum to: Analysis of late Quaternary faulting in San Diego Bay and Hazard to the Coronado Bridge* (Vol. 97). California Department of Conservation, Division of Mines and Geology.

Kennedy, M.P., 1975. Geology of the western San Diego metropolitan area, California: Del Mar, La Jolla, and Point Loma quadrangles. *Calif. Div. Mines and Geol. Bull. A*, *200*, pp.709-722.

Langbein, J. and Johnson, H., 1997. Correlated errors in geodetic time series: Implications for time-dependent deformation. *Journal of Geophysical Research: Solid Earth*, *102*(B1), pp.591-603.

Lindsey, E.O. and Fialko, Y., 2013. Geodetic slip rates in the southern San Andreas Fault system: Effects of elastic heterogeneity and fault geometry. *Journal of Geophysical Research: Solid Earth*, *118*(2), pp.689-697.

Lindvall, S.C. and Rockwell, T.K., 1995. Holocene activity of the Rose Canyon fault zone in San Diego, California. *Journal of Geophysical Research: Solid Earth*, *100*(B12), pp.24121-24132.

Le Pichon, X., Kreemer, C. and Chamot-Rooke, N., 2005. Asymmetry in elastic properties and the evolution of large continental strike-slip faults. *Journal of Geophysical Research: Solid Earth*, *110*(B3).

Lekic, V., French, S.W. and Fischer, K.M., 2011. Lithospheric thinning beneath rifted regions of Southern California. *Science*, *334*(6057), pp.783-787.

Legg, M.R., 1985. Geologic structure and tectonics of the inner continental borderland, offshore northern Baja California. *Mexico [Ph. D. thesis]: Santa Barbara, University of California*.

Legg, M.R., Wong, V. and Suarez, F., 1991. Geologic Structure and Tectonics of the Inner Continental Borderland of Northern Baja California: Chapter 9: Part III. Regional Geophysics and Geology.

Leonard, M., 2010. Earthquake fault scaling: Self-consistent relating of rupture length, width, average displacement, and moment release. *Bulletin of the Seismological Society of America*, *100*(5A), pp.1971-1988.

Marshall, M., 1997, April. Detailed Gravity Studies and the Tectonics of the Rose Canyon–Point Loma–La Nación Fault System, San Diego, California. In *The Seismic Risk in the San*

Diego Region: Special Focus on the Rose Canyon Fault Systems: Workshop Proceedings (pp. 80-100).

Magistrale, H., 1993. Seismicity of the Rose Canyon fault zone near San Diego, California. *Bulletin of the Seismological Society of America*, *83*(6), pp.1971-1978.

Magistrale, H., 2002. Relative contributions of crustal temperature and composition to controlling the depth of earthquakes in southern California. *Geophysical research letters*, *29*(10), pp.87-1.

Maloney, J.M., 2013. *Fault segments and step-overs: Implications for geohazards and biohabitats*. University of California, San Diego.

Maloney, J.M., Driscoll, N., Kent, G., Duke, S., Freeman, T., Bormann, J., Anderson, R. and Ferriz, H., 2016. Segmentation and step-overs along strike-slip fault systems in the inner California borderlands: Implications for fault architecture and basin formation. *Applied Geology in California, Environmental Engineering Geologists*, *26*, pp.655-677.

Marquez, E., 2017, Rose-Canyon fault zone architecture at releasing step, San Diego, CA, M.S. Thesis, San Diego State University.

Materna, K. and Bürgmann, R., 2016. Contrasts in compliant fault zone properties inferred from geodetic measurements in the San Francisco Bay area. *Journal of Geophysical Research: Solid Earth*, *121*(9), pp.6916-6931.

McNeilan, T.W., Rockwell, T.K. and Resnick, G.S., 1996. Style and rate of Holocene slip, Palos Verdes fault, southern California. *Journal of Geophysical Research: Solid Earth*, *101*(B4), pp.8317-8334.

Moore, G.W., 1972. Offshore extension of the Rose Canyon fault, San Diego, California. *Geol. Surv. Profess. Pap*, pp.800-2.

Nazareth, J.J. and Clayton, R.W., 2003. Crustal structure of the Borderland-continent transition zone of southern California adjacent to Los Angeles. *Journal of Geophysical Research: Solid Earth*, *108*(B8).

Platt, J.P. and Becker, T.W., 2010. Where is the real transform boundary in California?. *Geochemistry, Geophysics, Geosystems*, *11*(6).

Reveal, 2019, https://www.shearwatergeo.com/6/reveal-software, last accessed April 19, 2019.

Reyes, A., Brune, J., Barker, T., Canales, L., Madrid, J., Rebollar, J. and Munguia, L., 1975. A microearthquake survey of the San Miguel fault zone, Baja California, Mexico. *Geophysical Research Letters*, *2*(2), pp.56-59.

Rockwell, T.K., Masana, E., Sharp, W.D., Štěpančíková, P., Ferrater, M. and Mertz-Kraus, R., 2019. Late Quaternary slip rates for the southern Elsinore fault in the Coyote Mountains, southern California from analysis of alluvial fan landforms and clast provenance, soils, and U-series ages of pedogenic carbonate. *Geomorphology*, *326*, pp.68-89.

Rockwell, K.T., Hatch, E.M. and Schug, L.D., 1987. Late Quaternary rates Agua Blanca and borderland faults. *US Geological Survey Final Technical Report for Contract*, (14-08), pp.0001-22012.

Rockwell, T.K., Schug, D.L. and Hatch, M.E., 1993. Late Quaternary slip rates along the Agua Blanca fault, Baja California, Mexico. *Geological Investigations of Baja California, South Coast Geol. Soc., Ann. Field Trip Guideb. no*, *21*, pp.53-92.

Rockwell, T. K. 2010. The Rose Canyon Fault Zone in San Diego *Fifth International Conference on Recent Advances in Geotechnical Earthquake Engineering and Soil Dynamics and Symposium in Honor of Professor I.M. Idriss*, no. 7.06c: 1–9.

Ryan, H.F., Legg, M.R., Conrad, J.E., Sliter, R.W., Lee, H.J. and Normark, W.R., 2009. Recent faulting in the Gulf of Santa Catalina: San Diego to Dana Point. *Earth science in the urban ocean: The Southern California Continental Borderland: Geological Society of America Special Paper*, *454*, pp.291-315.

Ryan, H.F., Conrad, J.E., Paull, C.K. and McGann, M., 2012. Slip rate on the San Diego trough fault zone, inner California Borderland, and the 1986 Oceanside earthquake swarm revisited. *Bulletin of the Seismological Society of America*, *102*(6), pp.2300-2312.

Sahakian, V., Bormann, J., Driscoll, N., Harding, A., Kent, G. and Wesnousky, S., 2017. Seismic constraints on the architecture of the Newport-Inglewood/Rose Canyon fault: Implications for the length and magnitude of future earthquake ruptures. *Journal of Geophysical Research: Solid Earth*, *122*(3), pp.2085-2105.

Savage, J.C. and Burford, R.O., 1973. Geodetic determination of relative plate motion in central California. *Journal of Geophysical Research*, *78*(5), pp.832-845.

Segall, P., 2010. *Earthquake and volcano deformation*. Princeton University Press.

Schug, D.L., 1987. *Neotectonics of the western reach of the Agua Blanca fault, Baja California, Mexico*. Masters Thesis, San Diego State University, Department of Geological Sciences.

Suarez-Vidal, F., Armijo, R., Morgan, G., Bodin, P. and Gastil, R.G., 1991. Framework of Recent and Active Faulting in Northern Baja California: Chapter 16: Part III. Regional Geophysical and Geology.

ten Brink, U.S., Zhang, J., Brocher, T.M., Okaya, D.A., Klitgord, K.D. and Fuis, G.S., 2000. Geophysical evidence for the evolution of the California Inner Continental Borderland as a

metamorphic core complex. *Journal of Geophysical Research: Solid Earth*, *105*(B3), pp.5835-5857.

Treiman, J.A., 1993. *The Rose Canyon Fault Zone, southern California* (Vol. 93, No. 2). California Department of Conservation, Division of Mines and Geology.

USGS, 2019. U.S. Geological Survey and California Geological Survey, Quaternary fault and fold database for the United States, accessed March 1, 2019, at: https://www.usgs.gov/natural-hazards/earthquake-hazards/faults.

Van Wijk, J., Axen, G. and Abera, R., 2017. Initiation, evolution and extinction of pull-apart basins: Implications for opening of the Gulf of California. *Tectonophysics*, *719*, pp.37-50.

Vidal-Villegas, J.A., Munguía, L., González-Ortega, J.A., Nuñez-Leal, M.A., Ramírez, E., Mendoza, L., Castro, R.R. and Wong, V., 2018. The Northwest Mexico Seismic Network: Real-time seismic monitoring in northern Baja California and northwestern Sonora, Mexico. *Seismological Research Letters*, *89*(2A), pp.324-337.

Wesnousky, S.G., 1988. Seismological and structural evolution of strike-slip faults. *Nature*, *335*(6188), pp.340-343.

Wesnousky, S.G., 2006. Predicting the endpoints of earthquake ruptures. *Nature*, *444*(7117), pp.358-360.

Wetmore, J., Wetmore, P. H., Fletcher, J., Teran, O., Yelil, R., and Courtland, L. M., 2011. October. The Northwestern San Miguel-Vallecitors-Calabasas Fault System, Baja California, Mexico: Total Offset Constraints. In *2011 GSA Annual Meeting in Minneapolis, MN*.

Wetmore, P.H., Malservisi, R., Fletcher, J.M., Alsleben, H., Wilson, J., Callihan, S., Springer, A., González-Yajimovich, O. and Gold, P.O., 2019. Slip history and the role of the Agua Blanca fault in the tectonics of the North American–Pacific plate boundary of southern California, USA and Baja California, Mexico. *Geosphere*, *15*(1), pp.119-145.

Wright, T. L. 1991. Structural Geology and Tectonic Evolution of the Los Angeles Basin, California. *Chapter 3, Active Margin Basins*. AAPG Memoir.

Yeats, Robert. 1973. Newport-Inglewood Fault Zone, Los Angeles Basin, California. AAPG Bulletin. 57.

Table 3.1. Intra-cluster horizontal and vertical baselines. RMS values for north, east, and up components are calculated relative to a weighted mean.

Baseline	**Distance (km)**		**RMS (mm)**		
	Horz.	Vert.	North	East	Up
STG1 - STG2	79.361	-0.006	0.4	0.5	1.2
WDW1 - WDW2	61.659	-0.006	1.5	1.2	0.6
TJE1 - TJE2	70.667	-7.927	0.42	0.54	1.69
TJE1 - TJE3	109.63	-10.509	0.5	0.4	1.77
SWT1 - SWT2	56.318	-3.627	0.29	0.42	0.98
SWT1 - SWT3	75.826	-5.066	0.57	0.41	3.5
SWT1 - SWT4	156.952	-11.214	0.19	0.4	1.6
COW1 - COW2	31.275	6.418	0.47	0.37	0.57
COW1 - COW3	58.312	4.96	0.86	0.3	0.68
COW1 - COW4	68.009	7.539	0.43	0.36	0.48

Table 3.2. GPS velocities relative to ITRF14. Site SWT1-4, COW1-4, TJE1-3, STG1-2, and WDW1-2 are campaign sites.

Site	**Latitude**	**Longitude**	**Velocity (mm/yr)**			**Sigma (mm/yr)**		
			North	East	Vertical	North	East	Vertical
POTR	32.61841	243.40914	18.31	-39.85	6.24	0.81	0.82	3.63
DESC	32.82992	243.3582	17.84	-39.38	3.37	0.82	0.81	3.63
RAAP	33.04224	243.08275	16.72	-38.48	4.25	0.65	0.64	2.79
P473	32.73378	243.05049	17.83	-39.61	1.9	0.59	0.59	2.53
NSSS	32.57931	243.02732	17.89	-39.02	6.36	0.51	0.5	2.15
P475	32.6664	242.75606	19.85	-39.87	-2.56	0.82	0.82	3.61
DSME	33.03648	242.75046	17.57	-38.92	0.28	0.52	0.52	1.02
SIO5	32.84073	242.75031	18.68	-39.36	4.92	0.62	0.61	2.63
SWT1	32.68832	242.99153	18.87	-39.63	-0.29	0.48	0.47	0.96
SWT2	32.68868	242.99195	18.83	-39.45	-0.36	0.49	0.48	1
SWT3	32.6882	242.99232	18.78	-39.49	0.02	0.48	0.47	1
SWT4	32.68838	242.9932	18.91	-39.56	-0.1	0.49	0.48	0.99
COW1	32.81327	242.96784	18.76	-39.51	0.07	0.49	0.48	1.03
COW2	32.81306	242.96805	18.66	-39.23	0.31	0.49	0.48	1
COW3	32.81275	242.9679	18.46	-39.5	0.32	0.49	0.49	1.04
COW4	32.81271	242.96811	18.61	-39.4	0.01	0.49	0.48	0.99
P472	32.88921	242.89531	17.39	-39.89	2.33	0.56	0.55	2.36
TJE1	32.53633	242.89502	19.75	-39.93	-0.56	0.37	0.36	0.94
TJE2	32.53638	242.89427	19.88	-39.9	-0.01	0.37	0.36	0.94

Table 3.2. Continued. GPS velocities relative to ITRF14. Site SWT1-4, COW1-4, TJE1-3, STG1-2, and WDW1-2 are campaign sites.

Site	Latitude	Longitude	Velocity (mm/yr)			Sigma (mm/yr)		
			North	East	Vertical	North	East	Vertical
TJE3	32.53708	242.89426	19.69	-39.86	0.27	0.38	0.37	1
STG1	32.69733	242.75092	19.76	-40.37	-0.22	0.37	0.36	0.84
STG2	32.69665	242.75115	19.3	-40.23	-1.2	0.37	0.37	0.88
WDW1	32.70065	242.74578	19.34	-40.13	-0.36	0.37	0.37	0.87
WDW2	32.70009	242.7458	19.65	-40.04	0.22	0.4	0.39	0.86

Table 3.3. Slip rate and asymmetry parameter model estimates for elastic half space model. X^2 and $\widetilde{X^2}$ values are before normalization of GPS error.

	RCF Rate (mm/yr)	**A**	**X^2**	**$\widetilde{X^2}$**
Single fault homogeneous elastic half space (N=23)				
Reference Station				
SIO5	2.5 ± 2.2		19.1175	0.869
DESC	3.4 ± 1.1		8.8044	0.4002
POTR	2.2 ± 1.1		10.7289	0.4877
Double fault homogeneous elastic half space (N=23)				
SIO5	2.3 ± 2.1		19.3150	0.8780
DESC	2.9 ± 1.0		9.4246	0.4284
POTR	1.8 ± 1.2		11.6905	0.5314
Single fault asymmetric elastic half space (N=23)				
SIO5	5	0.171	11.2455	0.5355
DESC	4	0.371	3.7646	0.1793
POTR	4.3	0.111	9.4182	0.4485

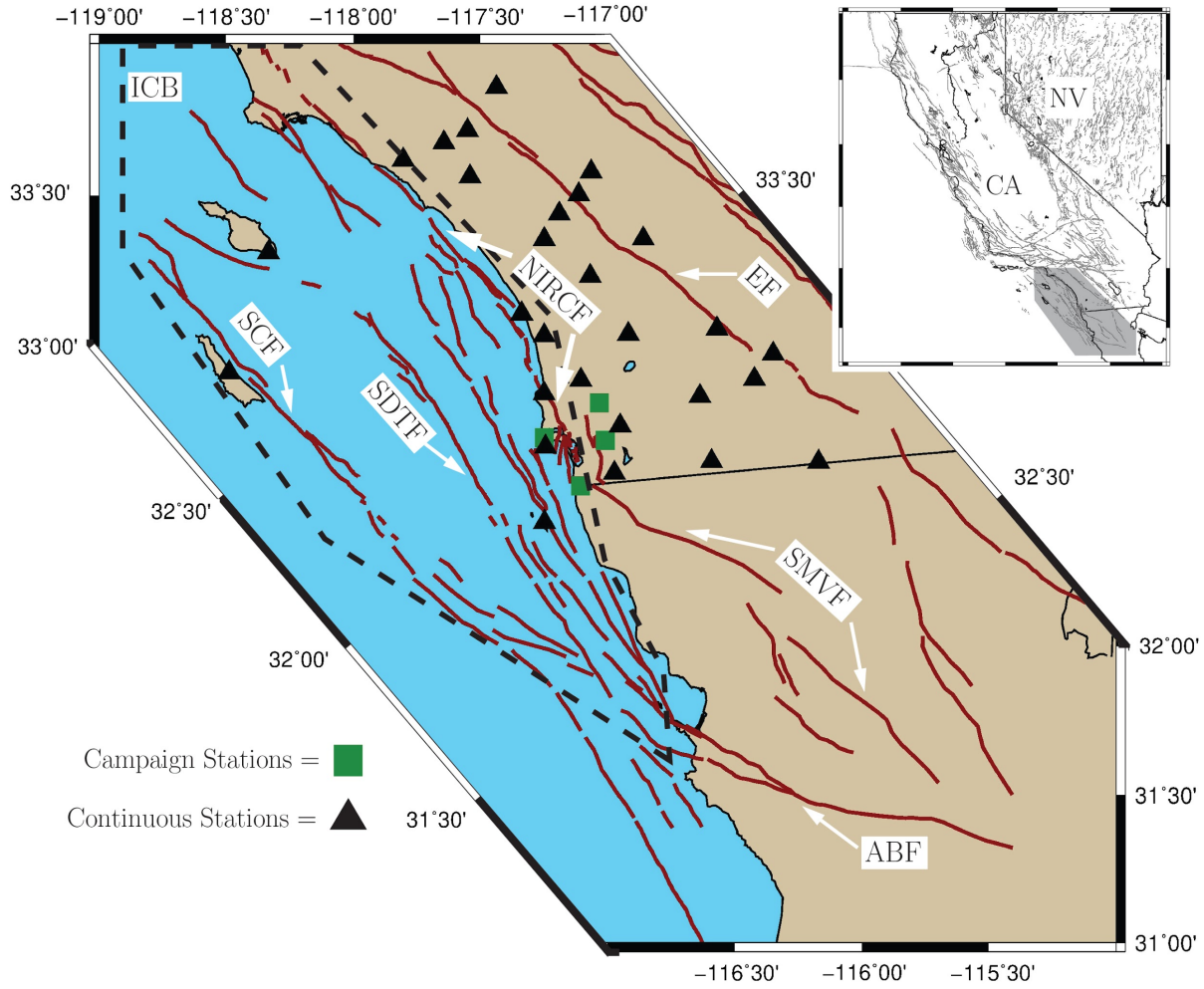

Figure 3.1. Overview map of ICB and coastal southern California and northern Baja California, Mexico. Red lines are the generalized traces of region fault systems. Squares and triangles are GPS stations used in this study to constrain network. Inset shows locations in California and Baja California, Mexico. NIRCF = Newport-Inglewood-Rose Canyon Fault, EF=Elsinore Fault, SCF=San Clemente Fault, SDTF=San Diego Trough Fault, SMVF=San Miguel-Vallecitos Fault, ABF=Agua Blanca Fault.

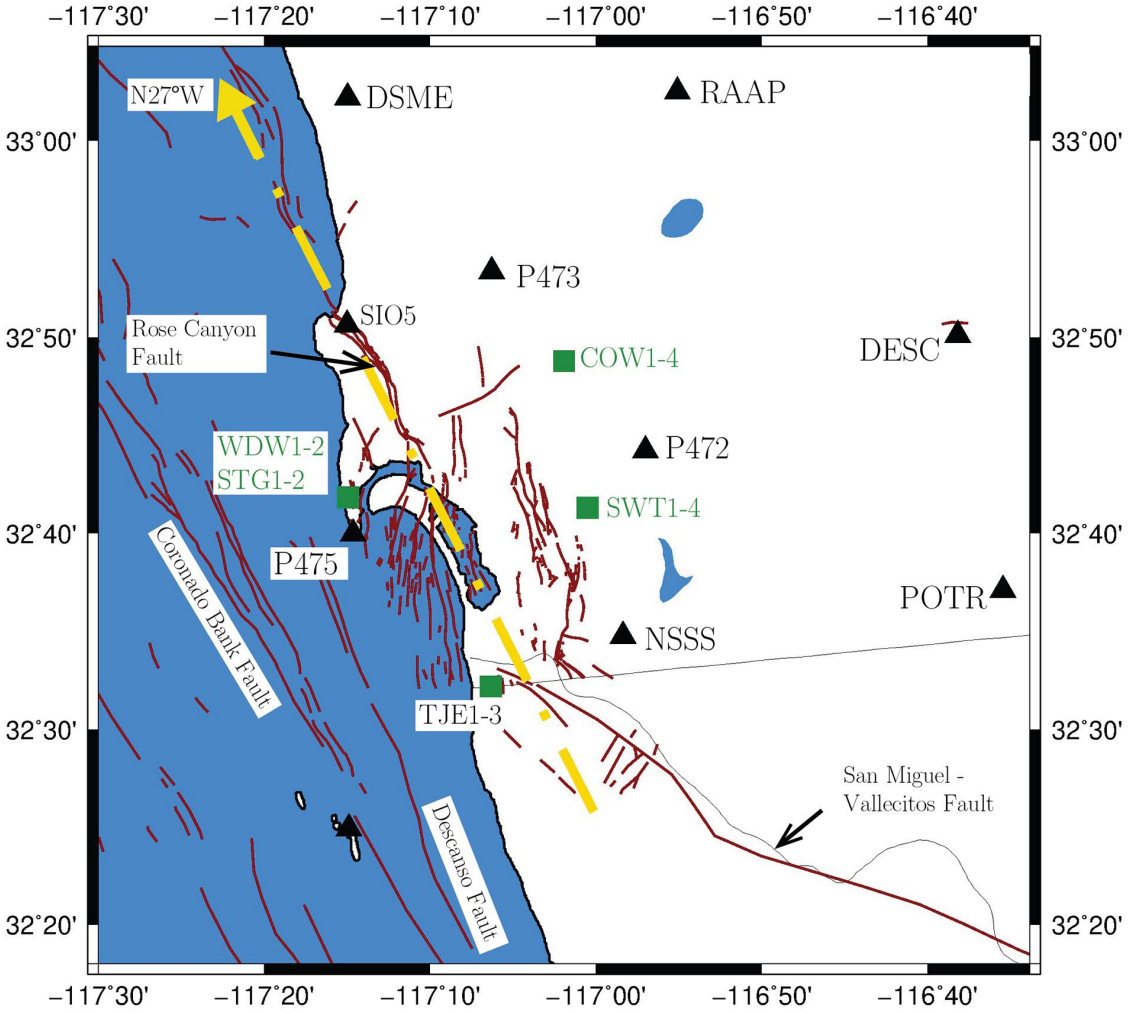

Figure 3.2. Map of the San Diego region with stations used in this study to constrain elastic half space models. Black triangles are continuous stations and green squares are campaign stations. Also shown is the average strike of the Rose Canyon Fault in yellow, and fault geometry (red lines). Fault traces north of the international border are from the USGS fault database (USGS, 2019), faults south of the border are from Fletcher et al. (2014).

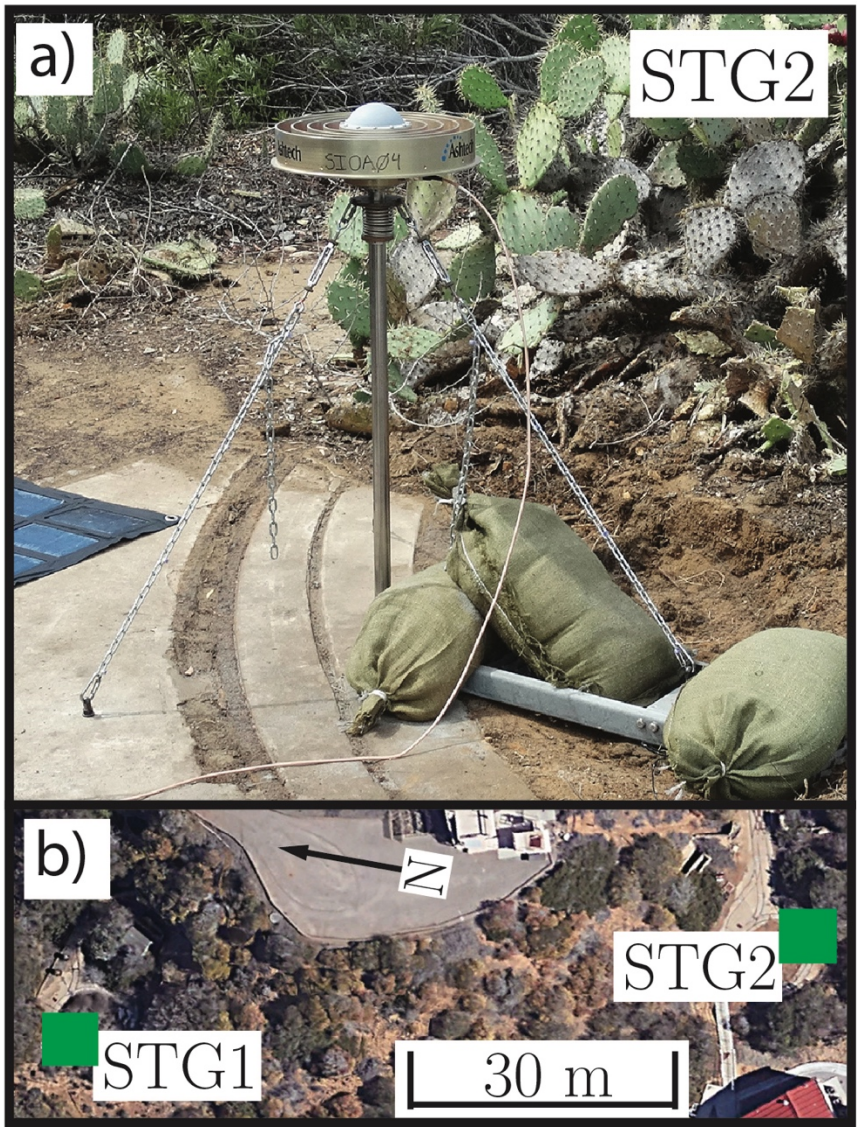

Figure 3.3. Fixed height campaign station. a) Photograph of monument STG2. b) Map view of intracluster baselines for sites STG1-STG2.

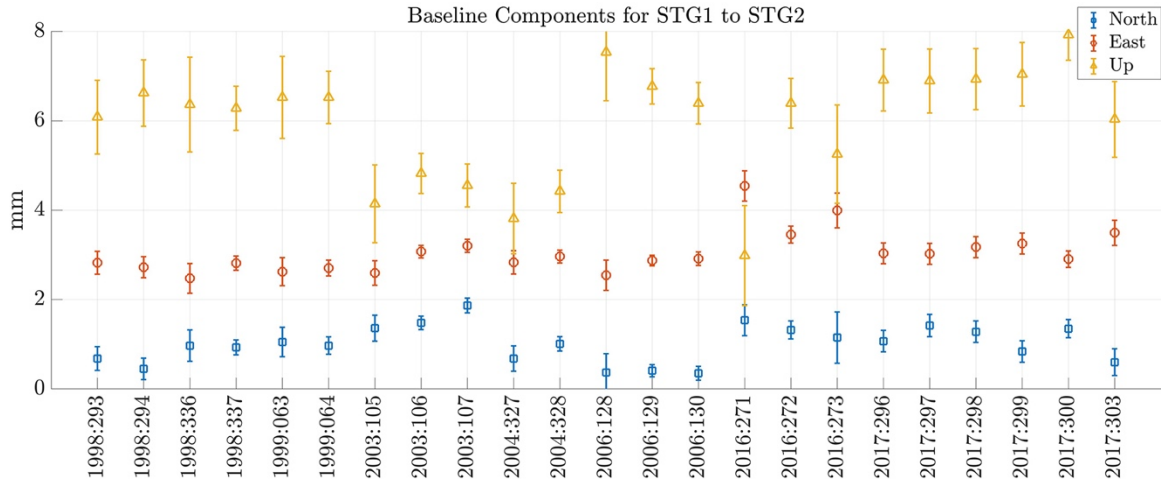

Figure 3.4. North, east, and up components of baseline between STG1 and STG2. Component values are shown after removal of a weighted mean and addition of arbitrary offset for visualization. X-axis labels show year and GPS day of year (yyyy:ddd).

Figure 3.5. Single and double fault homogeneous elastic half-space models with four reference slip rates. GPS surface velocities and associated errors are blue squares and error bars. A-C are single fault models for reference stations SIO5, DESC, and POTR; D-F are double fault models with the Elsinore Fault at 71 km. Fault locations mark with vertical red line. Green labels show campaign GPS stations and black show continuous GPS stations. Inset shows the χ^2 value versus slip rate for each model. Following Dixon et al. (2002), line P=0.90 represents the probability that the χ^2 value could have resulted from random errors, assuming the model is appropriate with errors that are normally distributed. This is used to estimate a one-sigma uncertainty for slip rate estimates in Table 3. χ^2 values included in table 3 are prior to reduced χ^2 normalization.

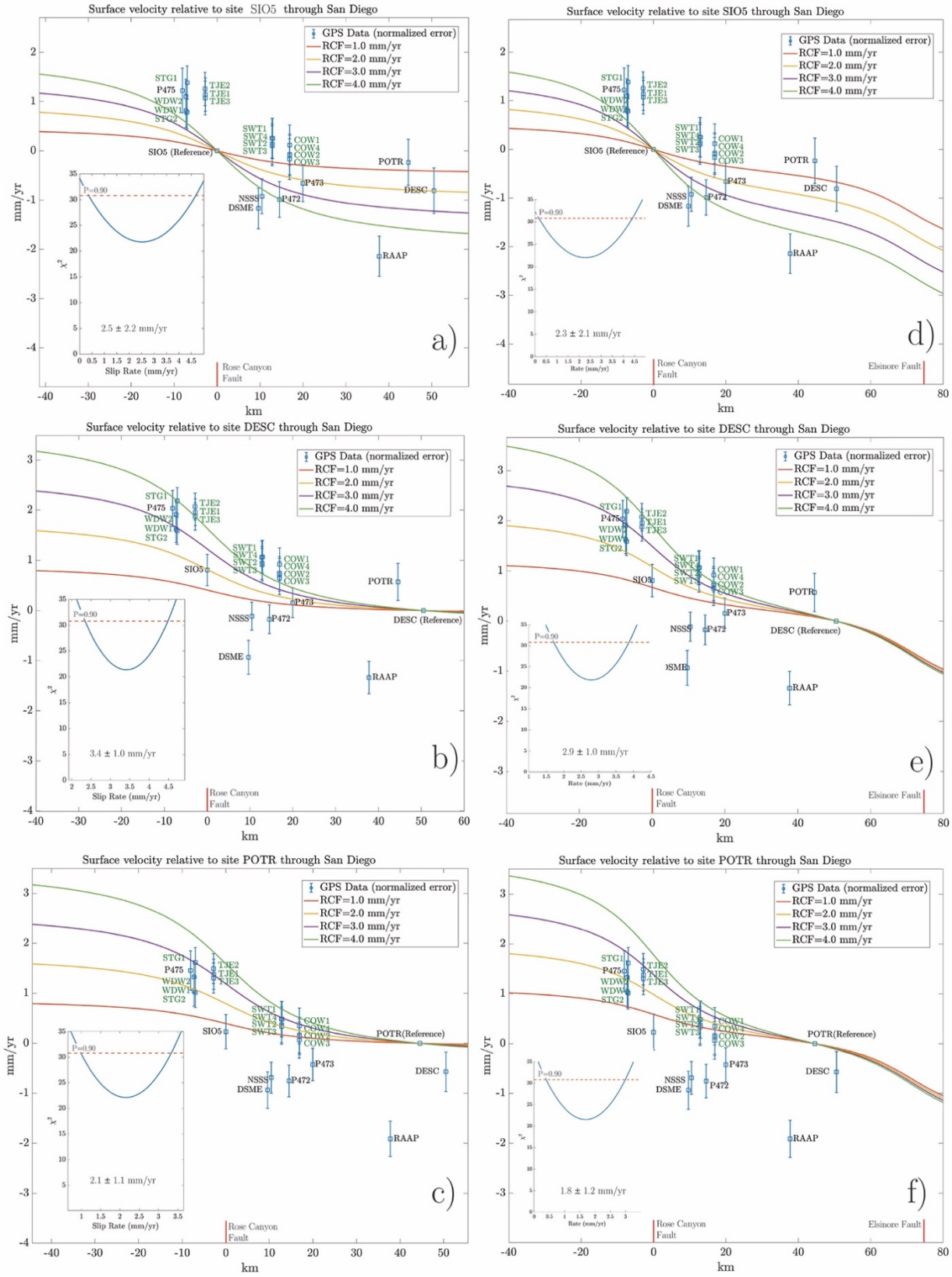
Surface velocity relative to site SIO5 through San Diego
GPS Data (normalized error)
RCF=1.0 mm/yr
RCF=2.0 mm/yr
RCF=3.0 mm/yr
RCF=4.0 mm/yr
STG1
P475
WDW2
WDW1
STG2
TJE2
TJE1
TJE3
SWT1
SWT4
SWT2
SWT3
COW1
COW4
COW2
COW3
SIO5 (Reference)
POTR
P473
DESC
NSSS
DSME
P472
RAAP
P=0.90
2.5 ± 2.2 mm/yr
Slip Rate (mm/yr)
Rose Canyon Fault
mm/yr
km
a)
Surface velocity relative to site SIO5 through San Diego
2.3 ± 2.1 mm/yr
Rate (mm/yr)
Elsinore Fault
d)
Surface velocity relative to site DESC through San Diego
DESC (Reference)
3.4 ± 1.0 mm/yr
b)
Surface velocity relative to site DESC through San Diego
2.9 ± 1.0 mm/yr
e)
Surface velocity relative to site POTR through San Diego
POTR(Reference)
2.1 ± 1.1 mm/yr
c)
Surface velocity relative to site POTR through San Diego
1.8 ± 1.2 mm/yr
f)

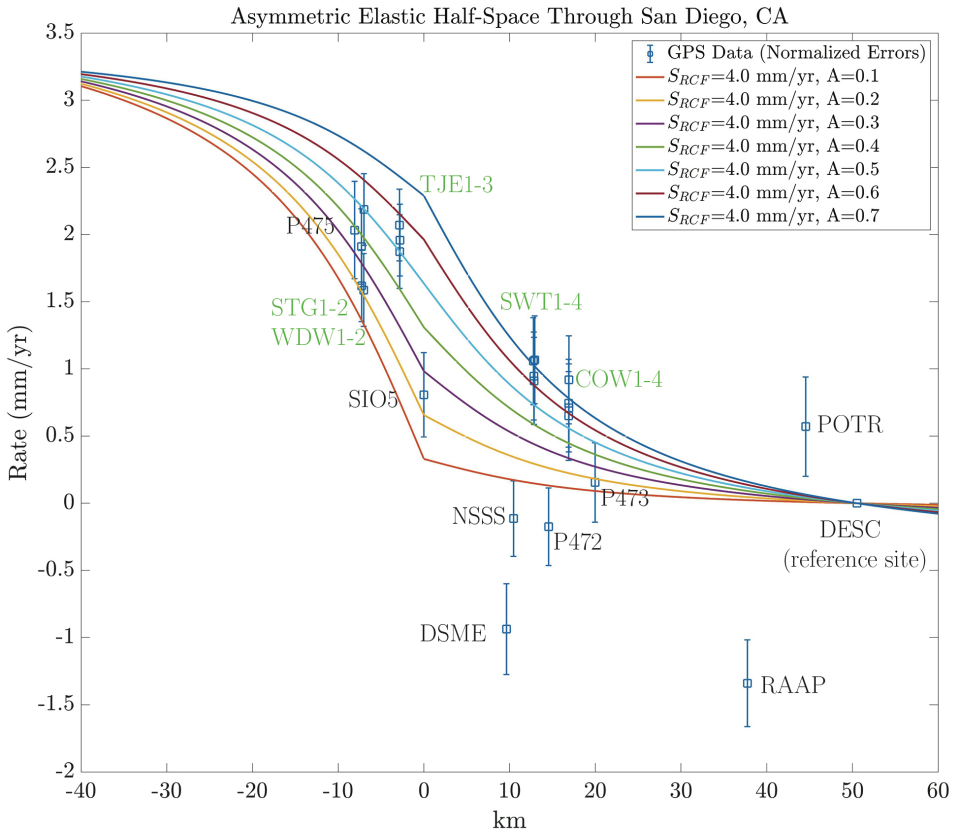

Figure 3.6. Asymmetric elastic half space model for DESC transect. GPS surface velocities and associated errors are plotted in blue. Also plotted are several model profiles with a slip rate of 4.0 mm/yr and varying values for *A*.

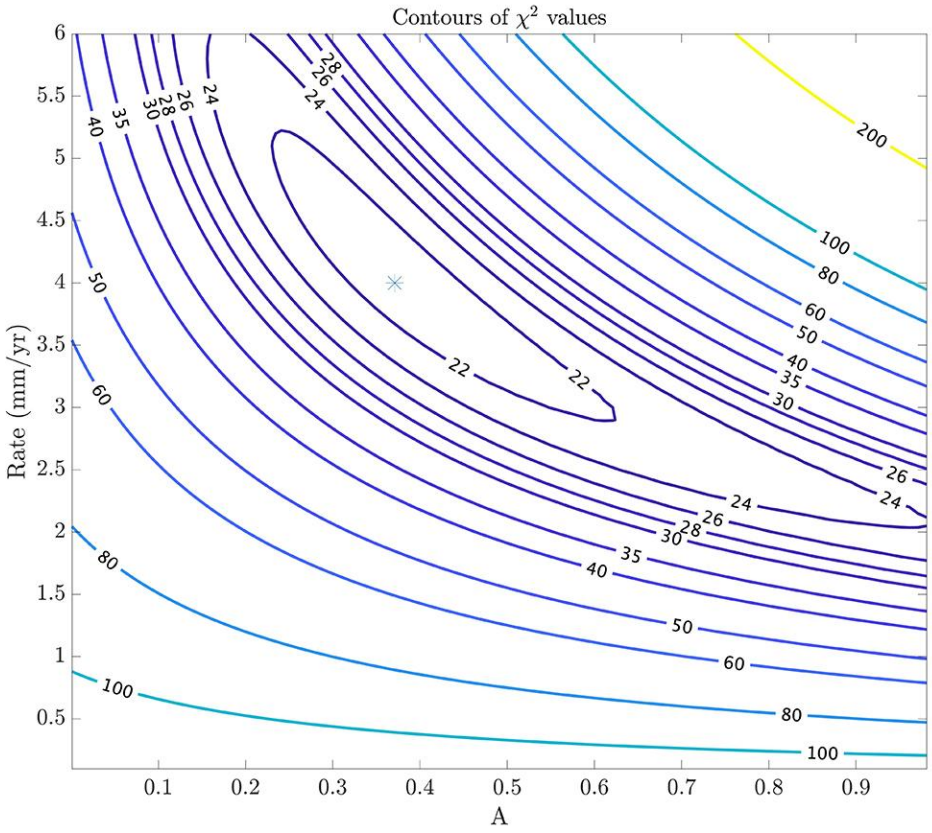

Figure 3.7. X^2 contour plot of asymmetric elastic half-space model for DESC transect. Star represents the best fitting model parameters.

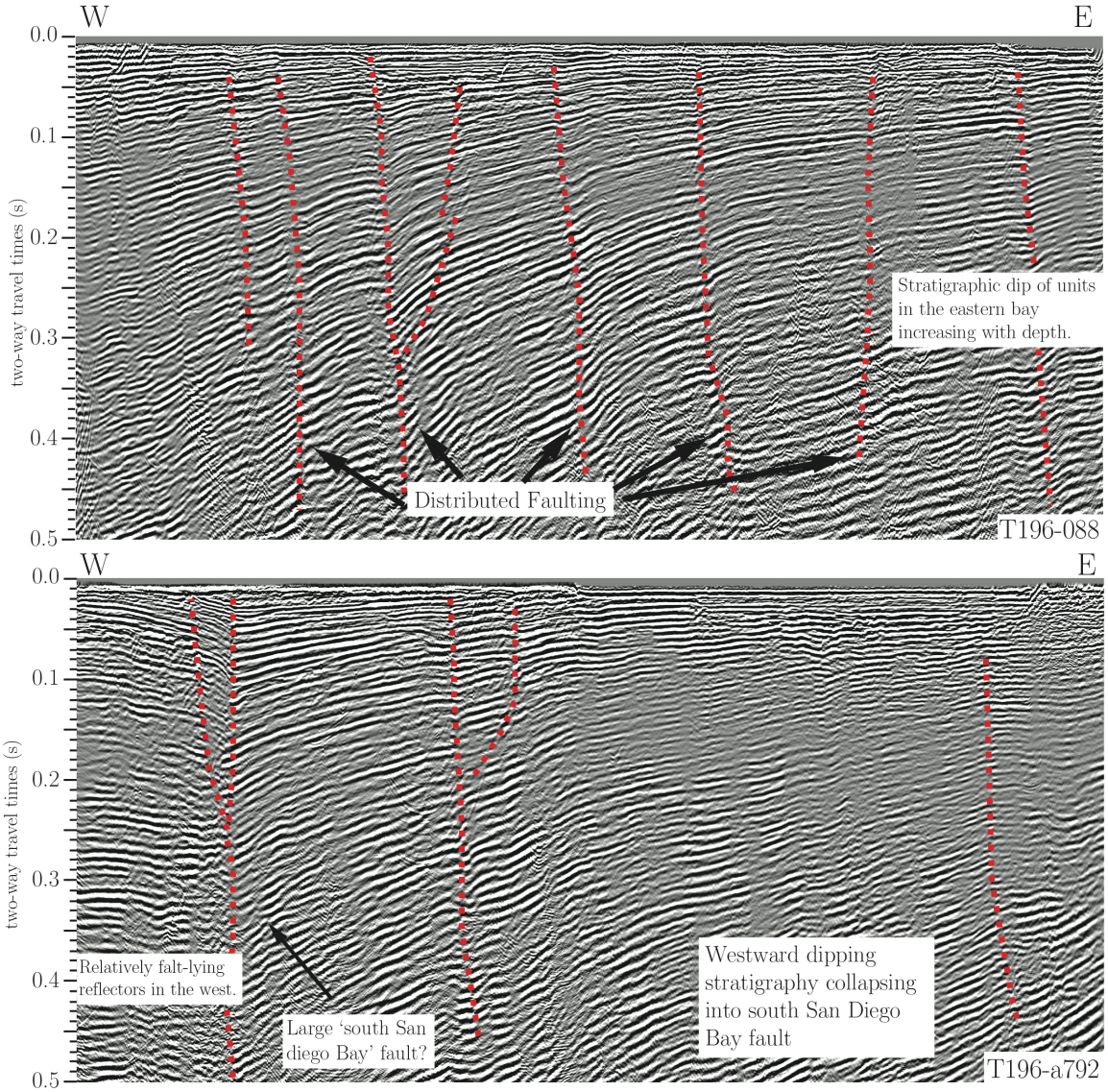

Figure 3.8. MCS profiles T196-088 (top) and T196-a792 (bottom) from south-central San Diego Bay. Sub-parallel distributed faulting is well imaged in T196-088 and is characteristic of fault structure in the northern portion of San Diego Bay in the center of the Rose Canyon Fault stepover. Further south faulting has consolidated onto a main strand seen in T196-a792 as well as a few auxiliary stands. Stratigraphic dips increase with depth against the large 'south San Diego Bay Fault' seen in T196-a792, which appears to hinge deposition in the southern portion of San Diego Bay. Location of profiles shown in Figure 9.

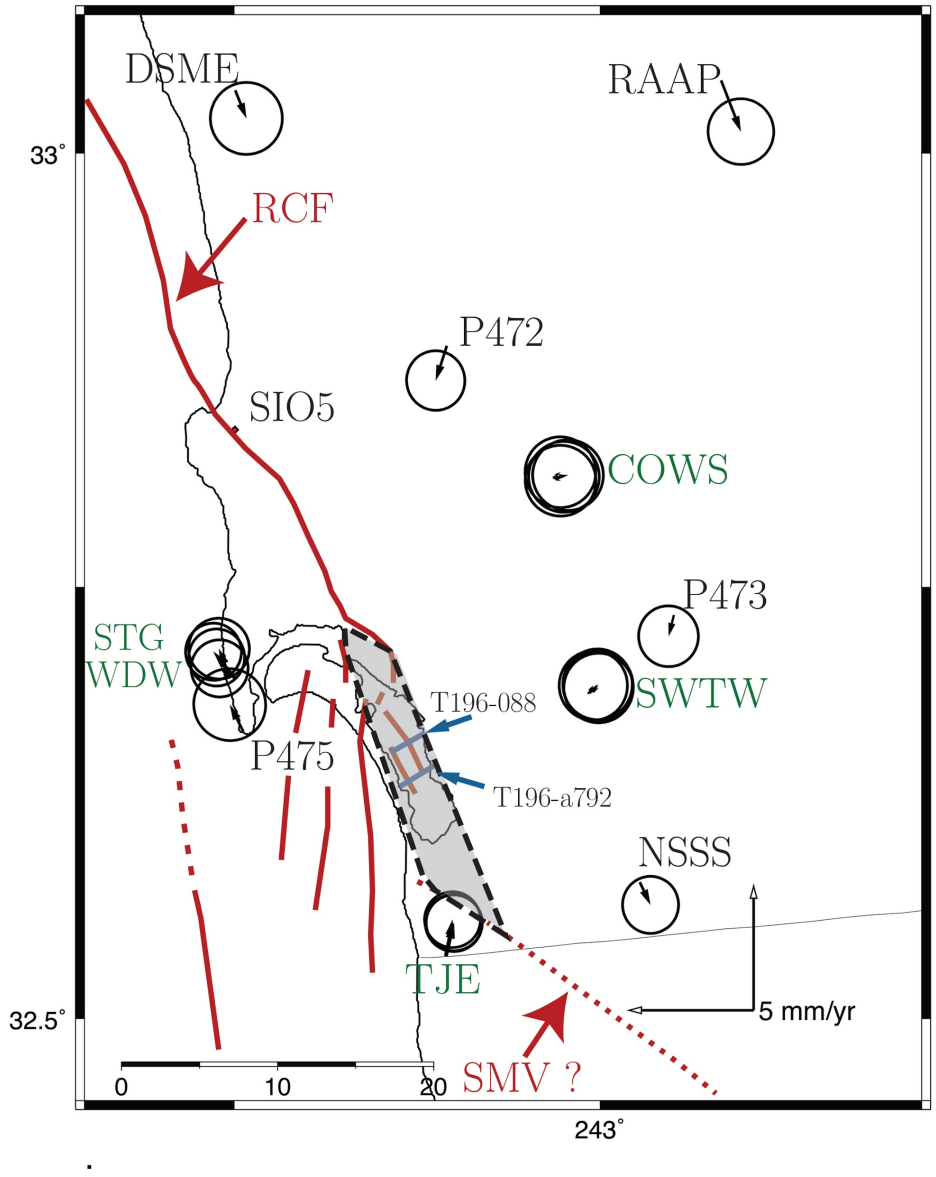

Figure 3.9. Map of surface velocity around San Diego relative to SIO5. SIO5 is within ~100 m of the surface trace of the Rose Canyon Fault. Velocities to the east of SIO5 are seen to move to the south-southeast, while stations to the west move to north-northwest consistent with right lateral motion on the Rose Canyon Fault. Based on the similarities in velocity vector, site TJE (composed of benchmarks TJE1-3) appears to be in the same crustal block as sites on Point Loma. Additionally, site TJE is seen moving in the opposite direction to NSSS, which may be evidence of a fault structure beneath Tijuana, Mexico and the Tijuana River. Shaded region represents the approximate central location of proposed rhombochasm graben of Marshall (1989) with either side collapsing into the shaded region.

4. Recency of faulting and subsurface architecture of the San Diego Bay pull-apart basin, California USA

4.1 Abstract

The Newport-Inglewood-Rose Canyon fault is well defined for most of its mapped trace from western Los Angeles to downtown San Diego, California. South of downtown San Diego, the southern segment (the Rose Canyon fault) splays out into a complex network of faults that accomplishes the subsidence of San Diego Bay. A pull-apart basin model between the Rose Canyon fault and the offshore Descanso fault has been suggested to explain the apparent subsidence and orientations of several prominent faults in northwestern San Diego Bay. However, this model does not explain observed northwest oriented faults in southeastern San Diego Bay or the La Nacion fault zone located 5-10 km outside of the proposed Rose Canyon-Descanso pull-apart. To investigate the subsurface fault architecture and stratigraphic character beneath San Diego Bay we combined a suite of reprocessed legacy multi-channel seismic profiles with high-resolution chirp data, with age and lithology control from geotechnical boreholes and vibracores. Gridded horizon surfaces, fault maps, and a kinematic fault analysis were carried out using the combined dataset. San Diego Bay is dominated by down-to-the-east motion on normal faults that are separated into two distinct groups. The orientations of these two groups (as well as the La Nacion fault) can be explained with a double pull-apart basin model for San Diego Bay. In our conceptual model, the western portion of San Diego Bay is controlled by a Rose Canyon-Descanso fault pull-apart basin, which matches both observations and laboratory models. The eastern portion of San Diego Bay is controlled by a proposed Rose Canyon–San Miguel-Vallecitos fault pull-apart basin that matches fault orientations, but that kinematic analysis indicates should have a significant component of strike-slip partitioning that is not observed in the seismic data. The potential of a Rose CanyonSan Miguel-Vallecitos fault connection has important implications for the seismic hazard of the San Diego-Tijuana

metropolitan area (collectively home to some three million people) and highlights the need for additional studies to better understand faulting south of San Diego Bay.

4.2 Introduction

In the San Diego region, the Rose Canyon fault represents the boundary between the Peninsula Range geologic province and the complex tectonic fabric of the Inner Continental Borderland (ICB). The Rose Canyon fault is the southern segment of the larger Newport-Inglewood-Rose Canyon fault system, which is the easternmost fault in the ICB and has been mapped as a continuous fault zone from Los Angeles to San Diego (Moore, 1972; Wright, 1991; Sahakian, et al., 2017; Maloney et al., 2016). The ICB is composed of a series of northwest trending sub-parallel strike-slip faults that are segmented by stepovers and regions of concentrated transpression and transtension (Bohannon and Geist, 1998; Maloney et al., 2016; Legg et al, 1991; Legg et al., 2015; Ryan et al., 2009). A broad area of transtension exists south of downtown San Diego, where the Rose Canyon fault splays out into a complex network of faults that together accomplish the subsidence of the San Diego Bay pull-apart basin (Figure 1).

San Diego Bay occupies what has been called the San Diego Graben, which is a series of horst and graben structures that is bounded by the offshore Descanso fault to the west and the La Nacion fault to the east; together with the Rose Canyon fault to the north and the Tijuana River Valley to the south these structures define the San Diego Bay pull-apart basin (Figure 2) (Kennedy, 1975; Marshall, 1989; Maloney, 2013). Faults in the northwestern portion of the bay are well described as linking faults oriented ~30-40° to the dextral Rose Canyon and Descanso faults in a classic pull-apart basin model. In southeastern San Diego Bay, a series of faults has been imaged that together with the La Nacion fault zone are oriented at a high angle to the Rose

Canyon and Descanso faults, suggesting additional factors are influencing deformation in San Diego Bay.

With the Newport-Inglewood-Rose Canyon fault representing a major boundary in the ICB and the closest fault to major population centers, its southern continuation has important consequences for not only understanding how strain enters the ICB, but also for regional seismic hazard. While the northwestern bay faults can be explained with a Descanso–Rose Canyon pull-apart basin model, the high angle faults to the southeast are problematic. Based on a variety of geologic and geophysical data, some studies have suggested that a possible connection between the Rose Canyon and the San Miguel-Vallecitos fault to the south may be present and may potentially be responsible for the orientations of the southeastern bay faults (Tremain, 1993; Marshall, 1989; Wiegrand, 1970). However, the exact mechanics of this connection remain uncertain and definitive evidence of faulting south of San Diego Bay has been elusive.

Onshore, paleoseismic evidence has shown the Rose Canyon fault is active, having experienced several surface rupturing earthquakes throughout the Holocene (Lindvall and Rockwell, 1995; Singleton et al., 2019). Several swarms of small earthquakes in the 1980s indicate that this activity is likely not confined to the onshore segments, but continues into San Diego Bay (Magistrale, 1993). Indeed, in the northwestern portion of the San Diego pull-apart basin evidence exists that the most recent sizable event in the San Diego Region (M~6 1862 A.D. San Diego Earthquake) may have initiated on one of the linking faults in the bay and continued onto the main strand of the Rose Canyon fault at Old Town (Legg and Agnew, 1979; Singleton et al., 2019; Marquez, 2017).

The northwestern portion of San Diego Bay is home to key infrastructure for the city of San Diego, including major Naval Bases and the Coronado Bridge. As a result, several studies have been conducted with the objective to resolve fault locations and activity (e.g., Kennedy and Clark, 1996; Maloney, 2013; Marquez, 2017; Weidman, 2019; Gingery et al., 2010). While some effort has been made to extend age control southward into the central portion of the bay, very little is known about the activity of faults south of the Coronado Bridge (Kennedy and Clarke, 1996). While there is evidence that some earthquakes may involve both the onshore Rose Canyon fault and certain offshore faults, the role that faults in San Diego Bay as a whole play in larger earthquakes is unknown.

In this study, we use a combination of high-resolution seismic chirp profiles, reprocessed multi-channel seismic (MCS) lines, and borehole-core sampling to resolve the stratigraphic character and fault structure beneath San Diego Bay. These datasets are used to construct gridded maps of the subsurface horizons and extended mapped traces of faults to develop a structural framework beneath San Diego Bay. In the southern part of our study area, short (~3-5 m) sediment cores are used to ground-truth chirp profiles that imaged the upper ~50 m of bay sediments with sub-meter vertical resolution and develop an age model since the last sea-level transgression to determine recency of faulting. Finally, a structural analysis of the fault orientations and regional plate boundary characteristics is performed to develop models to explain the observed features of the San Diego Bay pull-apart basin.

4.3 Regional Geology and Local Tectonics

The ICB is the offshore extension of the Big Bend Domain of the San Andreas plate boundary that dominates the tectonics of southern California. A boundary can be drawn from

the Salton Sea through San Diego Bay and offshore that separates faults with predominantly transpressional structures (leftward bends and jogs) to the north, from transtensional structures (rightward bends and jogs) in the south (Legg et al., 2015; Wetmore et al., 2018). Thus, the San Diego Bay pull-apart occupies a complex transitional area between two deformation regimes. Faults within the ICB play an important role in transferring 10-15% of plate motion from the Gulf of California around the big bend in the San Andreas fault and into the faults of the Western Transverse Ranges (Platt and Becker, 2010; Humphreys and Weldon, 1991). Slip is fed into the ICB by the faults of the Transpeninsula fault system in Baja California, Mexico, mainly the Agua Blanca (and associated strands) and the San Miguel-Vallecitos faults (Figure 1).

The Agua Blanca fault cuts across the Baja peninsula and transfers ~2-8 mm/yr of slip into the faults of ICB (Dixon et al., 2002; Legg et al., 1991). Within the ICB, the Descanso and Coronado Bank faults are associated strands of the Agua Blanca fault that help carry a portion of this slip northward, possibly partitioning it into the Rose Canyon fault through the San Diego Bay pull-apart basin (Legg, 1985; Legg et al., 1991). Studies in the 1980s and 1990s postulated that the Coronado Bank fault is a segment of an extensive Palos Verdes-Coronado-Agua Blanca fault system, but recently collected seismic data have shown that the Coronado Bank fault decreases in activity and continuity offshore Oceanside and does not have a clear connection to the Palos Verdes fault (Legg, 1985; Legg et al., 1991; Ryan et al., 2009; Brothers et al., 2015). Therefore, any slip carried northward by the Coronado Bank fault is likely transferred onto an adjacent fault structure (Conrad et al., 2018). The Descanso fault trends N25°W offshore San Diego (Figure 1 and 2), and may be the northern terminus of a larger

Estero-Descanso fault, but the exact location of the Descanso fault south of the international border is poorly understood due to a 'lack of good seismic data' (Legg, 1985).

Reprocessed industry MCS profiles suggest that at the latitude of San Diego Bay, the Descanso fault is an eastern strand of the larger Coronado Bank fault system (Maloney, 2013). Hanging wall rollover imaged in MCS data along the eastward dipping Coronado Bank fault indicates a degree of soling at depth that is likely a consequence of participation in the San Diego Bay pull-apart basin (Maloney, 2013). This hanging wall rollover also contributes to the Descanso fault's position as the western edge of the horst-and-graben structure of the San Diego Bay pull-apart basin. The west side down sense of displacement of the westward-dipping Descanso fault elevates the Point Loma peninsula relative to the surrounding region (Maloney, 2013). Combined high-resolution chirp and MCS data show the Descanso-Coronado Bank fault zone reaches its locally greatest width adjacent to the deepest portion of the San Diego Bay pull-apart basin where it displaces the transgressive surface; northward the fault zone narrows and chirp data indicate a non-faulted transgressive surface, suggesting a decrease in activity on the Descanso fault (Maloney, 2013). Recent faulting is observed on the Coronado Bank fault until the La Jolla Fan (Ryan et al., 2009). Several earthquakes (M<4) from 1981 to 1997 have been located between the Coronado Bank and Point Loma, providing additional evidence of a connection between these two fault systems (Astiz and Shearer, 2000).

The San Miguel-Vallecitos fault trends northwest across the Baja Peninsula and is well aligned to connect with the Rose Canyon fault (Figure 1 and 2). Mapped offsets of magmatic dikes suggest a small (~600-1000 m) total offset, while slip rate estimates vary considerably, with geologic estimates (~0.2 mm/yr) significantly lower than geodetic estimates (~2-4 mm/yr) (Hirabayashi et al., 1996; Dixon et al., 2002; Wetmore et al., 2011). These contrasting

characteristics may be an indication of the fault's incipient nature. The San Miguel-Vallecitos fault is the most active fault in the ICB hosting several M>6 surface rupturing earthquakes in the past century and high rates of microseismicity (Hirabayashi et al., 1996; Frez et al., 2000). The mapped trace of the San Miguel-Vallecitos fault ends ~30 km south of San Diego Bay, but previous studies have postulated a connection to the Rose Canyon fault zone based on the alignment of warm water wells, elongated north-south trending depressions (possible sag ponds), offset terraces, and stratigraphic and lithological changes across the proposed fault lineament (Wiegand, 1970; Gastil et al., 1979; Treiman, 1993). Youthful faulting may be obscured by fluvial sedimentation along the Rio De La Palma and Tijuana rivers.

Faults west of Tijuana river valley, in northernwestern Tijuana, Mexico, have been studied in detail by Minch (1967) and are referred to as the Los Buenos fault zone. The primary structural fabric in this area consists of north-south oriented normal faults that run parallel to the coastline, and secondary east-west and northwest-southeast oriented normal faults. The north-south faults are dominantly down-to-the-east (Minch, 1967), similar to faults in San Diego Bay. Pleistocene deposits are offset and folded along several faults, but most deformation appears to have occurred during the Miocene. The Pleistocene Avondale Terrace, mapped by Ellis and Lee (1919), is at an elevation of 350-400 feet and offset by faults in the Los Buenos fault zone, but north of the Tijuana River Valley the same terrace is at 200 feet and is not offset by faulting (Gastil et al., 1979). The Los Buenos fault zone may be a response to complex crustal stress conditions created by interactions between the San Miguel-Vallecitos, Descanso, and Rose Canyon fault systems.

North of San Diego, the Rose Canyon fault trends ~N25°W from offshore Oceanside 35 km south to La Jolla, where the fault takes a leftward compression bend uplifting Mt. Soledad

before continuing on a similar trend south along the I-5 corridor towards San Diego Bay (Figure 1). The Rose Canyon fault has ~4 km of total offset based on the displaced Eocene Mt. Soledad conglomerate and is thought to have initiated in Plio-Quaternary as the upper portion of the San Diego Formation is a tectono-stratigraphic unit that records the down-dropping and sedimentation in San Diego Bay (Kies, 1984; Tremain, 1993; Demere, 1983). The San Diego Formation is overlain by a series of marine terraces of Pleistocene age that are locally deformed in the San Diego region in response to movement on regional faults (Kern and Rockwell, 1992).

Just north of downtown San Diego, the Rose Canyon fault splays out into a complex network of faults that make up the San Diego Bay pull-apart basin (Figure 2). The northernmost splay trends offshore into San Diego Bay as the Spanish Bight fault. Through downtown, the fault zone is mapped as a western San Diego fault and an eastern zone of faulting that includes the "downtown graben" (Treiman, 1993; 2002; Weidman et al., 2019). These splays trend into the bay as the Coronado and Silver Strand faults, respectively. Gravity measurements indicate that San Diego Bay overlies a northwest oriented, ~20 km long, ~12 km wide, and 2-3 km deep basin that deepens southward reaching its greatest depth beneath south San Diego Bay (Marshall, 1989). The faults in the northwestern bay (Spanish Bight, Coronado, and Silver Strand) are well-defined and well-imaged (Figure 2). These faults have a north-northeasterly surface trend and have been mapped from the northern portion of San Diego Bay, across the Coronado Peninsula, and offshore to at least the International border, where poor data quality prevented the establishment of a southern continuation (Legg, 1985; Maloney, 2013). These three 'linking' faults all show predominantly down to the east displacement in

seismic data and displace sediment close to the bay floor with potential displacement of the bay floor on some strands (Maloney, 2013; Marquez, 2017).

South of the Silver Strand fault, in the southeastern portion of San Diego Bay are a series of north-northwest trending faults that also exhibit normal motion with down-to-the-east displacement (Figure 2). These southeastern bay faults appear to lie outside of the Rose Canyon-Descanso pull-apart basin. East of San Diego Bay, the La Nacion fault zone is composed of North-South oriented, west dipping, anastomosing normal faults with more than 60 m vertical offset of the Pliocene San Diego Formation (Hart, 1974). Holocene activity has not been observed in paleoseismic excavations (Hart, 1974) and the long-term slip rate is very low. The La Nacion fault has traditionally been interpreted as the eastern boundary of the San Diego Bay pull-apart basin.

4.4 Methods

The MCS data used in this study were collected as part of a seismic hazard assessment of the Coronado bridge in the mid-1990s (Kennedy and Clarke, 1996; 1999). The original survey collected 130 km lines of MCS with a 14-cubic inch sleeve-gun source, 24-channel streamer, and 3.125 m shot spacing. This work also included a transect of boreholes beneath the Coronado bridge (Kennedy and Clarke, 1996; 1999). Unfortunately, all of the original computer data (stored on magnetic tape files), were destroyed in a warehouse fire before they could be transferred to modern digital format, including the original navigation files. Thus, the only surviving copies of the seismic data were thought to be working paper copies (owned by the original investigators) and the figures included in the final report filed with the City of San Diego and the California Division of Mines and Geology (Kennedy and Clark, 1996).

However, a spring-cleaning effort at the offices of the US Geological Survey-Menlo Park unearthed a set of the original magnetic tape copies of the MCS lines collected in San Diego Bay. These lines were transferred to modern digital format and reprocessed through the Shearwater Reveal software package (Reveal, 2019).

Through the Reveal software package, a processing scheme was developed to increase the resolution of the MCS data. A linear moveout and f-k filter were first applied to knock down noise due to streamer motion and refracted arrivals, which were especially prevalent in shallow San Diego Bay and in portions of the bay with large cement structures such as Naval docks. A water bottom mute followed by common mid-point stacking with normal moveout correction and velocity semblance were also applied. Following this, the data were brute stacked and then time migrated. Reprocessing the older MCS data with improved computational techniques dramatically increased the resolution at depth allowing for better characterization of fault geometry and stratigraphy.

The magnetic tapes did not include navigation for the MCS lines, so the locations had to be digitized from the figures included in the original report. First the figures were scanned and georeferenced in ESRI ArcMap and the individual MCS lines were digitized. The total length of the digitized line was divided into equal spaced 'shots' at 3.125 m spacing, which is the shot spacing of the original acquisition (Kennedy and Clarke, 1996). Due to uncertainties in the digitization of the original figure, the final locations likely carry a location error of ~15-100 m. Borehole data were extracted from a cross-section collected beneath the Coronado bridge and include age constraints (radiocarbon, amino acid stratigraphy, and paleontological analysis) on underlying strata (Kennedy and Clarke, 1999).

During 2011-2013, and 2019, high-resolution seismic reflection data were collected in San Diego Bay using Scripps Institution of Oceanography's Edgetech chirp profiler, operated with a 50 ms swept pulse of 1-15 kHz and 0.7-3.0 kHz, providing sub-meter vertical resolution with sub-bottom penetration up to ~50 m, and location accuracy within 5 m. Chirp data were processed using *SIOSEIS* and Seismic Unix. Both the MCS and chirp data were interpreted using IHS Kingdom Suite to examine changes in stratigraphy and fault geometry.

With no tie-lines collected in the southern portion of the bay during the original MCS survey, we relied on several distinctive stratigraphic sequences to correlate stratigraphy between survey lines that were spaced on average ~400 m apart. Five distinctive sets of high-amplitude reflectors separated packages of more chaotic to homogenous low-amplitude packages, and were used to separate the stratigraphy into four main units. These five horizons were mapped across the study area to observe changes in stratigraphic character. Using IHS Kingdom Suite software, gridded surfaces of the mapped horizons were generated for improved visualization. Due to the geometry of the original MCS survey, occasional large (~800 m) areas of the gridded surfaces are without data to constrain the interpolation.

In the southern portion of San Diego Bay, shore-based vibracores provide ground-truthing and age correlation for the southern chirp profiles. The cores were split, photographed, and described, before being scanned for magnetic susceptibility to aid in stratigraphic correlation. The cores were then sampled for datable material, which were dated for radiocarbon ages by accelerated mass spectrometry at the University of California-Irvine Keck Carbon Lab. An age model was constructed using OxCal v4.3.2 and Marine Calibration Curve 13 (Bronk Ramsey, 2017; Reimer et al., 2013) with a local reservoir age of 171 ± 154 years before present (Holmquist et al., 2015).

To develop kinematic models of the San Diego Bay pull-apart basin, the surface trends of faults potentially involved with the San Diego Bay pull-apart basin were measured within 1.5 x 1.5 km grid cells from an overlay of a recent fault map (Kennedy and Tan, 2005). Averages of fault trends were calculated using Fisher statistics. Assuming plate motion provides boundary conditions, and deformation of a continuum provides the best kinematic analysis (McKenzie and Jackson, 1983; Fossen and Tikoff, 1993), the relationship between plate motion, instantaneous strain axes, and degree of strike-slip partitioning were used to distinguish between two end members: wrench (simple-shear) dominated and pure-shear dominated deformation (Fossen and Tikoff, 1993). Together with the regional plate motion boundary conditions, the orientations of regional faults and the deformation indicated by the kinematic analysis were used to construct a potential model to explain faulting in the San Diego Bay pull-apart.

4.5 Results

4.5.1 Observations from nested MCS and chirp datasets with age control

Reprocessing the legacy MCS data resulted in good-quality, usable data down to ~450-500 ms two-way travel time (twtt), and imaged many of the fault segments previously mapped in San Diego Bay. The processed chirp data resulted in sub-meter vertical resolution seismic images down to ~50 ms twtt (~40 m using a sonic velocity of 1500 m/s). Previous studies in San Diego Bay have delineated relatively narrow fault zones in the northwestern portion of the bay that trend north-south across the width of the bay (e.g., the Spanish Bight, Coronado, and Silver Strand faults) (Kennedy et al., 1975; Kennedy and Clarke, 1996; Maloney, 2013; Marquez, 2017; USGS, 2019). The southeastern portion of the bay is characterized by short

discontinuous fault segments and is comparatively understudied (USGS, 2019; Kennedy and Clarke, 1996).

In the northernmost portion of the bay, previous observations are confirmed as both the Spanish Bight and the Coronado faults exhibit dips of ~75° and ~85° eastward, respectively, northerly trends, and down-to-the-east sense of displacements. The Silver Strand fault is a major fault in San Diego Bay and dips ~82° east with ~100 m of down-to-the-east displacement of the horizon 5 surface observed in the Glorietta Bay area (Figure 3). However, poor data quality on the western side of the Silver Strand fault hampered efforts to correlate stratigraphy across the fault confidently, therefore the amount of displacement may be significantly different. Nevertheless, the amount of displacement on the Silver Strand fault appears to decrease northward toward downtown San Diego.

South of the Coronado Bridge, fault segments are generally northwest trending, discontinuous, and exhibit a down-to-the-east sense of displacement (Kennedy and Clarke, 1996; Kennedy and Moore, 1975). Occasional small, ~50-300 m, northeast trending fault segments with variable senses of displacement are also observed. By combining the MCS and chirp datasets, the surface traces of short discontinuous fault segments are extended to form longer continuous faults in San Diego Bay (Figure 2). Two of these continuous faults (D1 and SB1) appear to be major structures in the southeastern portion of the bay and exert a control on deposition. Fault D1 is located just south of the Coronado Bridge and trends ~N10°W towards the Silver Strand. To the east, Fault SB1 trends ~N25°W and is aligned with the long axis of the bay. Given the uncertainty associated with the MCS navigation from georeferencing, fault locations are determined from chirp profiles where possible.

The combined MCS and chirp datasets show a continuation of the previously mapped D1 fault from Kennedy and Clarke (1996). We confirm and extend its trace south from the Coronado Bridge towards the Silver Strand (Figure 2 and Figures 3-5 moving north to south). Fault D1 dips steeply to the east for its entire length, but changes its sense of slip from locally down-to-the-west in the north near the intersection with the Silver Strand fault and the faults of the "downtown graben", to down-to-the-east southward. As first noted by Kennedy and Clarke (1996), at the latitude of the Coronado Bridge, Fault D1 forms a localized horst and graben structure with the adjacent Silver Strand and downtown graben faults (Figure 3). Faulting associated with D1 is distributed across several closely spaced strands that are typically observed in the footwall of the main fault, and appear to act as a localized nested graben to accomplish the down-to-the-east sense of motion (Figure 4). Towards the southern end of the mapped trace fewer auxiliary strands are observed (Figures 4 and 5). Occasional strands located in the hanging wall dip west and exhibit a down-to-the-west sense of motion as a result of hanging wall collapse (Figure 5).

Increasing stratigraphic dips and progressively larger offsets with depth are observed along D1 in the MCS data indicating its control on deposition in the south central portion of the bay (Figures 4 and 5). Figure 6 shows that as Fault D1 extends away from the intersection with the Silver Strand fault, the horizon 5 surface reaches its locally greatest depth of ~163 m and begins to shallow southward. Furthermore, Fault D1 appears to control the pathway of Chollas Creek, which is diverted southward upon contact with the fault trace and follows the fault towards the Silver Strand (Figures 4, 5, 7, 8, and 9). Chollas Creek follows Fault D1 south with the western channel bank potentially aligning with a paleo-scarp of Fault D1; the paleochannel intersects with the larger Sweetwater River paleochannel and exits San Diego Bay through the

Silver Strand (Figures 7 and 9). The exact location where the paleochannels breach is unknown due to gap in data coverage, but chirp profiles indicate that these paleochannels did not flow south of the current Sweetwater channel and likely exited between Crown Cove and Fiddlers Cove (Figure 9).

Potential recency of faulting for D1 is difficult to establish due to the shallow location of the first multiple reflection in chirp data and a general lack of coherent reflectors in the water saturated upper ~5 ms of data. The inset of Figure 3 shows a chirp profile near pier 18 that crosses Fault D1. The high-amplitude irregular surface that is displaced across Fault D1 and adjacent faults has been dated by amino acid stratigraphy and paleontological analysis (from a borehole adjacent to pier 18) to most likely correlate with MIS stage 5e (Kennedy and Clarke, 1996). Additional radiocarbon dates from beneath the Coronado Bridge may suggest that this fault is Holocene active, but conclusive evidence is not present in the high-resolution chirp profiles (Kennedy and Clarke, 1999).

Fault SB1 is a large fault in the southernmost portion of the study area that dips steeply to the east and exhibits a down-to-the-east sense of motion (Figure 2 and Figures 4, 5, 8, 10). The character and geometry of Fault SB1 is variable along strike; in the south displacement is concentrated onto a single fault and occasional hanging wall splay (Figure 10), as the fault trends northward deformation becomes distributed onto a series of sub-parallel fault strands that continue to have down to the east sense of motion (Figure 4). Figure 10 shows a nested chirp and MCS line that images Fault SB1's down-to-the-east sense of displacement, which develops into a negative flower structure towards the surface.

Figure 11 shows a fence diagram of southern chirp lines used to extend SB1's northern segment and connect it with a similar length segment that extends beyond our data coverage

into the southern extreme of San Diego Bay. The MCS data show progressively increasing offsets and stratigraphic dips with depth associated with the Fault SB1. Observed down-to-the-east offsets across SB1 in Figure 10 include an offset of ~11 m for horizon 1, an offset of ~21 m for horizon 2, an offset of ~25 m for horizon 3 and 4, and an offset of ~32 m for horizon 5 (Figure 10). Additionally, growth strata terminating against the fault are imaged in the high-resolution chirp data (Figures 10, 11, and 12).

Fault SB1 may offset a high amplitude irregular reflector with characteristics suggesting a sea level low-stand, although the location of the multiple makes interpretations difficult (Figures 10 and 11). In Figure 10, a bright high-amplitude reflector is observed to terminate directly above the potential low-stand reflector and trace of Fault SB1. This truncated reflector could be an indication of recent faulting, or may be the result of data resolution loss from fluid flow which is seen in the water column and has indented the seafloor above SB1. Therefore, although SB1 appears to exert some control on the geometry of the older Pleistocene low-stand deposit, no definitive evidence of Holocene movement is observed.

The gridded horizon 5 surface shows that the stratigraphy of southern San Diego Bay generally dips towards the west with several depositional basins formed by down-to-the-east movement along the Silver Strand, D1, and SB1 faults (Figure 6). For Fault D1, the horizon 5 gridded surface shows that subsidence reaches its greatest depth just south of the intersection with the Silver Strand fault and faults of the downtown graben, a pattern similar to that observed along the Silver Strand fault. Amino acid stratigraphy and paleontological analysis of material collected adjacent to pier 18 of the Coronado Bridge suggests mid-Pleistocene deposits at a depth of at least ~140 m, a depth similar to the interpreted depth of horizon 5 in the area. In the south central portion of San Diego Bay, a smaller more westerly oriented area of subsidence

is located between the overlapping tips of Fault D1 and Fault SB1 (Figure 6). This localized westerly oriented area of subsidence appears to correspond with a decrease in subsidence associated with Fault SB1 moving northward, and Fault D1 moving southward.

Stratigraphic dips are variable across the three main faults in south San Diego Bay. In the vicinity of the Coronado Bridge, the Silver Strand fault separates moderate to steeply westward dipping stratigraphy in the east, from gently flat lying to gently westward dipping stratigraphy to the west (Figure 3). Moving southward the stratigraphy of the eastern portion of the bay continues to dip west, but Fault D1 begins to accommodate more of the subsidence, and strata are observed to dip more steeply into D1 than in the north (Figures 4 and 5). Similar to the Silver Strand, the stratigraphy west of Fault D1 continues to dip gently westward, possibly a result of the offshore Silver Strand fault. South of the localized area of more westerly oriented subsidence between D1 and SB1 in the south central portion of the bay, this pattern of westward dips across faults shifts (Figures 6 and 8). The stratigraphy in the eastern portion of the bay continues to dip westward, but becomes more concentrated on Fault SB1. The steepness of dips progressively increases from north to south along SB1, with the steepest dips observed along the southernmost profile. Interestingly, the stratigraphy on the west side of SB1 changes from gently flat lying to slightly eastward dipping southward (Figures 8 and 10).

The spatial width of faulting is also variable along strike (Figure 2). Near the intersection between the Silver Strand, “downtown graben” faults, and Fault D1, faulting is confined to a relatively narrow zone. Southward of this intersection, the spatial width between the main fault strands and the number of associated strands increases toward the central part of the bay. This trend appears to reverse with faulting becoming more concentrated by the

southernmost MCS line (T196-a792; Figure 10) with a majority of the displacement observed on Fault SB1 and a couple of adjacent fault strands in the MCS data.

In the southwest corner of the study area, chirp data image two subparallel northeast trending auxiliary faults that extend from beneath the Silver Strand ~500 m into the bay to form a localized pop-up structure (Figure 13). The western strand appears to displace sediment within ~ 2 ms twtt of the bay floor and displaces the locally extensive irregular reflector interpreted to represent sea level low-stand, approximately ~5.7 m (Figure 14). In this area (Crown Cove), both the chirp profiles and the northeast trending fault are within 10-50 m of the shore and offer an opportunity for low-cost shore-based coring to ground truth the chirp data. Three cores were collected on a sand spit that has built out ~80 m since dredging of the area in 1945. Figure 15 shows the core locations, chirp profiles, and shorelines for a variety of periods. The 1941 aerial photograph (Figure 15d) and 1927 Nautical Chart (Figure 15e) show that the cores were collected at the pre-development shoreline on a subaerially exposed salt marsh or tidal flat.

The lithology of the cores consists of three main packages (Figure 16). The upper ~3 m of the cores are interpreted to be related to the post-dredge sand spit build out and deposition based on sediment characteristics and modern radiocarbon dates (Table 1 and Figure 17). Most of this artificial fill section consists of medium to fine grained clastic sands with abundant broken shell fragments. The lower portions of the artificial section vary between cores, with CC11 and CC13 exhibiting peaty sand deposits overlying a silty-sand section and core CC12 exhibiting cross-bedding of medium to fine sands, interpreted to be related to sand spit build out. A potential sand blow or liquefaction feature is observed in the cross-bedded section of core CC12 located above the interpreted dredge surface. The dredge surface is a sharp contact

that separates coarse sands above from clayey-silts below that are interpreted as marine or estuarine origin. The marine/estuarine clayey-silts are generally dark grey to very dark grey with occasional medium to fine sand stringers and scattered shells, both fragmented and whole. The lowest portion of the cores consists of alternating medium-coarse sands and marine silts that give way to oxidized coarse sands as seen in cores CC13 and CC12 (Figure 16). The contact between the basal sands and marine silts is sharp, and the lower basal sands are interpreted to represent the most recent sea-level transgression. Datable material collected throughout the natural portion of the cores gives an approximate age of ~1294 years before present (yrs BP) for the inundation of the Silver Strand bay side shoreline (Figure 17).

Figure 13 shows chirp line SSB02 with the location and approximate depth of the three cores. The sharp contact between the basal sands and overlying marine/estuarine silts should produce a high enough acoustic impedance contrast to be imaged in the chirp data. At the base of the cores in Figure 13, a medium to high amplitude irregular surface is seen diverging from the pop-up structure at the corresponding depth to be the inundation / transgressive surface observed in the cores. This surface is separated from the lower low-stand surface by a transparent homogenous package infilling the accommodation space that appears created by movement on the pop-up structure faults. To the east of the cores, the interpreted inundation surface looks to merge with the interpreted low-stand surface as part of the pop-up structure, and may then diverge again to the east (Figure 13).

Line SSB05 runs north-south perpendicular to SSB02 and images the western strand of the pop-up structure faults (Figure 14). SSB05 also images a small portion of the undredged San Diego Bay and shows a mostly homogenous sediment package overlying the interpreted low-stand surface. The western strand of the pop-up structure displaces sediment that may

correspond to the inundation surface observed in the Crown Cove cores, which would indicate movement in the last ~1,300 years.

4.5.2 Structural Analysis

Traditional conceptual models for pull-apart basins cannot fully explain the deformation patterns and fault geometry we observe in the San Diego Bay pull-apart basin (Figure 18). A Rose Canyon-Descanso fault pull-apart basin model can predict the orientation of faults in the northwestern portion of the basin (the Spanish Bight, Coronado, and Silver Strand faults), which are oriented at ~30-40° to the master strike slip faults. However, the northwest trending faults in the southeastern portion of the bay, as well as the La Nacion fault, are oriented at a high angle to the Rose Canyon fault, conflicting with a classical pull-apart basin model and suggesting the possibility for additional influences from other regional faults. Therefore, towards developing a more accurate model for the San Diego Bay pull-apart basin, we conduct a kinematic analysis using the regional fault orientations and plate boundary conditions to explain the faulting seen in the San Diego pull-apart basin in terms of two end member models, simple shear dominated and pure shear dominated transtension.

The north-northeastly trending oblique faults in the northwestern half of the San Diego Bay pull-apart basin (hereafter referred to as Group-1 faults) have three primary splays: the Spanish Bight, Coronado, and Silver Strand faults (Figure 1 and 2) (Kennedy and Welday, 1980; Kennedy and Clarke, 1999). Group-1 faults have an average strike of N1.5°E. The north-northwesterly trending faults in the southeastern part of San Diego Bay (hereafter referred to as Group-2 faults) have an average strike of N22.7°W. Faults in the La Nacion Fault zone have an average strike of N8.7°W.

Table 2 provides the average surface trends represented in Figure 18 for faults in Group-1, Group-2, and the La Nacion Fault zone (thin solid lines), the trends of major strike-slip faults (thick dashed lines), plate motion vectors (large outlined arrows) and maximum and minimum horizontal stress directions (solid black arrows). We assume faulting observed in the sedimentary basin is representative of faults in the basement. The maximum horizontal compressional stress orientation, σ_c, is assigned N7°E (Hardebeck and Hauksson, 1999; Hardebeck and Hauksson, 2001) and the maximum horizontal extension direction, σ_e, is assumed to be 90° to σ_c.

The Group-1 trend is nearly parallel to σ_c, perpendicular to σ_e, and is oriented ~40° to the trend of the Rose Canyon and Descanso faults. This geometry is well described by both analog and numerical models of pull apart basins (e.g. Dooley and McClay, 1997; Dooley and Schreurs 2012; van Wijk et al, 2017). Testing our observations with kinematic models yields a similar result. Following the method of Teyssier et al., (1995), we assign α to be the angle between the plate margin and plate motion vector (N43°W), and θ to be the angle between the direction of maximum instantaneous horizontal extension (assumed to be coaxial with σ_e) and the plate margin. Assuming that the average trend of Rose Canyon fault and Descanso fault (~N26°W) acts as the plate margin boundary for the San Diego Bay pull-apart basin, we find that $\alpha = 17°$ and $\theta = 57°$. These values are in close agreement to the predicted value of 54° using $\theta = 1/2(\alpha + 90)$ (Tikoff and Teyssier, 1994). Furthermore, these values for α and θ also indicate that the proposed Rose Canyon-Descanso basin would be simple shear dominated, with ~80% of the deformation between the Rose Canyon fault and the Descanso fault being accommodated through normal faulting. Figure 19b represents our conceptual model to explain the orientation of Group-1 faults in terms of a Rose Canyon-Descanso fault connection.

Although no definitive evidence for a connection between the Rose Canyon fault and San Miguel-Vallecitos fault has been published, we believe based on kinematic relationships that the structure of the Group-2 and La Nacion faults are partially controlled by the San Miguel-Vallecitos fault, with its northernmost segment, the Vallecitos fault, mapped ~30 km southeast of San Diego Bay. The Group-2 and La Nacion fault zones are oriented at 27° and 41°degrees to the San Miguel-Vallecitos fault, which trends ~N50°W. If we assume dextral motion along a Rose Canyon–San Miguel-Vallecitos system, rather than the Rose Canyon–Descanso system, provides plate boundary conditions for Group-2 faults, we can apply the same ideas to test for kinematic relationships. This geometry yields values of $\alpha = 5°$and $\theta = 45°$, which are in close agreement with the predicted value of $\theta = 50°$ (Tikoff and Teyssier, 1994). This geometry would implie that the eastern San Diego pull-apart basin would be strongly simple shear dominated with 0% strike-slip partitioning (Teyssier et al., 1995).

However, the oblique angle of Group-2 faults and the La Nacion fault system to the maximum compressional stress σ_c, may be an indication that the maximum horizontal extensional stress direction, σ_e, is not the best representation of the minimum instantaneous shortening direction for the eastern portion of the San Diego Bay pull-apart basin. Alternatively, if we assume that the minimum instantaneous shortening direction is oriented perpendicular to the average trend of Group-2 faults we determine a value of $\alpha = 5°$and $\theta = 75°$, which would indicate a strongly simple shear dominated basin but with 90% strike-slip partitioning. Assuming that the minimum instantaneous shortening direction is perpendicular to the average trend of the La Nacion fault zone we find that $\alpha = 5°$and $\theta = 61°$, again indicating a strongly simple shear component to deformation but with slightly less strike slip partitioning at 80%. Either way, the observed geometry in Figure 18 and the kinematic analysis suggests

Group-2 is experiencing simple-shear transtension influenced by the San Miguel-Vallecitos system. The difference between Group-2 and La Nacion trends may be attributed to a mid-basin transition zone, where the western margin of Group-2 is influenced by the Rose Canyon-Descanso stepover, but the La Nacion fault zone is oriented optimally if a stepover exists between San Miguel-Vallecitos fault and Rose Canyon fault (Figure 19c).

4.6 Discussion

4.6.1 Subsurface architecture, fault linkage, and stratigraphic controls beneath San Diego Bay

As shown in the gridded horizon surface and MCS profiles presented in this chapter, faults D1 and SB1 exert a major influence on the stratigraphic character of southeastern San Diego Bay. Together with the faults of Group-1, the collective east side down displacement results in the distribution of localized depositional centers throughout San Diego Bay, and may therefore be manifestations of terraced sidewall faults that are observed in analog models of pull-apart basins (Figure 6) (Dooley and McClay, 1997; Rahe et al., 1997; Dooley and Schreurs, 2012). The two groups of faults would represent terraced sidewall faults for two separate pull-apart basins (Figure 19b,c), with Group-1 faults representing the western boundary of a western basin, and Group-2 faults representing the western boundary of an eastern basin, with a transition zone in between.

The spatial pattern of subsidence observed in the gridded surface for horizon 5 in the southeastern portion of San Diego Bay suggests that the potential terraced sidewall faults (faults D1 and SB1) may be playing a more significant role than simply accommodating localized subsidence and deposition. As mentioned previously, the localized westerly oriented

area of subsidence in the south-central portion of San Diego Bay lies between D1 and SB1, and corresponds to a decrease in the apparent displacement on both faults. Fault SB1 accommodates a larger amount of apparent displacement southward (compared to its northern segment), while Fault D1 accommodates greater displacement northward (again compared to its southern segment). A possible explanation for the apparent change in displacement gradients is that the faults located in the westerly localized area of subsidence represent a relay structure that is connecting these two potential sidewall faults (Figure 5 and 6) (Dooley and McClay, 1997; Fossen and Rotevatn, 2016). Relay structures typically form in areas of overlap between two closely spaced normal faults (Fossen and Rotevatn, 2016).

The relay faults would act to transfer displacement from fault D1 to fault SB1, effectively placing the fault tips of SB1 and D1 in a stress shadow and shutting down displacement on the fault sections between the relay structure and the fault tip (Fossen and Rotevatn, 2016). The presence of relay faults linking these two terraced sidewall faults would imply that the western pull-apart basin may be starting to develop through-going linking faults between the master strike slip segments. Such a through-going fault is a common feature in models of pull-apart basins (Dooley and McClay, 1997; van Wijk et al., 2015; Wu et al, 2009; Rahe et al., 1997; Dooley and Schreurs, 2012). The subsidence associated with the relay faults is a potential indication that the relay structure has been breached and a linked sidewall fault has developed (Dooley and McClay, 1997; Fossen and Rotevatn, 2016). However, the variable spatial distribution of the MCS lines does not allow for complete mapping of the relay structure so the full extent of the connection is uncertain.

If the short discontinuous segments in the southern extreme of San Diego Bay that are similarly oriented to SB1, are in fact one continuous fault (Figure 1 and 2), then the linked D1-

SB1 fault would extend ~9 km and be oriented sub-parallel to the long axis of the bay. The linked D1-SB1 fault would then be favorably oriented with the gravity anomalies and the interpreted crystalline basement that underlies the San Diego pull-apart basin (Marshall, 1989; Elliot, 1970). Additionally, the deepest portion of the basin is located beneath south San Diego Bay and coincides with the approximate area where SB1 begins to accommodate increased subsidence (Figure 10) (Marshall, 1989). The similar orientation between the potential linked sidewall basin fault (D1-relay-SB1 structure) and the gravity anomalies/crystalline basement suggests a connection between potential basement faults and faults D1-SB1.

In addition to the development of linked sidewall faults, the spatial distribution of faults and the sense of displacement in San Diego Bay is also consistent with analog and dynamic models of pull apart basins. In the northern portion of the bay, the Spanish Bight and Coronado faults are located near the northern termination of the potential Rose Canyon-Descanso fault pull-apart basin (Figure 2 and 19b). High-resolution chirp data image stratal-collapse into the fault zone and rotated wedges associated with both faults in the upper ~50 m of bay sediments (Maloney, 2013, Marquez, 2017). These types of sedimentary structures are typically associated with areas of localized transtension and the development of negative flower structures in strike-slip environments (Yeats et al., 1997). Offshore of the Coronado Peninsula, combined chirp and MCS data image predominately dip slip displacement for the Group-1 faults (Maloney, 2013). Both observations are consistent with analog models of pull-apart basins that predict the formation of negative flower structures and nested grabens close to the principal displacement zones, and increasing dip slip motion towards the center of the pull-apart basin (e.g., Dooley and McClay, 1997; Rahe et al., 1997; Dooley and Schreurs, 2012).

The Group-2 faults located in the southeastern portion of San Diego Bay exhibit a similar characteristic with normal, down-to-the-east displacement observed to decrease on fault D1 towards downtown San Diego, as well as a consolidation of adjacent fault strands to form a localized nested graben structure with the Silver Strand and downtown graben faults near the edge of the interpreted eastern pull-apart basin (Figure 19c) (Kennedy and Clarke, 1996). Towards the center of the proposed eastern pull apart basin, increased dip slip motion is observed on D1 as well as an increase in the number of adjacent strands. Both observations are consistent with analog models of pull-apart basins (Dooley and Schreurs, 2012). However south of the potential relay structures, fault SB1 deviates from the analog model. As observed in the southernmost seismic profiles (Figures 8 and 10), the stratigraphy west of fault SB1 changes from gently westward dipping north of the relay structures, to flat-lying and then gently eastward dipping towards the south. This collapse into the main strand of SB1 and the formation of a negative flower structure observed in line T196-a792 suggests that this region of the eastern San Diego Bay pull apart basin may be experiencing an increased strike-slip component of deformation. The presence of the localized pop-up structure to the west of SB1 provides additional evidence of an increased strike-slip component. The location of such a structure (characteristic of transpression) in the middle of a pull-apart basin is interesting, but may be explained as the formation of a cross-basin fault, which frequently exhibit localized transpression in analog pull-apart basins models (Dooley and McClay, 1997; Rahe et al., 1997; Dooley and Schreurs, 2012). Alternatively, the localized pop-up may be the result of a reversed polarity structure from unidirectional rupture on the master strike-slip segments (Ben Zion et al., 2012).

The diversion of Chollas Creek southward by fault D1 and the paleochannel's western bank alignment with the fault's potential paleoscarp, may be evidence for D1's activity during the last glacial maximum (LGM) when Chollas Creek would have been draining through the subaerially exposed San Diego Bay. Offshore San Diego Bay, recent work has successfully mapped several paleochannels interpreted to be formed during MIS stage 2 that extend away from San Diego Bay and the Point Loma peninsula (Graves, 2017). The location of interpreted extension of the Sweetwater paleochannel offshore, matches very well with the location of interpreted breaching of the Silver Strand by the combined Sweetwater-Chollas Creek paleochannel imaged within the bay (Figure 9) (Graves, 2017). Additionally, the presence of potential fluid flow along SB1 imaged in the southern chirp profiles suggests that the faults of the southeastern San Diego Bay pull-apart may provide a vertical pathway for the regional subsurface hydrologic system.

4.6.2 Conceptual model for the San Diego Bay pull-apart basin

Since the 1970s, considerable work has focused on understanding the nature of pull-apart basins and regions experiencing transtensional deformation. Three different approaches are typically used to model 3-dimensional deformation and slip patterns in relation to fault geometry and structural development: (1) Analog models involving laboratory experiments using clay and sand as proxies to crustal deformation (Dooley and McClay, 1997; Rahe et al, 1998; Wu et al., 2009), (2) kinematic models based on static stress and strain conditions, plate motion boundary conditions, and assumed material properties (Sanderson and Marchini, 1984; Fossen and Tikoff, 1993; Teyssier et al., 1995; Tikoff and Teyssier, 1994), and (3) dynamic models grounded in continuum mechanics and conservation laws focused on temporal changes in a system by use of finite element simulations (Rogers, 1980; Golke et al., 1994; van Wijk et

al., 2017). With conventional pull-apart basin models unable to explain the various orientations of the Group-1, Group-2, and La Nacion faults, we provide a new structural interpretation for the San Diego Bay pull-apart basin and compare it to results from these three types of models.

As discussed previously, the ~40° orientation between the linking Group-1 faults and the master strike slip segments (the Rose Canyon and Descanso faults) is consistent with most classical descriptions of pull-apart basins and with all three model approaches discussed above (Mann, 1983; Burchfiel et al., 1987). Both analog and dynamic models show sidewall faults at a ~35-40° angle to non-overlapping principle displacement zones (representative of the Rose Canyon–Descanso system), and the formation of a single basin (Rahe et al., 1998; Rogers, 1980; Golke et al., 1994; van Wijk et al., 2017). The results of the kinematic analysis suggest that wrench dominated transtension (simple shear) with minimal amounts strike-slip partitioning is expected between a Rose Canyon-Descanso system. Since the basin faults are kinematically linked to the master strike-slip faults this result is expected, and supported by observations of progressively increasing dip slip towards the center of the western pull apart basin, with minor amounts of potential strike-slip deformation observed near the edge of the stepover on the Spanish Bight and Coronado Bank faults. Figure 19b illustrates our conceptual model for Group-1 faults.

Based on the near parallel alignment between Group-2 faults and a potential Rose Canyon–Descanso pull-apart (Figure 19a,b); analog, kinematic, and numerical models of pull-apart basin development would predict strike-slip dominated motion along Group-2 faults and would imply they are simply a southern extension of the Rose Canyon fault. However, most evidence shows normal dominated deformation in the opposite sense, away from the pull-apart basin. In addition, the presence of the La Nacion fault system, which is between 5 and 10 km

outside the master fault segments, is difficult to explain by the Rose Canyon-Descanso fault stepover model (Figure 19b). Therefore, we proposed that the faults in the eastern portion of the basin are controlled/influenced by a Rose Canyon-San Miguel-Vallecitos connection. The more favorable orientation of Group-2, and especially the La Nacion faults, to a potential Rose Canyon-San Miguel-Vallecitos pull apart model (~27° and ~41° respectively), provide some evidence that such a model is valid (Figure 19c). However, the results of the kinematic analysis suggest that the deformation between the principal displacement zones in such a model should exhibit a strong degree of strike-slip partitioning; contrasting with the normal dominated displacement observed in the proposed eastern basin. Interestingly, several indicators of increased strike-slip deformation are observed in the southernmost seismic data (i.e., negative flower structure above SB1 and the auxiliary pop-up structure), which may be an indication of increasing strike-slip deformation.

With the pervasive down-to-the-east fault motion in San Diego Bay, it appears that the right-step between the Rose Canyon and Descanso faults dominates the overall basin architecture. However, based on the more favorable geometry of the San Miguel-Vallecitos system it appears to be responsible for the different orientation of Group-2 faults, the La Nacion fault zone as well as the uplifted, faulted region in northwest Tijuana, Mexico. Translation and rotation of crustal blocks has been invoked to explain the tectonic evolution of the ICB (e.g., Nicholson et al., 1994), therefore we conceptually describe the kinematics of the San Diego region as an interaction between three brittle, upper crustal blocks. In Figure 20 consider block B as a reference block, with blocks A and C both moving northwest at different rates, but nearly identical azimuths. Boundaries between blocks are defined by major faults: the Rose Canyon fault (block A and B boundary), the Descanso fault (block A and C boundary)

and the San Miguel-Vallecitos fault (block C and B boundary). The orientation of the boundary faults relative to block motion vectors can explain the various structural domains in and around the San Diego Basin. Regions 1-4 in Figure 20 are distinct deformation zones corresponding to Group-1 faults (1), Group-2 faults (2), the Los Buenos fault zone (3) and the transition zone between Group-1 and Group-2 faults (4).

Regions 1 and 2 are described by the corresponding pull-apart basin models (figures 19b,c), with some complex overprinting occurring at the boundary and in region 4. As first noted by Kennedy and Clarke (1996), 'fault D1 is a major fault in San Diego Bay that separates the northwest trending faults of south San Diego Bay from the more northerly trending faults in the north bay'; therefore, the transition between Group-1 and Group-2 is likely to exist between the D1 and Silver Strand faults, and may be located directly beneath the current Silver Strand tombolo. Region 4 likely experiences competing hanging wall subsidence associated with Group-1 faults overprinting footwall effects of Group-2, or vice versa. The uplift of region 3, based on elevation differences between Pleistocene terrace deposits (Ellis and Lee, 1919) can be described by footwall uplift across a broad zone of down-to-the-east normal faults. This creates a heterogeneous strain field responsible for the complex deformation in northwestern Tijuana, where transtensional deformation from the San Diego basin is overprinting regional scale (and likely older) transpressional deformation.

We put forward this conceptual block model to provide a first order starting point to begin resolving questions about the San Diego pull-apart basin. San Diego Bay appears to occupy a complex region of subsidence overlying two competing pull-apart basins. Our conceptual model does not however address several observations and features related to the San Diego Bay pull-apart basin. For example, no clear connection between the La Nacion fault

system and the Rose Canyon fault has been identified, as our model predicts would exist. Additionally, no conclusive evidence for recent movement on the La Nacion fault has been published despite its apparent structural relationship to the San Diego Bay pull-apart basin. The apparent asymmetry of the San Diego Bay pull-apart basin with both Group-1 and Group-2 faults appearing to collapse into the La Nacion fault (or an unmapped eastern strand of the Rose Canyon fault) is not addressed by our model.

4.6.3 Recency of Faulting and Seismic Hazard

The Pleistocene marine terraces and sea level low-stand observed in the seismic data are used for subsidence and slip rate estimates in San Diego Bay. The offset bright amplitude reflector image by chirp data adjacent to pier 18 of the Coronado Bridge (inset Figure 3), likely corresponds to the MIS stage 5e Nestor Terrace as indicated by amino acid stratigraphy and paleontological analysis. The Nestor Terrace is located at an elevation of 22-23 m at Point Loma and dates to ~120 ka (Muhs et al., 1988; Kern and Rockwell, 1992). Using an average elevation ~ -18 m for the Nestor Terrace adjacent to the Coronado Bridge and assuming that both locations are experiencing the same regional uplift rate of 0.13-0.14 mm/yr, an approximate subsidence rate for the central portion of San Diego Bay is 0.34 mm/yr. Using the apparent 4 m offset of the Nestor Terrace across the associated strand of fault D1 yields an apparent vertical slip rate of 0.03 mm/yr for that auxiliary strand. Alternatively, the high amplitude reflector interpreted to represent the Nestor Terrace, may have been overprinted with the MIS stage 5a Bird Rock Terrace (~80 ka), as has been observed in other locations around San Diego (Kern and Rockwell, 1992). Using a 9-11 m elevation for the Bird Rock Terrace on Point Loma yields an estimated subsidence rate of 0.36 mm/yr for the central portion of San Diego Bay.

In the Crown Cove area, the interpreted sea level low-stand is offset ~5.7 m as a result of movement on the localized pop-up structure. We assume an age of 20-15 ka for a stable sea level low-stand in southern California responsible for the apparent erosional surface (Reynolds and Simms, 2015). Therefore, the faults associated with the pop-up structure have an apparent vertical slip rate of 0.29-0.38 mm/yr. The offset of the interpreted latest transgressive surface observed in SSB05 (Figure 14) in the Crown Cove area suggests that the pop-up structure faults are Holocene active and may have ruptured in the past ~1,300 years. The homogeneous character of the sediments above the interpreted sea level low-stand in the southern chirp profiles does not facilitate the determination of post-LGM movement on other faults in Group-2. However, several truncated reflectors directly above the mapped fault strands may be evidence for recent faulting (Figure 10).

Fault stepovers have long been recognized as areas of potential earthquake nucleation and termination (e.g., Oglesby, 2005; Wesnousky, 2008). Empirical data of historical earthquake surface ruptures indicate that stepover distances greater than ~5 km typically act as barriers to through-going earthquake ruptures. Therefore, a through-going rupture across the ~10 km wide Rose Canyon–Descanso fault stepover is not predicted. The proposed Rose Canyon–San Miguel-Vallecitos stepover would be on the order of ~3-4 km wide, a distance that historical ruptures have jumped. Additionally, the linkage of D1 and SB1 via relay faults may indicate the formation of a through-going cross basin fault, which would provide a fault structure for potential future earthquakes to continue through San Diego Bay. The smaller stepover distance and potential cross basin fault would allow for potentially longer earthquake ruptures, which in turn would results in larger magnitude earthquakes. However, without conclusive evidence of faulting south of San Diego Bay to connect the two larger strike-slip

systems, a potential cross basin fault earthquake pathway remains speculative. Regardless, small earthquakes and static stress change within the San Diego pull-apart basin might act to trigger earthquakes on any of the three major faults, as has potentially happened in the past (Oglsbey, 2005; Marquez, 2017; Singleton et al., 2019). Additional studies into faulting south and east of San Diego Bay are warranted to better resolve regional fault connections.

4.7 Conclusion

The results of this study show the value of legacy MCS data to investigate fault structures in urban waterways where data collection may no longer be feasible. Additionally, the improved resolution from reprocessing the legacy MCS dataset allowed for the correlation of stratigraphy across San Diego Bay. When combined with the high-resolution chirp profiles, the nested dataset allowed for a more comprehensive interpretation of stratigraphy and recency of faulting beneath San Diego Bay. The results of the gridded surface for horizon 5 show several localized depositional centers adjacent to the linking faults imaged in San Diego Bay. These faults likely form a set of terraced sidewall faults that are predicted by analog models of pull-apart basins. The relative amount, and sense of displacement observed on the faults in San Diego Bay in the nested seismic dataset is consistent with predicted results from models of pull-apart basins. In the southeastern portion of San Diego Bay, fault D1-SB1 looks to be a continuous fault structure connected by relay faults. The D1-SB1 linked fault appears to control deposition in the southern portion of San Diego Bay and is similarly oriented to gravity anomalies beneath the bay.

The San Diego Bay pull-apart basin can be divided into a western and eastern basin based on the different orientation of two groups of faults (Group-1 and Group-2/La Nacion

fault zone). Group-1 faults are located in the northwestern portion of San Diego Bay and are well described by classical pull-apart basin models, and support a Rose Canyon–Descanso fault pull-apart basin to explain the subsidence of San Diego Bay. The near parallel orientation of Group-2 and the La Nacion faults to the Rose Canyon fault are in contrast to this model and suggest an additional influence from other regional faults. A potential pull-apart basin between the Rose Canyon and the San Miguel-Vallecitos faults would explain the orientations of the Group-2 and La Nacion faults. Kinematic analysis of the Rose Canyon–San Miguel-Vallecitos pull-apart model predicts a significant component of strike-slip partitioning, which is not observed in the seismic profiles. However, on the southernmost profiles, several indicators of strike-slip motion suggest an increase in strike-slip deformation in the southern portion of the bay. The favorable orientation of the Group-2 and La Nacion faults as well as the potential formation of a linked D1-SB1 fault, may be evidence for a Rose Canyon–San Miguel-Vallecitos fault connection, but further work is warranted.

4.8 Acknowledgments

We would like to thank Jared Kluesner for his assistance and helpful discussions while reprocessing the legacy MCS data. We would also like to thank the SDSU and UCSD earth science graduate students for their assistance in the field. This research was supported by the Southern California Earthquake Center (SCEC), award number 19107 and contribution number 10099. SCEC is funded by National Science Foundation Cooperative Agreement EAR1033462 and U.S. Geological Survey Cooperative Agreement G12AC20038. This research was also supported by the Shepard Foundation at Scripps Institution of Oceanography.

Chapter 4, in part is currently being prepared for submission for publication of the material. Singleton, D. M., Maloney, J. M., Brothers. D., Klotsko, S., Driscoll, N., Rockwell, T. Recency of faulting and subsurface architecture of the San Diego Bay pull-apart basin, California USA. The dissertation author was the primary investigator and author of this material.

4.9 References

Agnew, D.C., and Legg, M., 1979. Earthquake history of San Diego. *Earthquakes and Other Perils: San Diego Region, San Diego Association of Geologists, San Diego, Calif*, pp.123-128.

Astiz, L. and Shearer, P.M., 2000. Earthquake locations in the inner Continental Borderland, offshore southern California. *Bulletin of the Seismological Society of America*, *90*(2), pp.425-449.

Ben-Zion, Y., Rockwell, T.K., Shi, Z. and Xu, S., 2012. Reversed-polarity secondary deformation structures near fault stepovers. *Journal of Applied Mechanics*, *79*(3).

Bohannon, R.G. and Geist, E., 1998. Upper crustal structure and Neogene tectonic development of the California continental borderland. *Geological Society of America Bulletin*, *110*(6), pp.779-800.

Bronk Ramsey, C., 2017. OxCal Program, Version 4.3. *Oxford Radiocarbon Accelerator Unit: University of Oxford*.

Brothers, D.S., Conrad, J.E., Maier, K.L., Paull, C.K., McGann, M., and Caress, D.W., 2015, The Palos Verdes Fault offshore Southern California: Late Pleistocene to present tectonic geomorphology, seascape evolution, and slip rate estimate based on AUV and ROV surveys: Journal of Geophysical Research: Solid Earth, v. 120, p. 4734–4758, doi:10.1002/2015JB011938.

Burchfiel, B.C., Hodges, K.V. and Royden, L.H., 1987. Geology of Panamint Valley-Saline Valley pull-apart system, California: Palinspastic evidence for low-angle geometry of a Neogene range-bounding fault. *Journal of Geophysical Research: Solid Earth*, *92*(B10), pp.10422-10426.

Conrad, J., Brothers, D., Maier, K.L., Ryan, H.F., Dartnell, P., and Sliter, R.W., 2018, Right-lateral fault motion along the slope-basin transition, Gulf of Santa Catalina, Southern California: SEPM Special Publication No. 110, doi:10.2110/sepmsp.110.07

Demere, T.A., 1983. The Neogene San Diego basin: a review of the marine Pliocene San Diego formation.

Dixon, T., Decaix, J., Farina, F., Furlong, K., Malservisi, R., Bennett, R., Suarez-Vidal, F., Fletcher, J. and Lee, J., 2002. Seismic cycle and rheological effects on estimation of present-day slip rates for the Agua Blanca and San Miguel-Vallecitos faults, northern Baja California, Mexico. *Journal of Geophysical Research: Solid Earth*, *107*(B10), pp.ETG-5.

Dooley, T. and McClay, K., 1997. Analog modeling of pull-apart basins. *AAPG bulletin*, *81*(11), pp.1804-1826.

Dooley, T.P. and Schreurs, G., 2012. Analogue modelling of intraplate strike-slip tectonics: A review and new experimental results. *Tectonophysics*, *574*, pp.1-71.

Ellis, A.J. and Lee, C.H., 1919. Geology and ground waters of the western part of San Diego County, California. Supply Pap. *US geol. Surv*, *446*, pp.121-123.

Fletcher, J.M., Teran, O.J., Rockwell, T.K., Oskin, M.E., Hudnut, K.W., Mueller, K.J., Spelz, R.M., Akciz, S.O., Masana, E., Faneros, G. and Fielding, E.J., 2014. Assembly of a large earthquake from a complex fault system: Surface rupture kinematics of the 4 April 2010 El Mayor–Cucapah (Mexico) Mw 7.2 earthquake. *Geosphere*, *10*(4), pp.797-827.

Fossen, H. and Tikoff, B., 1993. The deformation matrix for simultaneous simple shearing, pure shearing and volume change, and its application to transpression-transtension tectonics. *Journal of Structural Geology*, *15*(3-5), pp.413-422.

Fossen, H. and Rotevatn, A., 2016. Fault linkage and relay structures in extensional settings—A review. *Earth-Science Reviews*, *154*, pp.14-28.

Frez J, González JJ, Acosta JG, Nava FA, Méndez I, Carlos J, García-Arthur RE, Alvarez M. 2000. A detailed microseismicity study and current stress regime in the Peninsular Ranges of northern Baja California, Mexico: The Ojos Negros region. Bulletin of the Seismological Society of America. 1;90(5):1133-42.

Gastil, R.G., Patterson, D.L., and Abbott, P.L. 1979. The Valle Formation-physical stratigraphy and depositional model, southern Vizcaino Peninsula, Baja California Sur. In *Baja California Geology, Field Guides and Papers. Geological Society of America Annual Meeting Guidebook, San Diego, California* (pp. 73-76).

Gingery, J.R., Rugg, S.H., Rockwell, T.K. and Hilton, B.R., 2010. Fault Hazard Characterization for a Transportation Tunnel Project in Coronado, California.

Gölke, M., Cloetingh, S. and Fuchs, K., 1994. Finite-element modelling of pull-apart basin formation. *Tectonophysics*, *240*(1-4), pp.45-57.

Graves, L., 2017. *Tectonic and eustatic control on channel formation, erosion, and deposition in the San Diego Bight, CA* (Doctoral dissertation, UC San Diego).

Hardebeck, J.L. and Hauksson, E., 1999. Role of fluids in faulting inferred from stress field signatures. *Science*, *285*(5425), pp.236-239.

Hardebeck, J.L. and Hauksson, E., 2001. Crustal stress field in southern California and its implications for fault mechanics. *Journal of Geophysical Research: Solid Earth*, *106*(B10), pp.21859-21882.

Hart, M.W., 1974. Radiocarbon Ages of Alluvium Overlying La Nacion Fault, San Diego, California. *Geological Society of America Bulletin*, *85*(8), pp.1329-1332.

Hirabayashi, C.K., Rockwell, T.K., Wesnousky, S.G., Stirling, M.W. and Suarez-Vidal, F., 1996. A neotectonic study of the San Miguel-Vallecitos fault, Baja California, Mexico. *Bulletin of the Seismological Society of America*, *86*(6), pp.1770-1783.

Holmquist, J.R., Reynolds, L., Brown, L.N., Southon, J.R., Simms, A.R. and MacDonald, G.M., 2015. Marine radiocarbon reservoir values in southern California estuaries: interspecies, latitudinal, and interannual variability. *Radiocarbon*, *57*(3), pp.449-458.

Kennedy, M.P., 1975. Geology of the western San Diego metropolitan area, California: Del Mar, La Jolla, and Point Loma quadrangles. *Calif. Div. Mines and Geol. Bull. A*, *200*, pp.709-722.

Kennedy, M.P. and Clarke, S.H., 1996. *Analysis of late Quaternary faulting in San Diego Bay and Hazard to the Coronado Bridge* (Vol. 97). California Department of Conservation, Division of Mines and Geology.

Kennedy, M.P. and Clarke, S.H., 1999. *Age of Faulting in San Diego Bay in the Vicinity of the Coronado Bridge, An Addendum to: Analysis of late Quaternary faulting in San Diego Bay and Hazard to the Coronado Bridge* (Vol. 97). California Department of Conservation, Division of Mines and Geology.

Kennedy, M.P. and Tan, S., SS, 2005. *Geologic map of the San Diego*, *30*, p.x60.

Moore, G.W. and Kennedy, M.P., 1975. Quaternary faults at San Diego Bay, California. *J Res US Geol Surv*, *3*, pp.589-595.

Kennedy, M.P. and Welday, E.E., 1980. Character and recency of faulting offshore, metropolitan San Diego. *California: California Division of Mines and Geology Map Sheet*, *40*(1), pp.50-000.

Kern, J.P. and Rockwell, T.R., 1992. Chronology and deformation of Quaternary marine shorelines, San Diego County, California, in Quaternary Coasts of the United States: Marine and Lacustrine Systems, SEPM Special Publication No. 48. P. 377-382

Kies, R.P., 1982. *Paleogene sedimentology, lithostratigraphic correlations and paleogeography, San Miguel Island, Santa Cruz Island, and San Diego, California* (Doctoral dissertation, San Diego State University, Department of Geological Sciences).

Legg, M.R., 1985. *Geological structure and tectonics of the Inner Continental Borderland offshore northern Baja California, Mexico*. PhD Thesis. University of California, Santa Barbara.

Legg, M. R., Wong, V., & Suarez, F. 1991. Geologic Structure and Tectonics of the Inner Continental Borderland of Northern Baja California: Chapter 9: Part III. Regional Geophysics and Geology.

Legg, M. R., M.D. Kohler, N. Shintaku, and D.S.Weeraratne, 2015, High-resolution mapping of two large-scale transpressional fault zones in the California Continental Borderland: Santa Cruz-Catalina Ridge and Ferrelo faults, J. Geophys. Res. Earth Surf., 120, doi:10.1002/2014JF003322.

Lindvall, S.C. and Rockwell, T.K., 1995. Holocene activity of the Rose Canyon fault zone in San Diego, California. *Journal of Geophysical Research: Solid Earth*, *100*(B12), pp.24121-24132.

Magistrale, H., 1993. Seismicity of the Rose Canyon fault zone near San Diego, California. *Bulletin of the Seismological Society of America*, *83*(6), pp.1971-1978.

Maloney, J.M., 2013. *Fault segments and step-overs: Implications for geohazards and biohabitats*. University of California, San Diego.

Maloney, J.M., Driscoll, N., Kent, G., Duke, S., Freeman, T., Bormann, J., Anderson, R. and Ferriz, H., 2016. Segmentation and step-overs along strike-slip fault systems in the inner California borderlands: Implications for fault architecture and basin formation. *Applied Geology in California, Environmental Engineering Geologists*, *26*, pp.655-677.

Mann, P., Hempton, M.R., Bradley, D.C. and Burke, K., 1983. Development of pull-apart basins. *The Journal of Geology*, *91*(5), pp.529-554.

Marquez, E., 2017, Rose-Canyon fault zone architecture at releasing step, San Diego, CA, M.S. Thesis, San Diego State University.

Mann, P., Hempton, M.R., Bradley, D.C. and Burke, K., 1983. Development of pull-apart basins. *The Journal of Geology*, *91*(5), pp.529-554.

Jackson, J. and McKenzie, D., 1983. The geometrical evolution of normal fault systems. *Journal of Structural Geology*, *5*(5), pp.471-482.

Minch, J.A., 1967. Stratigraphy and structure of the Tijuana-Rosarito Beach area, northwestern Baja California, Mexico. *Geological Society of America Bulletin*, *78*(9), pp.1155-1178.

Moore, G.W., 1972. Offshore extension of the Rose Canyon fault, San Diego, California. *Geol. Surv. Profess. Pap*, pp.800-2.

Muhs, D.R., Kennedy, G.L. and Rockwell, T.K., 1988. Uranium-series ages of corals from marine terraces, Pacific coast of North America: Implications for the timing and magnitude of late Pleistocene sea level changes. In *Programs and Abstracts of the 10th Biennial Meeting* (p. 140).

Nicholson, C., Sorlien, C.C., Atwater, T., Crowell, J.C. and Luyendyk, B.P., 1994. Microplate capture, rotation of the western Transverse Ranges, and initiation of the San Andreas transform as a low-angle fault system. *Geology*, *22*(6), pp.491-495.

Oglesby, D.D., 2005. The dynamics of strike-slip step-overs with linking dip-slip faults. *Bulletin of the Seismological Society of America*, *95*(5), pp.1604-1622.

Rahe, B., Ferrill, D.A. and Morris, A.P., 1998. Physical analog modeling of pull-apart basin evolution. *Tectonophysics*, *285*(1-2), pp.21-40.

Reimer, P.J., Bard, E., Bayliss, A., Beck, J.W., Blackwell, P.G., Ramsey, C.B., Buck, C.E., Cheng, H., Edwards, R.L., Friedrich, M. and Grootes, P.M., 2013. IntCal13 and Marine13 radiocarbon age calibration curves 0–50,000 years cal BP. *Radiocarbon*, *55*(4), pp.1869-1887.

Reveal, 2019, https://www.shearwatergeo.com/6/reveal-software, last accessed April 19, 2019.

Reynolds, L. C., & Simms, A. R. 2015. Late Quaternary relative sea level in southern California and Monterey Bay. *Quaternary Science Reviews*, *126*, 57-66.

Rogers, D.A., 1980. Analysis of pull-apart basin development produced by en echelon strike-slip faults. Sedimentation in oblique-slip mobile zones: Int. Association of Sedimentologist Special Publication 4.

Ryan, H. F., M.R. Legg, J.E. Conrad, and R.W. Sliter, 2009, Recent faulting in the Gulf of Santa Catalina: San Diego to Dana Point, in Earth Science in the Urban Ocean: The Southern California Continental Borderland, edited by H. Lee and W. Normark, Geol. Soc. Am. Spec. Pap., 454, 291–315.

Sahakian, V., Bormann, J., Driscoll, N., Harding, A., Kent, G. and Wesnousky, S., 2017. Seismic constraints on the architecture of the Newport-Inglewood/Rose Canyon fault:

Implications for the length and magnitude of future earthquake ruptures. *Journal of Geophysical Research: Solid Earth*, *122*(3), pp.2085-2105.

Sanderson, D.J. and Marchini, W.R.D., 1984. Transpression. *Journal of structural Geology*, *6*(5), pp.449-458.

Singleton, D.M., Rockwell, T.K., Murbach, D., Murbach, M., Maloney, J.M., Freeman, T. and Levy, Y., 2019. Late-Holocene rupture history of the Rose Canyon fault in Old Town, San Diego: Implications for cascading earthquakes on the Newport–Inglewood–Rose Canyon fault system. *Bulletin of the Seismological Society of America*, *109*(3), pp.855-874.

Teyssier, C., Tikoff, B. and Markley, M., 1995. Oblique plate motion and continental tectonics. *Geology*, *23*(5), pp.447-450.

Tikoff, B. and Teyssier, C., 1994. Strain modeling of displacement-field partitioning in transpressional orogens. *Journal of Structural Geology*, *16*(11), pp.1575-1588.

Treiman, J.A., 1993. The Rose Canyon fault zone, southern California: California Division of Mines and Geology Open File Report 93-02, 45 p.

Treiman, J.A., 2002. Silver Strand fault, Coronado fault, Spanish Bight fault, San Diego fault, and downtown graben: Southern Rose Canyon fault zone, San Diego, California: California Division of Mines and Geology Fault Evaluation Report FER-245, 13 p.

USGS, 2019. U.S. Geological Survey and California Geological Survey, Quaternary fault and fold database for the United States, accessed March 1, 2019, at: https://www.usgs.gov/natural-hazards/earthquake-hazards/faults.

Van Wijk, J., Axen, G. and Abera, R., 2017. Initiation, evolution and extinction of pull-apart basins: Implications for opening of the Gulf of California. *Tectonophysics*, *719*, pp.37-50.

Wesnousky, S.G., 2008. Displacement and geometrical characteristics of earthquake surface ruptures: Issues and implications for seismic-hazard analysis and the process of earthquake rupture. *Bulletin of the Seismological Society of America*, *98*(4), pp.1609-1632.

Weidman, L., J. Maloney, T. Rockwell, 2019. Geotechnical data synthesis for GIS-based analysis of fault zone geometry and hazard in an urban environment, Geosphere, v. 15, no. 6, p, 1999–2017, doi: 10.1130/GES02098.1

Wetmore, J., Wetmore, P. H., Fletcher, J., Teran, O., Yelil, R., and Courtland, L. M., 2011. October. The Northwestern San Miguel-Vallecitors-Calabasas Fault System, Baja California, Mexico: Total Offset Constraints. In *2011 GSA Annual Meeting in Minneapolis, MN.*

Wetmore, P.H., Malservisi, R., Fletcher, J.M., Alsleben, H., Wilson, J., Callihan, S., Springer, A., González-Yajimovich, O. and Gold, P.O., 2019. Slip history and the role of the Agua Blanca fault in the tectonics of the North American–Pacific plate boundary of southern California, USA and Baja California, Mexico. *Geosphere*, *15*(1), pp.119-145.

Wiegand, J.W., 1970. Evidence of a San Diego Bay-Tijuana fault. *Bull. Assoc. Eng. Geol.;()*, *7*.

Wright, T. L. 1991. Structural Geology and Tectonic Evolution of the Los Angeles Basin, California. *Chapter 3, Active Margin Basins*. AAPG Memoir.

Wu, J.E., McClay, K., Whitehouse, P. and Dooley, T., 2009. 4D analogue modelling of transtensional pull-apart basins. *Marine and Petroleum Geology*, *26*(8), pp.1608-1623.

Yeats, R. S., Sieh, K. E., & Allen, C. R. 1997. *The geology of earthquakes*. Oxford University Press, USA.

Table 4.1. Radiocarbon dates used to construct an age model of sampled material in the Crown Cove cores (Figure 16).

Sample #	*Core (depth cm)*	*14C age (yrs BP)*	±	*Material*
13.3-78/79	CC-13 (368-369)	3070	15	Shell (whole)
13.3-113/114	CC-13 (404-405)	2575	15	Shell (whole)
12.2-208/210	CC-12 (379-380)	2180	15	Shell (whole)
12.2-192/194	CC-12 (355-357)	2000	15	Shell (whole)
13.3-74/75	CC-13 (361-362)	1815	15	Shell (whole)
13.3-4/5	CC-13 (294-295)	815	15	Shell (whole)

Table 4.2. Average fault trends and plate motion boundary conditions used in the structural analysis of the San Diego Bay pull-apart basin.

Feature	*Trend*
Rose Canyon fault	N 27° W
Descanso fault	N 25 ° W
San Miguel-Vallecitos fault	N 50° W
Group-1 average	N 1.5° E
Group-2 average	N 22.7° W
La Nacion fault zone Average	N 8.7 ° W
Maximum horizontal compressional stress	N 7° E
Plate boundary vector	N 43° W

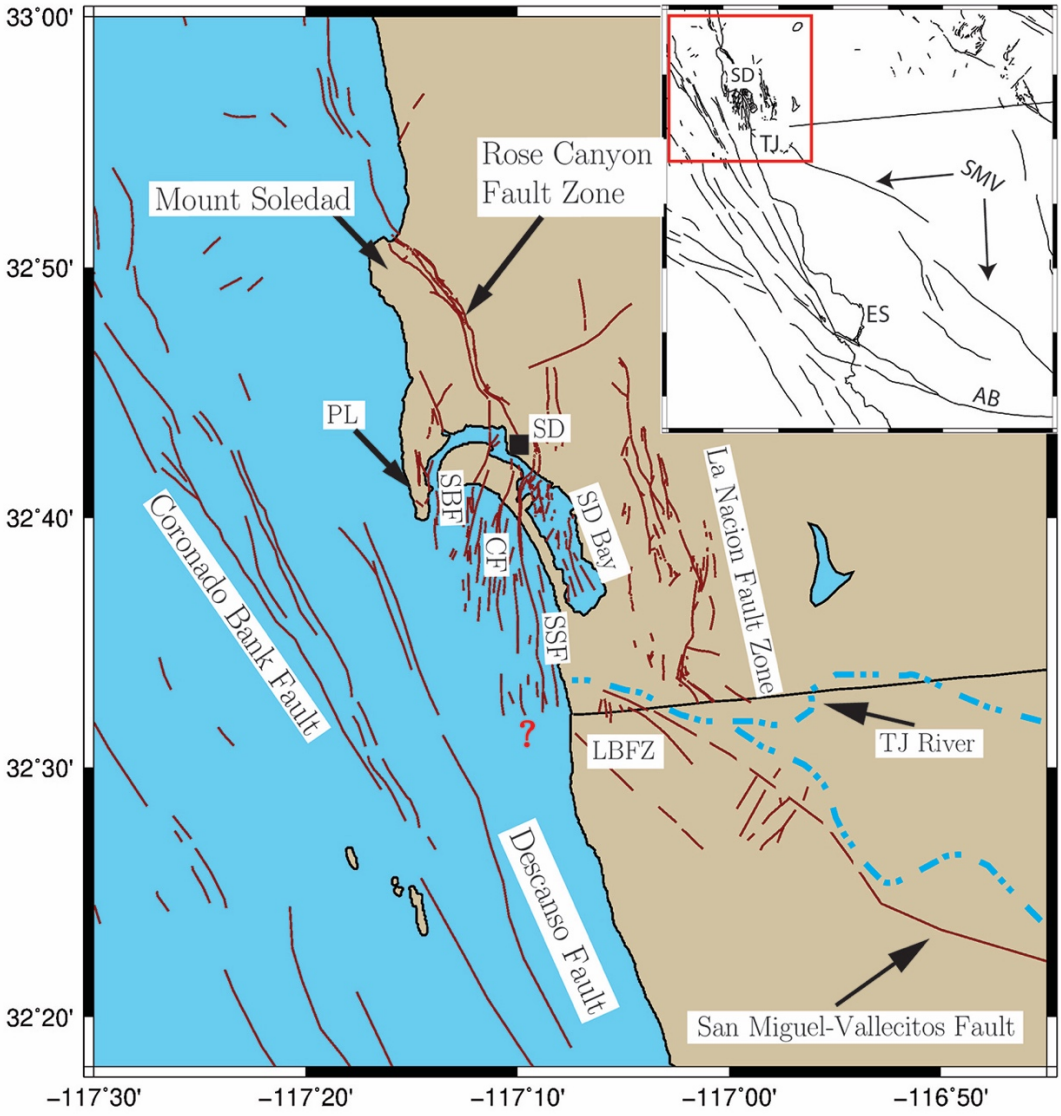

Figure 4.1. Overview map of San Diego region with regional faults (red lines). The faults that trend south away from San Diego Bay (i.e., SBF, CF, SSF) likely continue beyond the international border, but lack reliable data to extend the mapped trace. Inset shows location in northwestern Baja California and southwest California (red box) with transpeninsula faults (black lines). SD=San Diego, TJ=Tijuana, PL=Point Loma, ES=Ensenada, SMV=San Miguel-Vallecitos fault, AB=Agua Blanca fault, SBF=Spanish Bight fault, CF=Coronado fault, SSF=Silver Strand fault, LBFZ=Los Buenos fault zone. Fault traces north of the international border are from the USGS fault database (USGS, 2019), faults south of the border are from Fletcher et al. (2014).

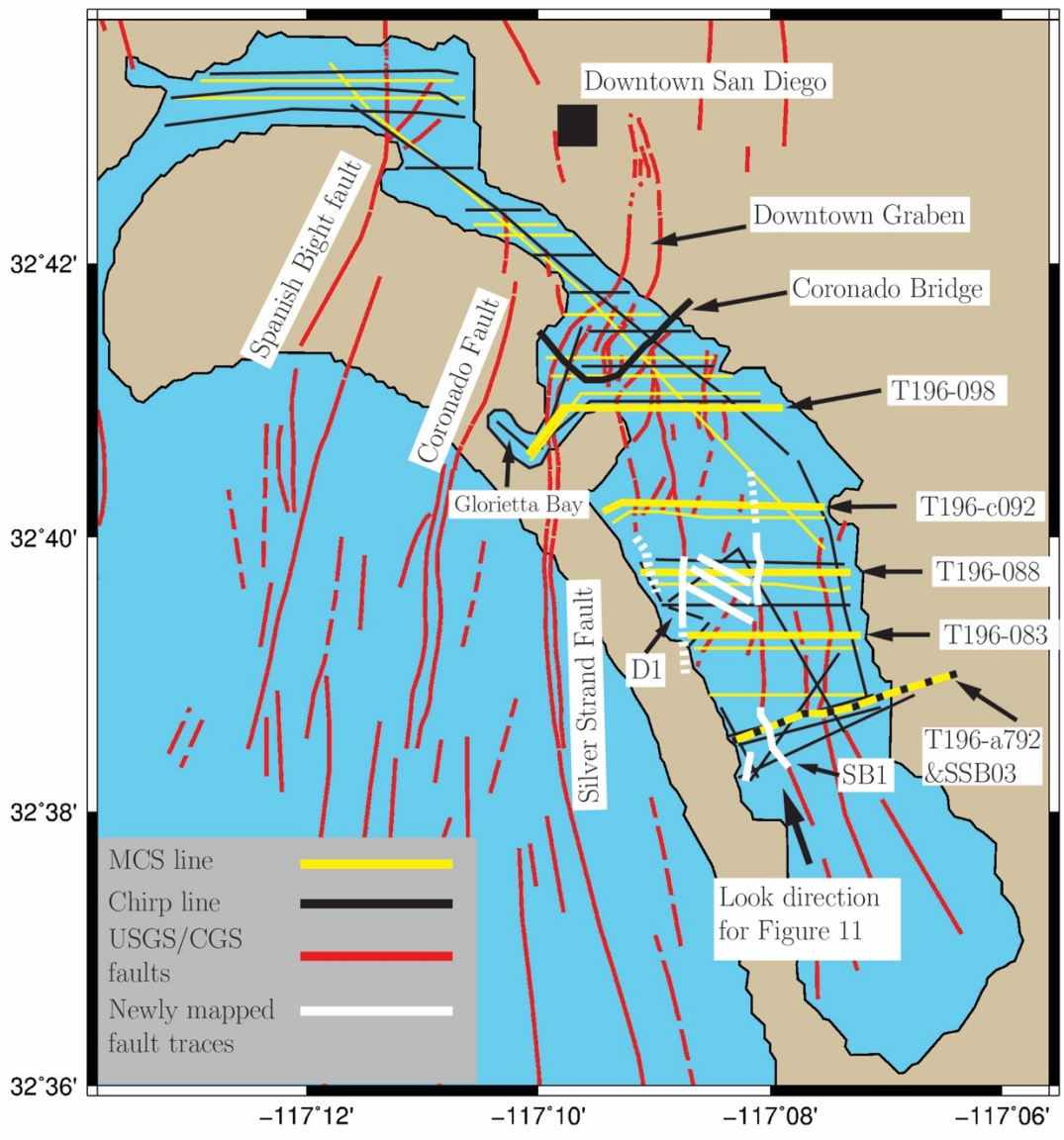

Figure 4.2. Map of San Diego Bay showing previously mapped fault traces from USGS quaternary fault database (red lines) (USGS, 2019), seismic data used in this study (yellow and black lines), and extended fault traces as part of this study (white lines). Bolded seismic lines are the location of figures presented in the text.

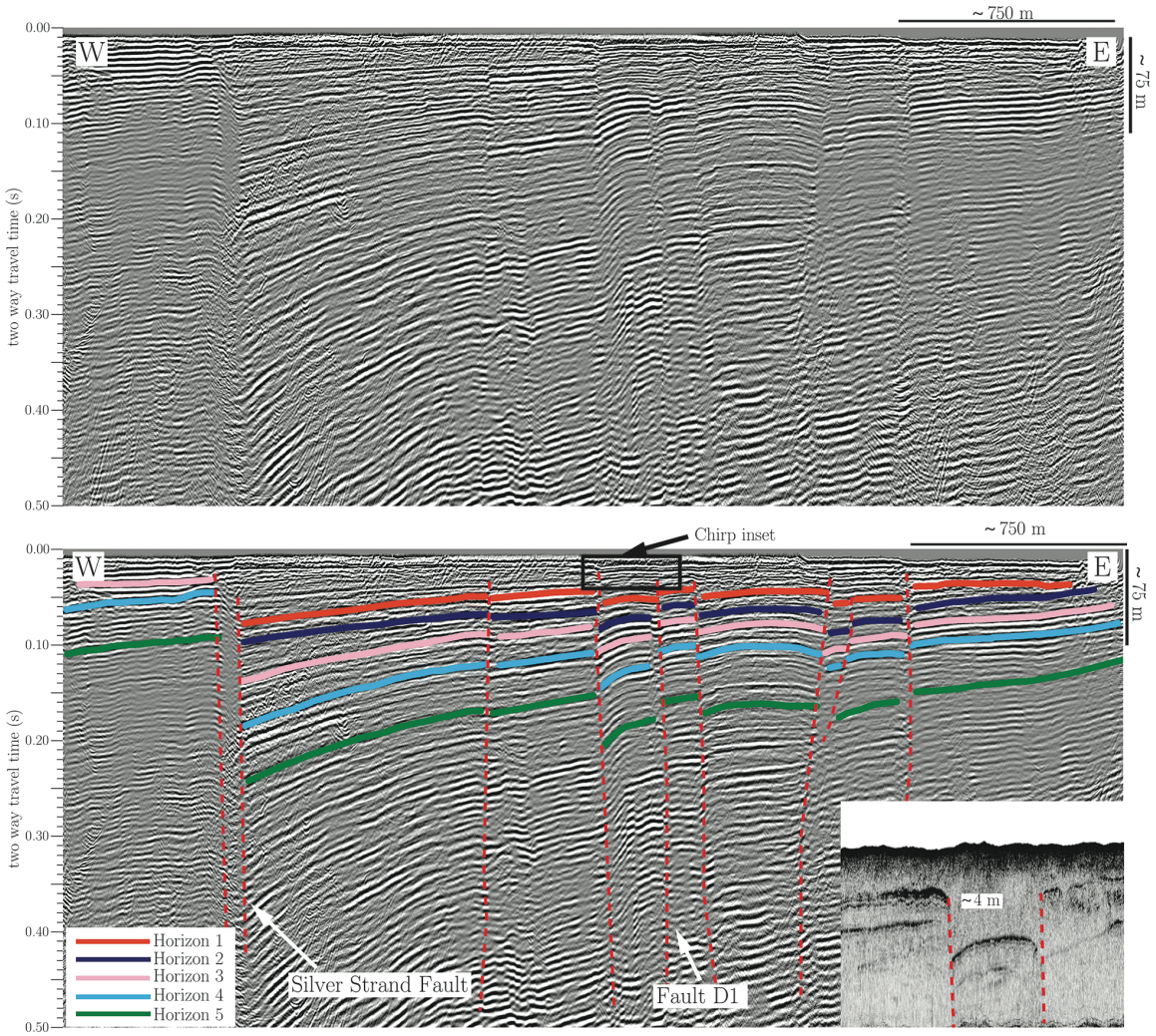

Figure 4.3. MCS profile T196-098 showing large displacement across the Silver Strand fault and westward dip of stratigraphy into both the Silver Strand fault and Fault D1. West of the Silver Strand fault, stratigraphy is flat lying to gently west dipping. Large apparent offset across the Silver Strand fault and uniform character of reflectors west of the fault make interpretations difficult. Inset shows offset high amplitude irregular reflector interpreted to represent the MIS stage 5e Nestor Terrace. Shown in the bottom panel are the five horizons used to observe changes in stratigraphy across San Diego Bay. Profile location shown in Figure 2.

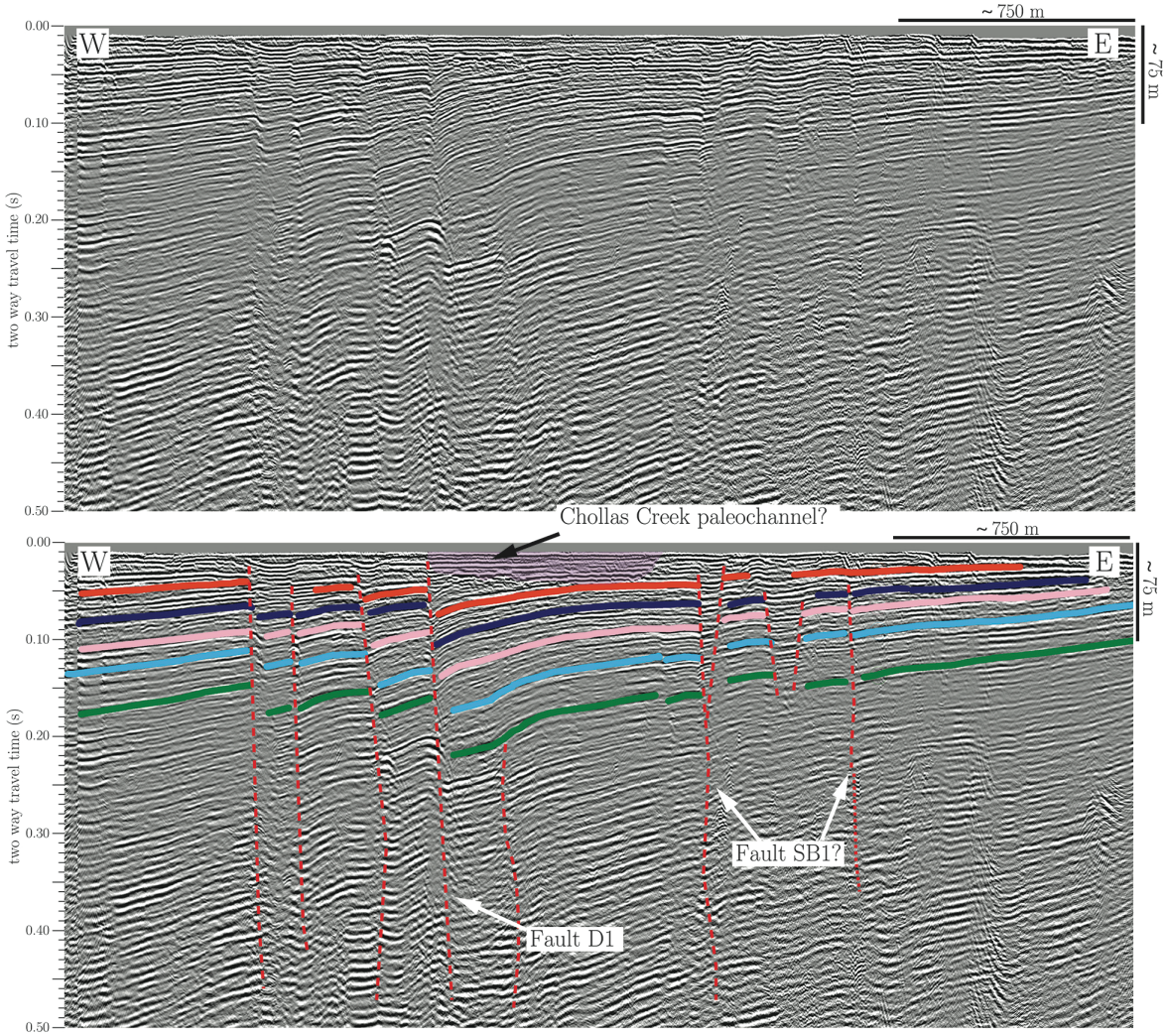

Figure 4.4. MSC profile T196-c092 showing increasing subsidence associated with D1. Horizons are the same as Figure 3. Location shown in Figure 2.

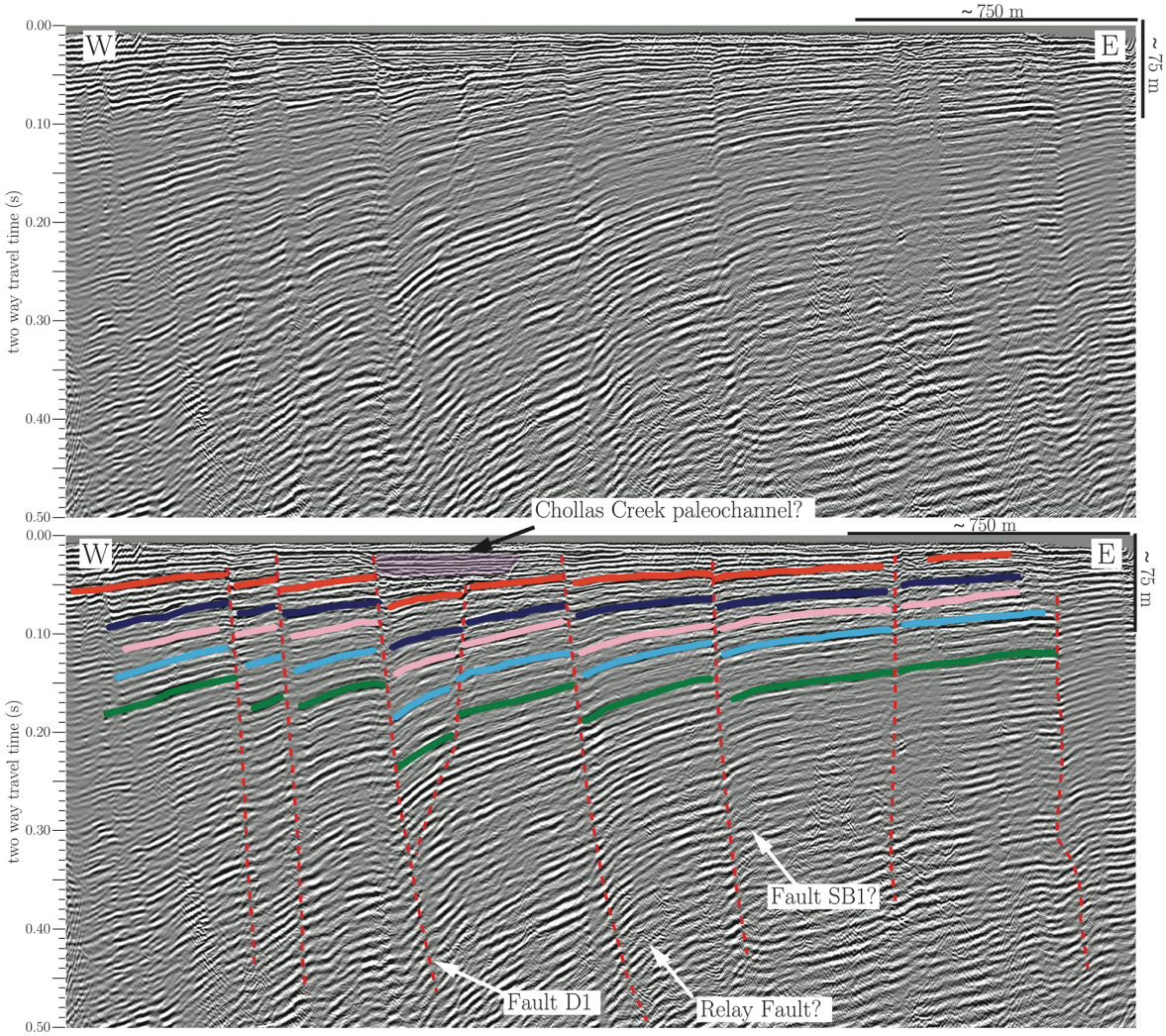

Figure 4.5. MCS profile T196-088 showing distributed faulting and potential relay structure between faults D1 and SB1. Horizons are the same as Figure 3. Location shown in Figure 2.

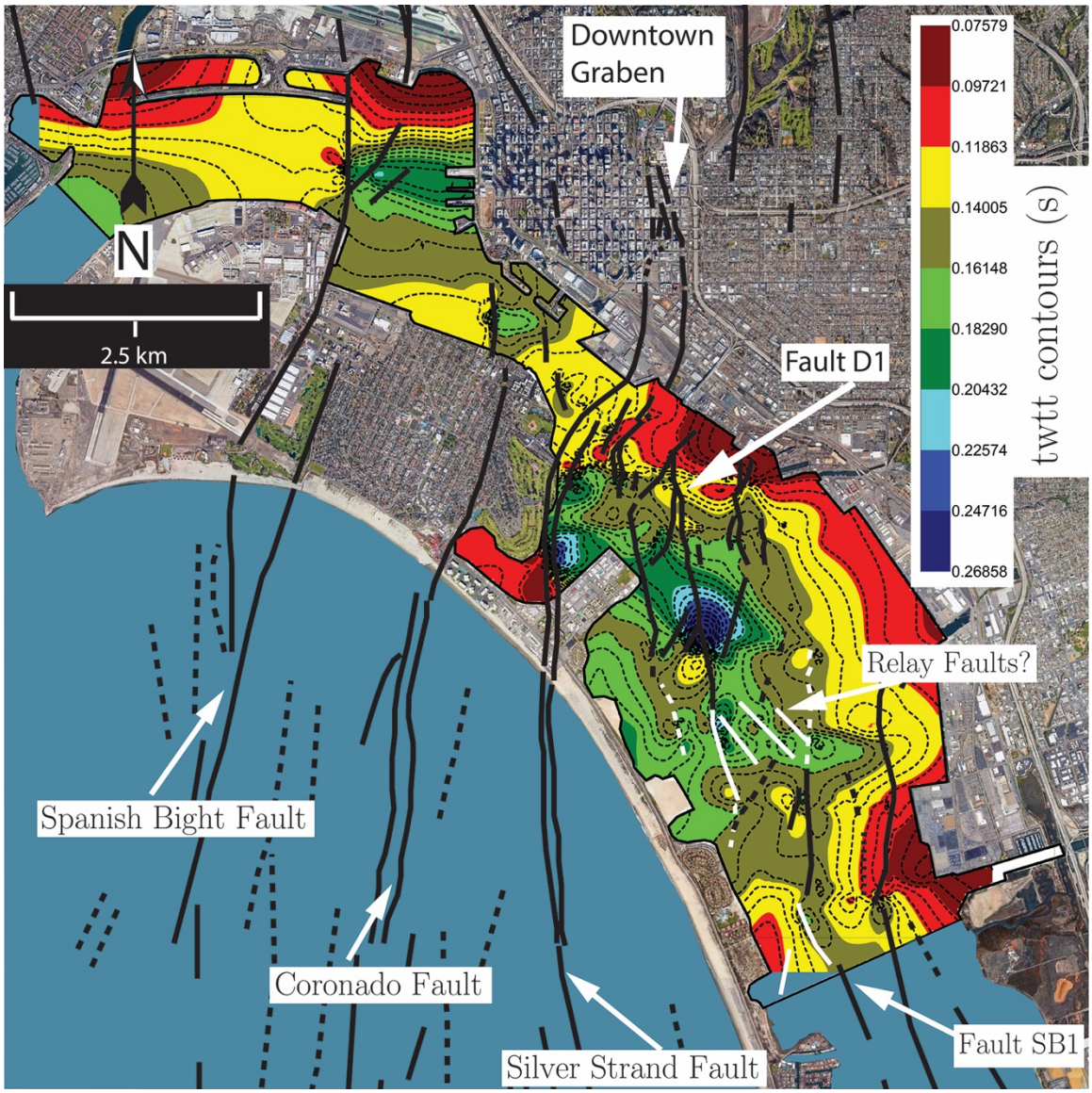

Figure 4.6. Horizon 5 gridded surface. Faults from the USGS quaternary fault database are shown as black lines (USGS, 2019). White lines are the extended fault traces from this study. Localized depositional centers are seen adjacent to D1, SB1, and the Silver Strand faults. Background satellite image from *Google Earth* (earth.google.com/web).

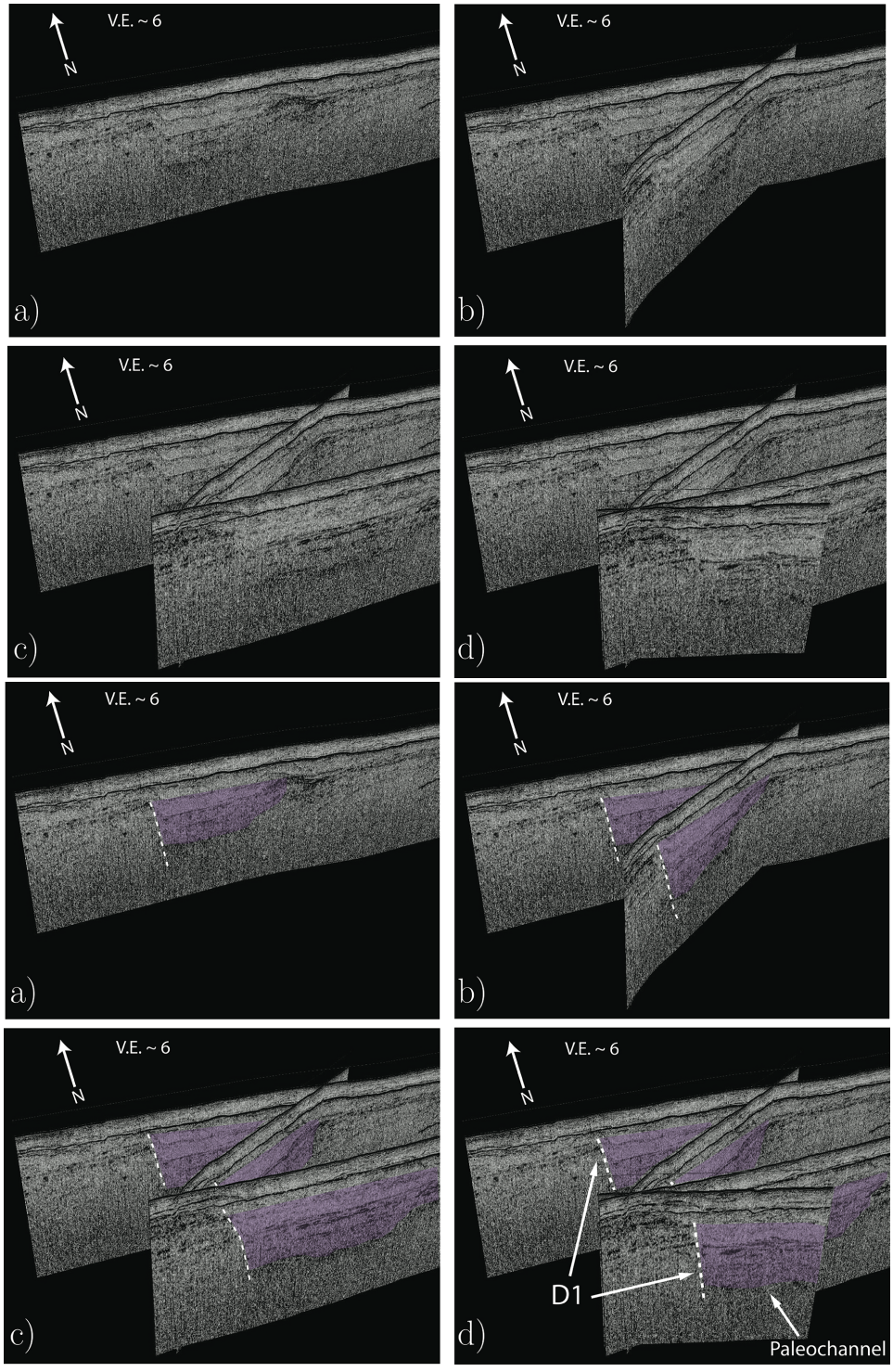

Figure 4.7. Unannotated (top) and annotated (bottom) fence diagrams showing trend of Fault D1 (white dashed vertical line) and its effect on the pathway of Chollas Creek (purple fill). See Figure 9 for look direction.

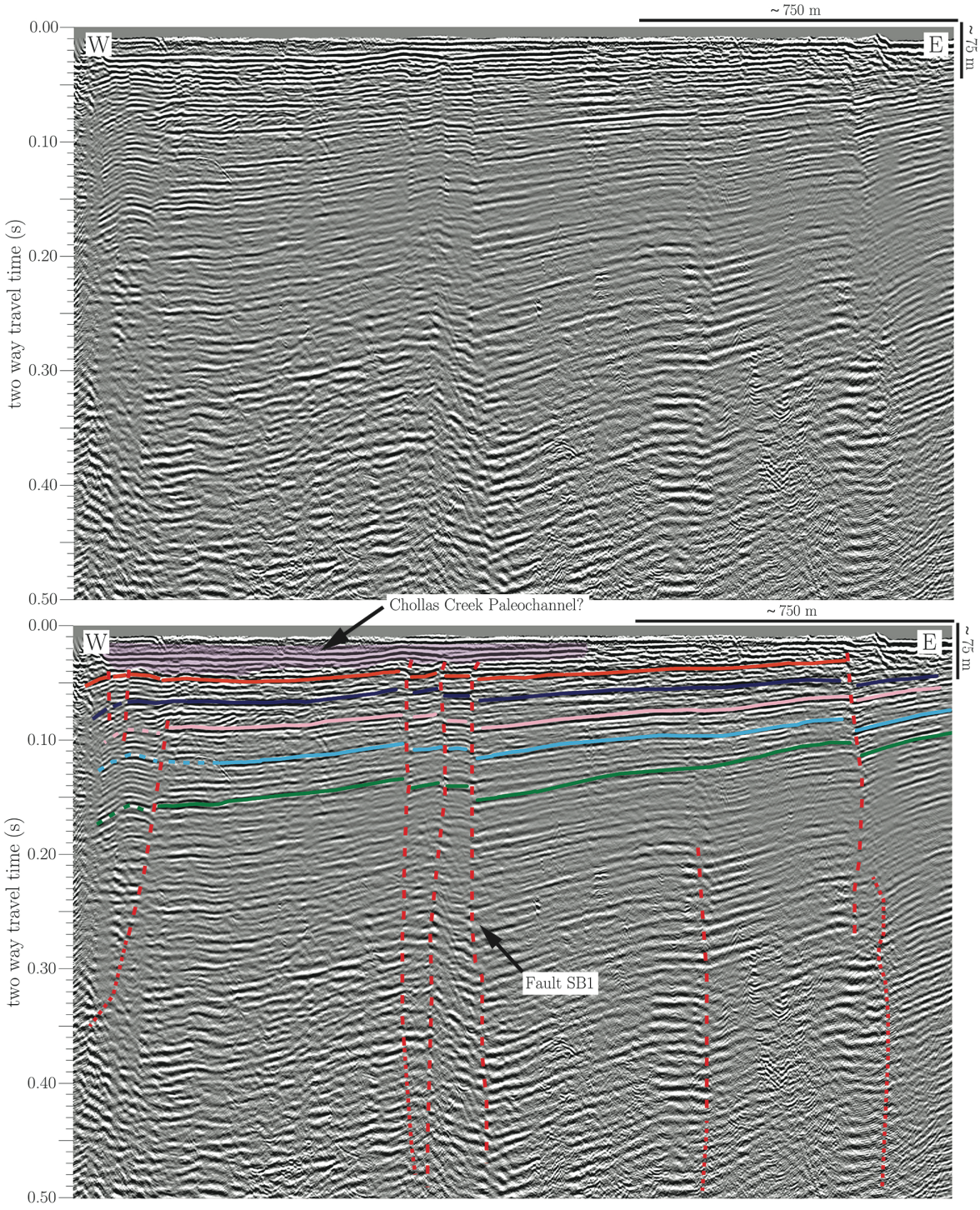

Figure 4.8. MCS profile T196-083 showing coalescing of fault strands adjacent to SB1 and more gently dipping stratigraphy to the west of SB1. Horizons are the same as Figure 3. Location shown in Figure 2.

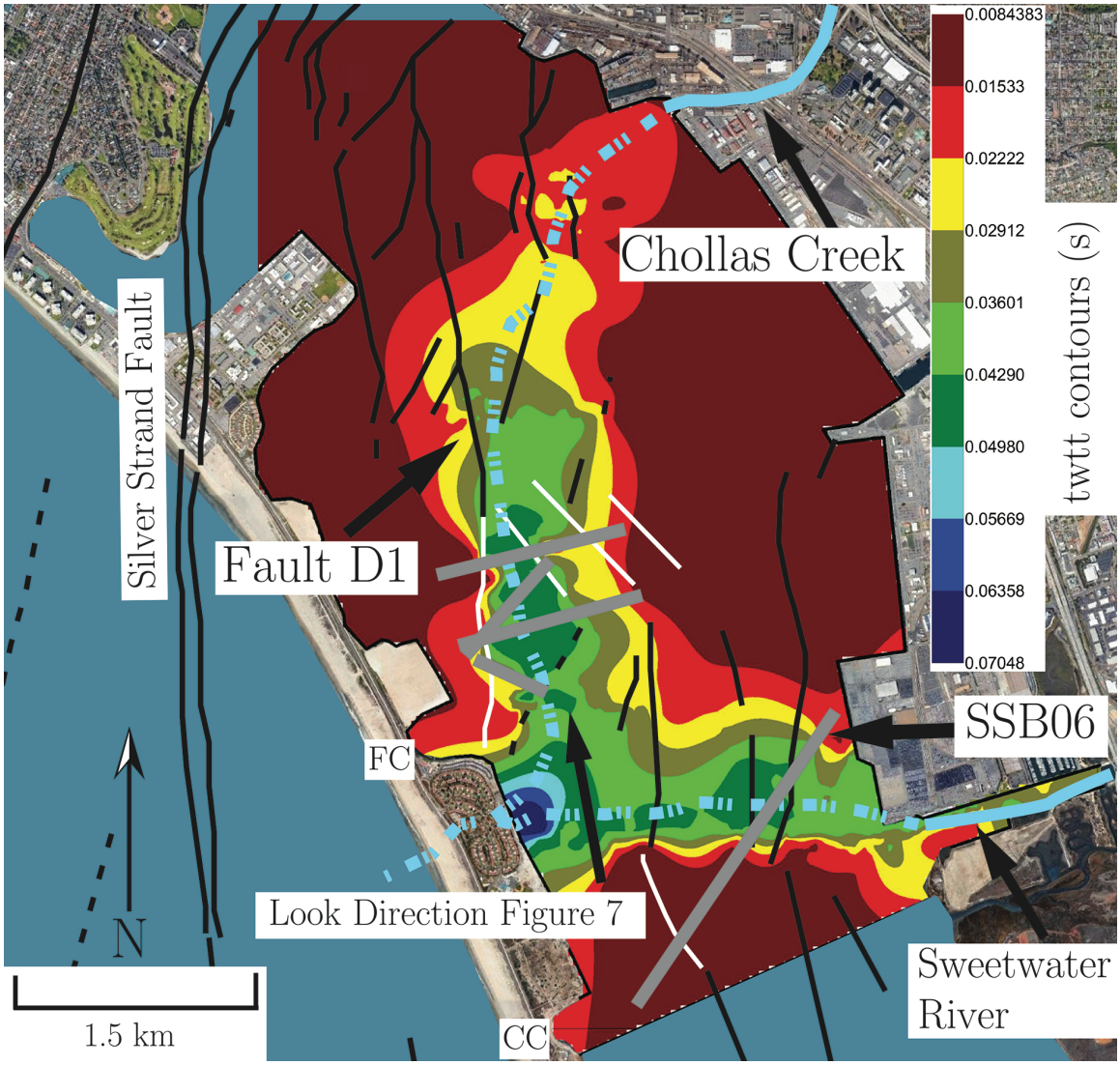

Figure 4.9. Gridded surface of paleochannels observed in combined MCS and chirp dataset. Previously mapped faults are shown in black, newly mapped faults in white. Blue dashed lines are the approximate locations of paleochannels. Grey lines are locations of chirp profiles. FC=Fiddlers Cove, CC=Crown Cove. Background satellite image from *Google Earth* (earth.google.com/web).

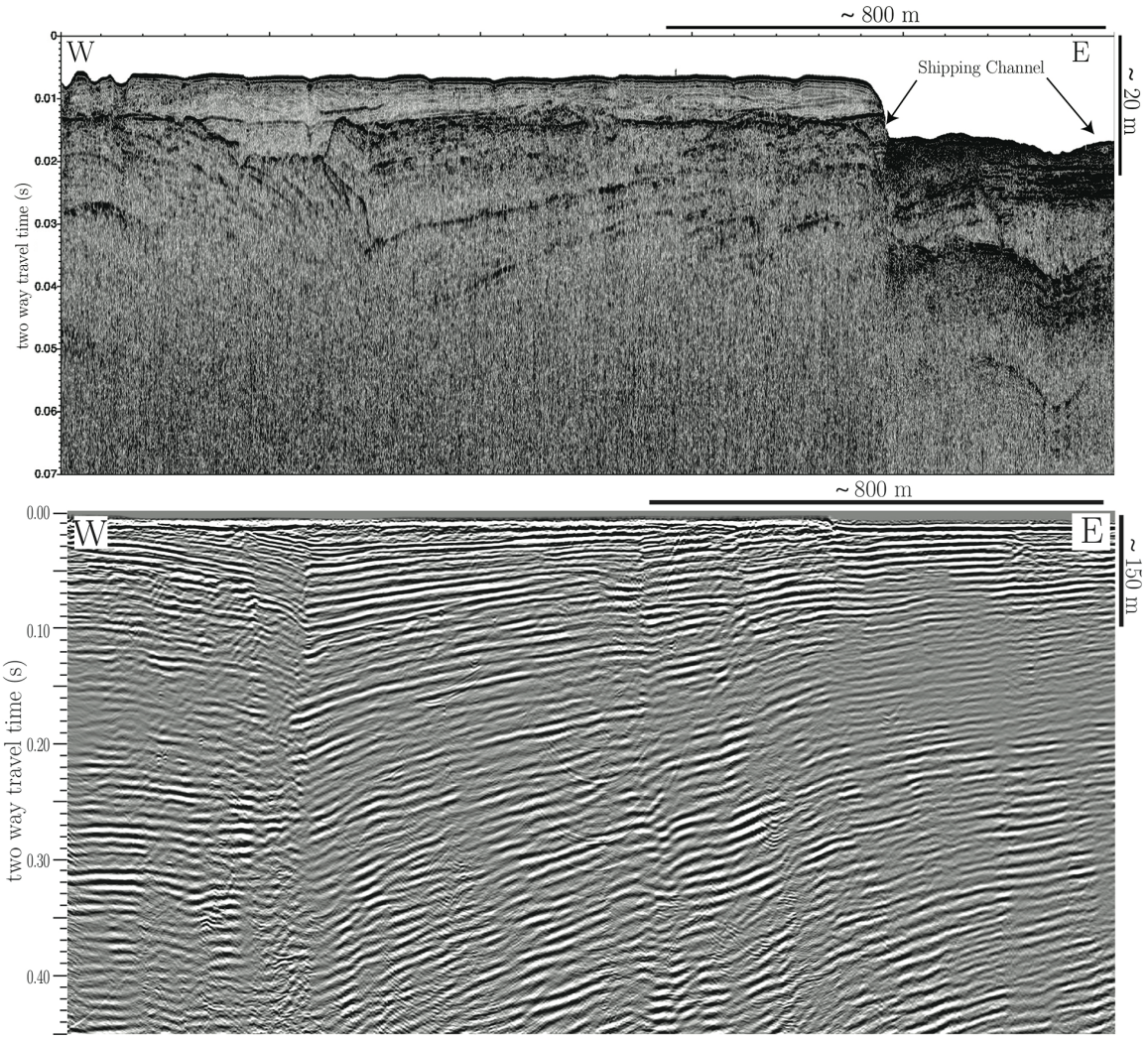

Figure 4.10. Unannotated (upper panel) and annotated (lower panel) nested chirp profile SSB03 (top profile) and MCS profile T196-a792 (bottom profile). Effect of Fault SB1 is seen as increasing dips with depth in the MCS profile, and growth strata terminating against the fault in the chirp profile. Green dashed horizon in chirp profile is the interpreted subaerially exposed surface from the latest sea level low-stand. Horizons in MCS image are the same as Figure 3. Location shown in Figure 2.

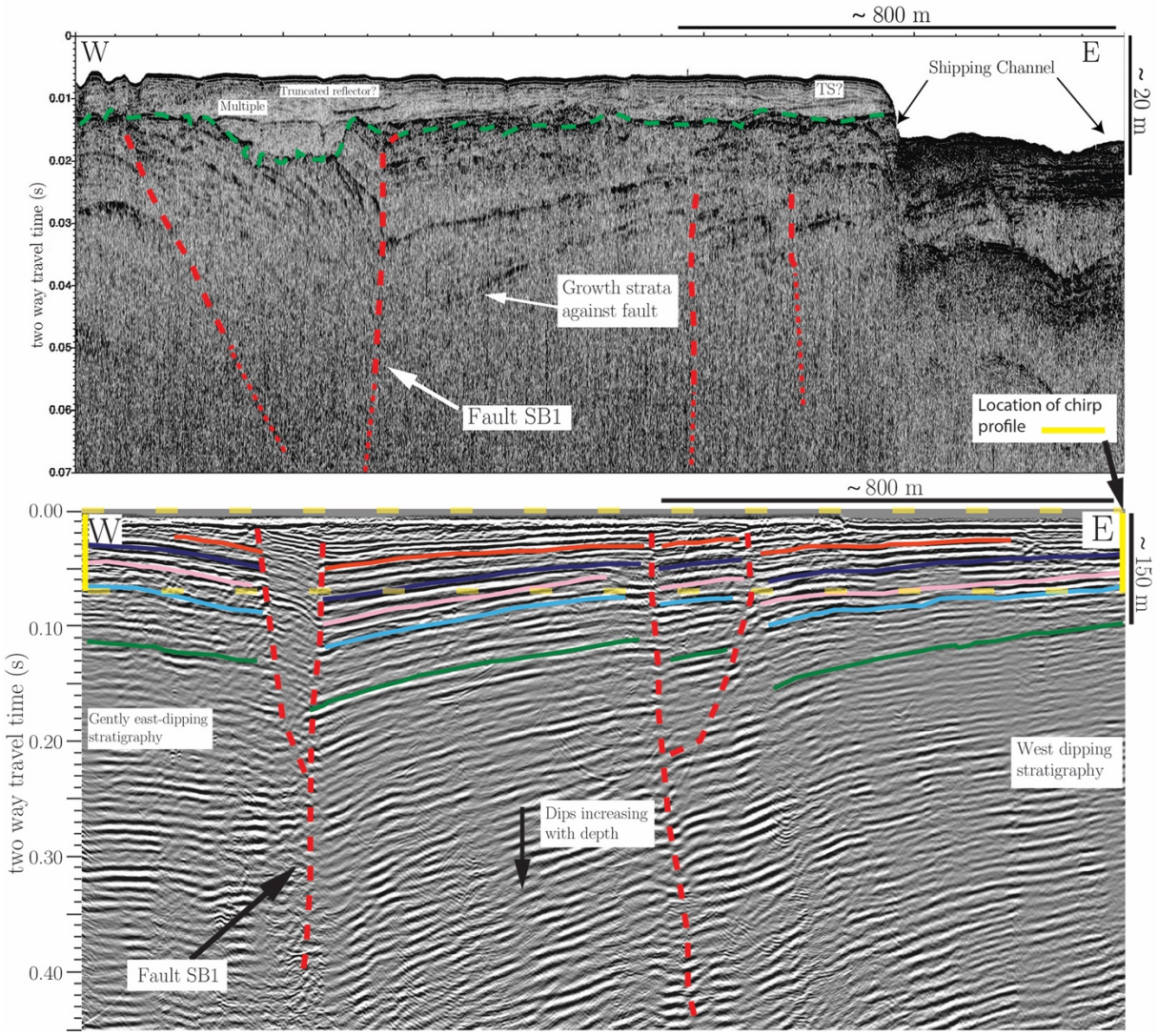

Figure 4.10. Continued. Unannotated (upper panel) and annotated (lower panel) nested chirp profile SSB03 (top profile) and MCS profile T196-a792 (bottom profile). Effect of Fault SB1 is seen as increasing dips with depth in the MCS profile, and growth strata terminating against the fault in the chirp profile. Green dashed horizon in chirp profile is the interpreted subaerially exposed surface from the last glacial maximum sea level low-stand. Horizons in MCS image are the same as Figure 3. Location shown in Figure 2.

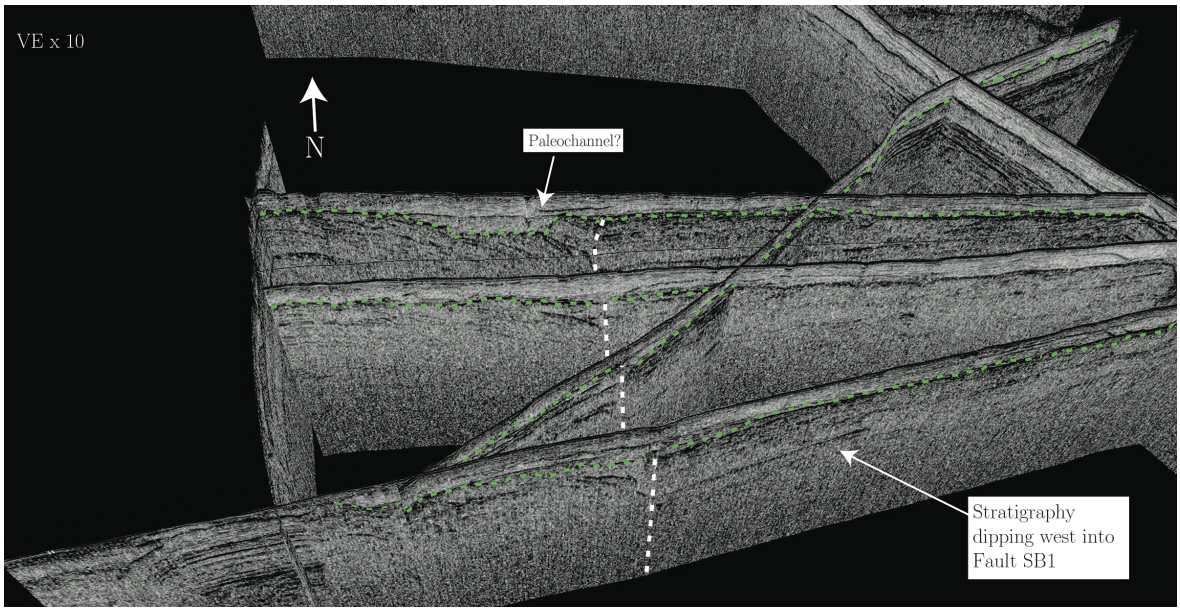

Figure 4.11. Fence diagram of southernmost chirp lines that image Fault SB1. Vertical white dashed line is trace of SB1. Green dashed line is the interpreted sea level low-stand surface. See Figure 2 for location.

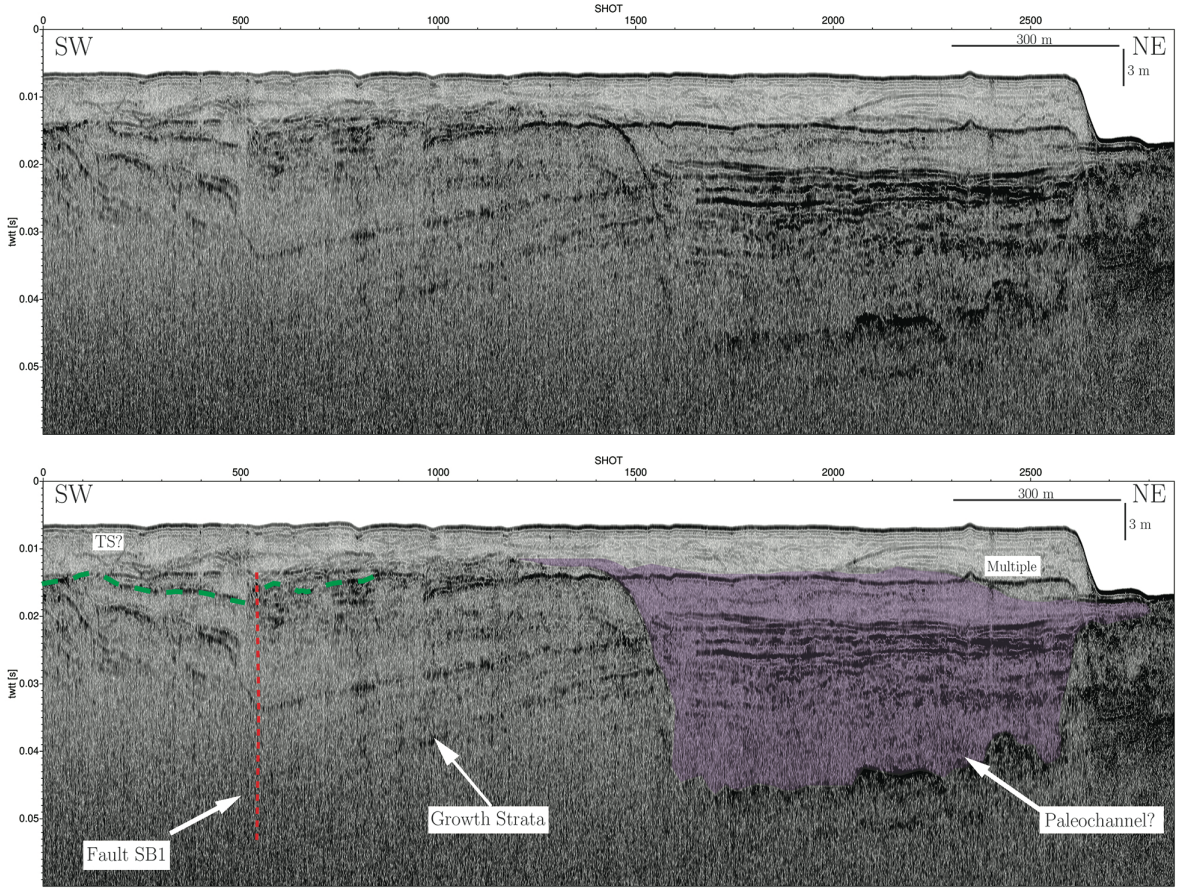

Figure 4.12. Chirp profile SSB06 across the Sweetwater paleochannel. Red dashed line is location of SB1. Green dashed line is the interpreted latest sea level low-stand surface. Location shown in Figure 9.

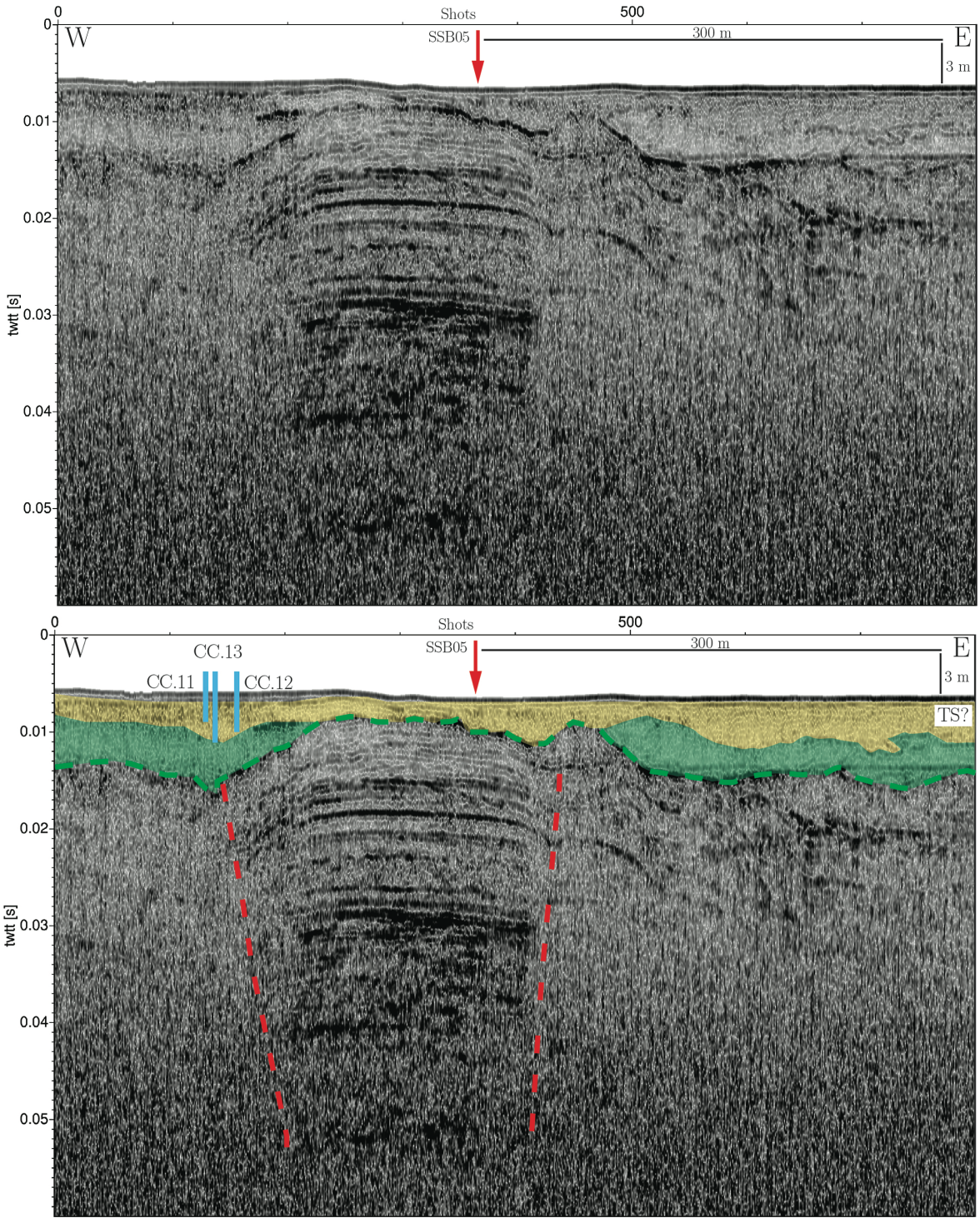

Figure 4.13. Chirp profile SSB02 with core correlation. Yellow horizon is potential inundation surface/latest transgressive surface. Green horizon is deposition from the last sea level low-stand until inundation. Red arrow marks location of north-south oriented SSB05 profile. See Figure15a for location.

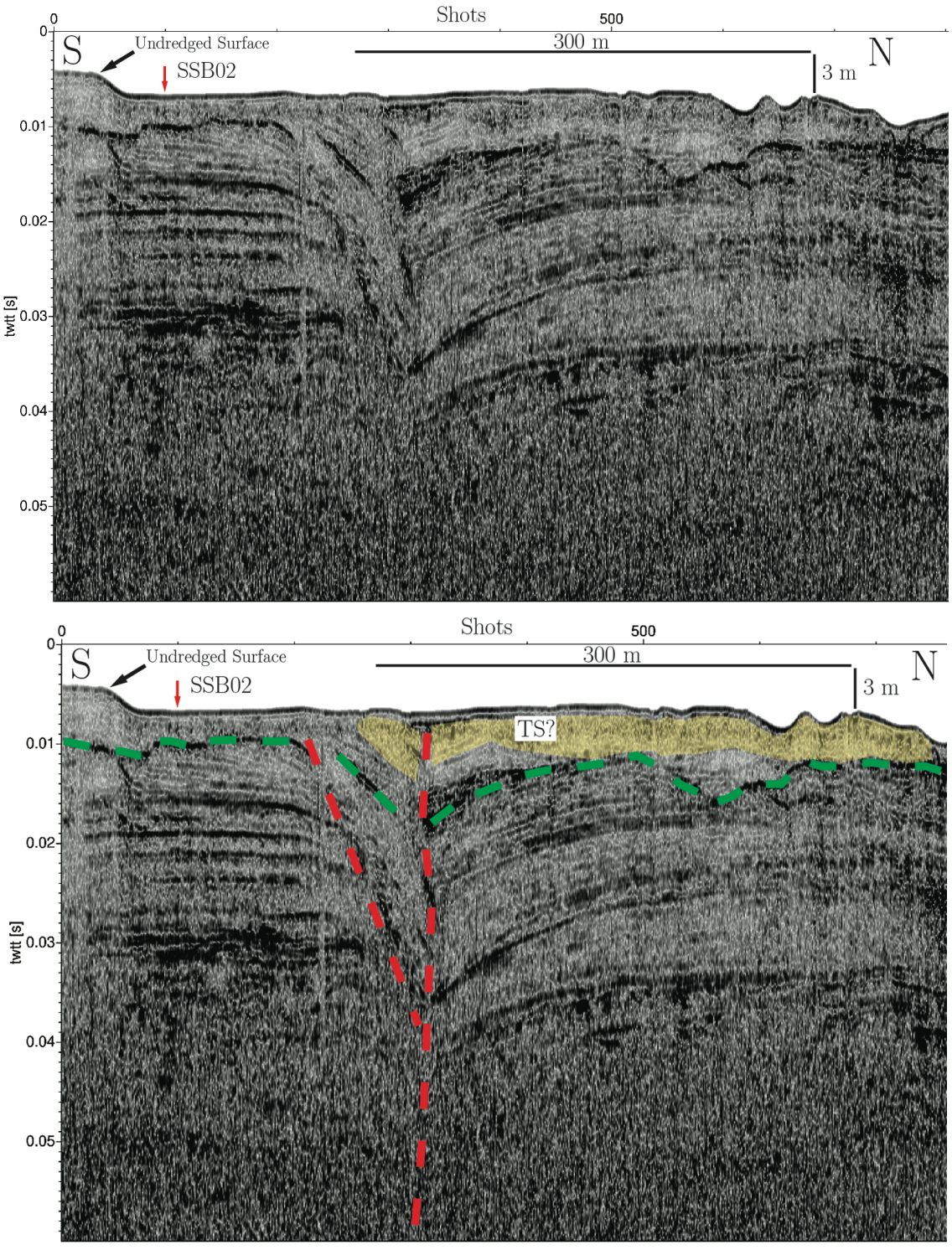

Figure 4.14. SSB05 showing offset associated with western pop-up structure fault. Green dashed line is the interpreted sea level low-stand surface. Yellow transparent unit is the interpreted transgressive surface / inundation surface. Red arrow marks location of east-west oriented SSB02 profile. See Figure15a for location.

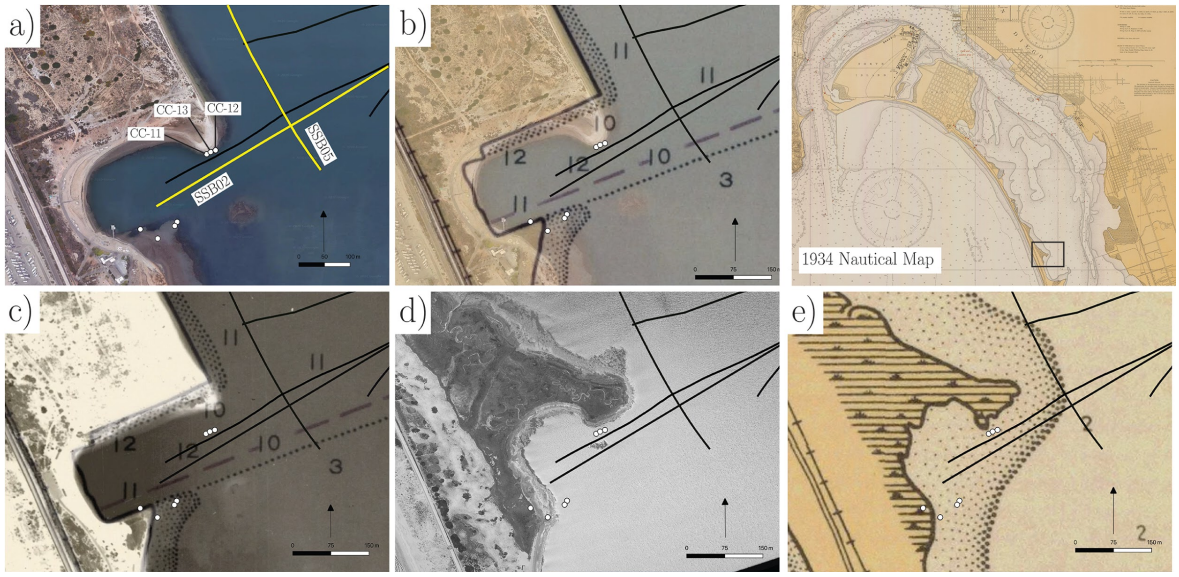

Figure 4.15. Map of Crown Cove Cores. a) Modern Day satellite image. b) 1945 Nautical Chart overlaid on Modern Day Satellite image. c) 1945 Nautical Chart overlaid on 1951 Aerial Image. d) 1941 Aerial Image. e) 1927 Nautical Chart. Black Box in 1934 Nautical Chart shows location in San Diego Bay. White dots are locations of cores and black lines are chirp profiles.

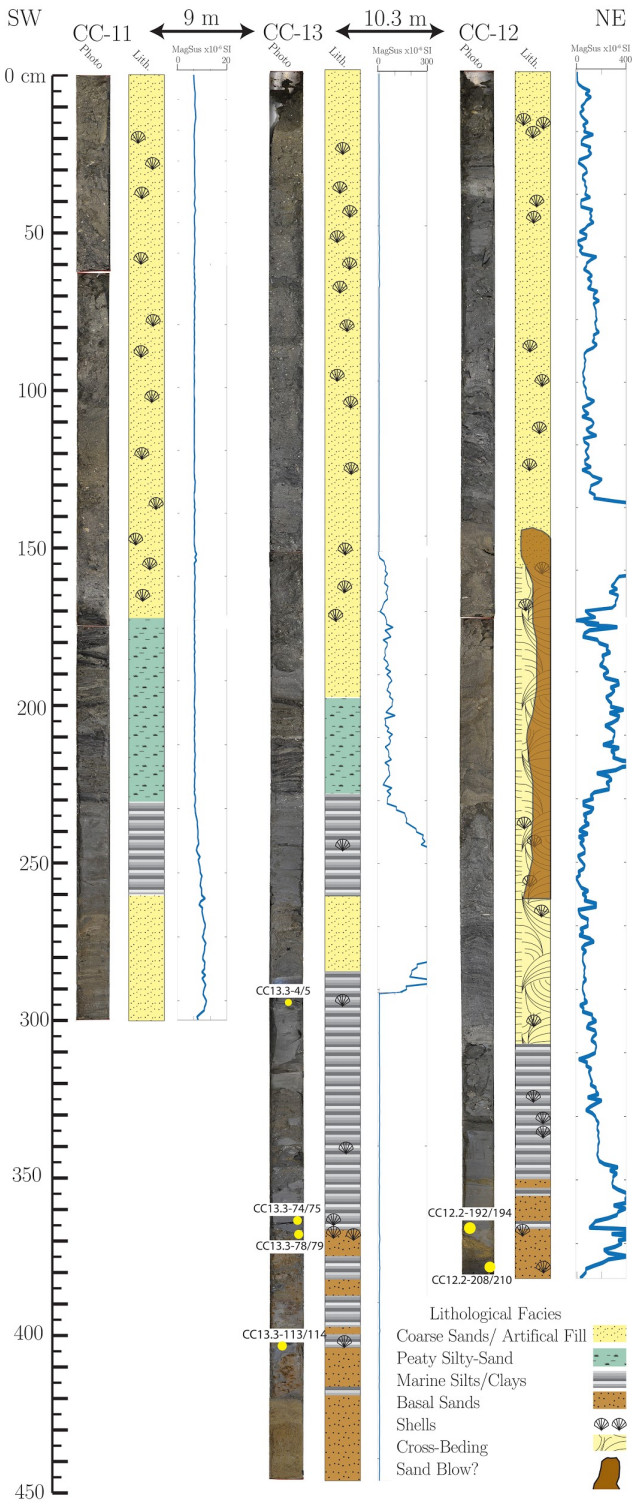

Figure 4.16. Crown Cove cores. Shown is a photograph of the core, a simplified lithology, and magnetic susceptibility. Yellow dots are sample locations for radiocarbon dating.

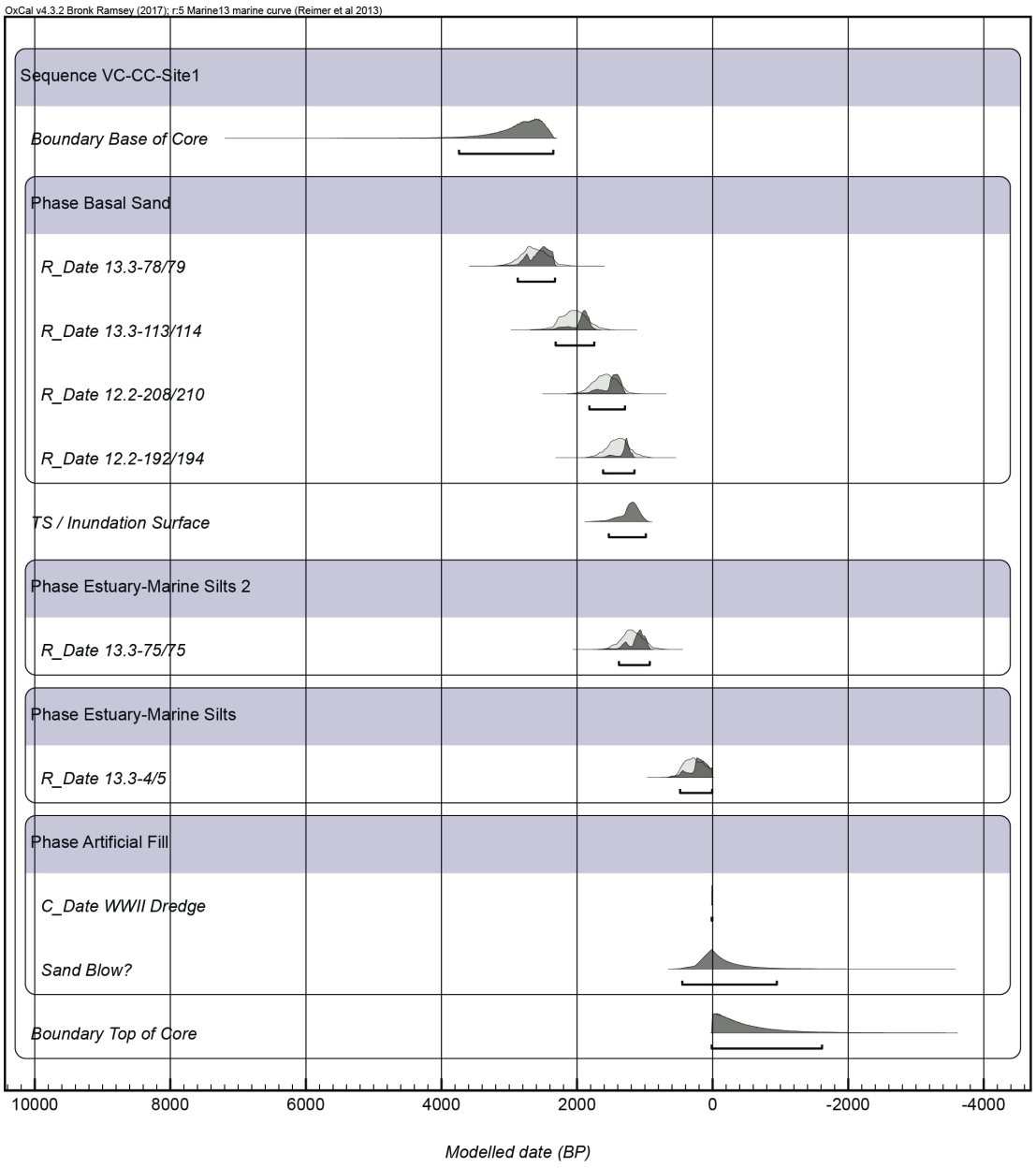

Figure 4.17. OxCal Age Model for Crown Cove cores.

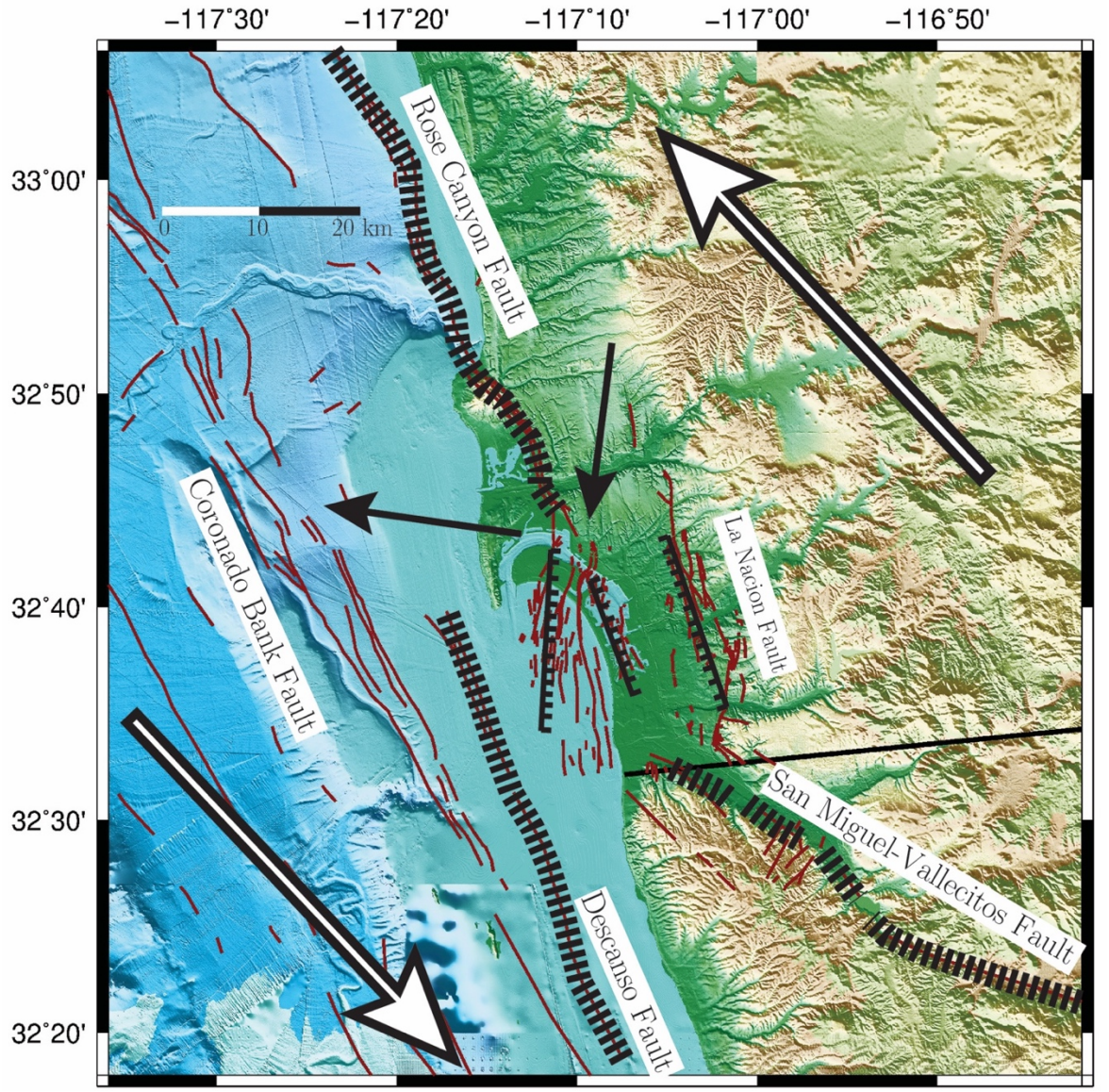

Figure 4.18. Regional fault orientations and plate boundary parameters used for kinematic interpretation. Solid black arrows are maximum and minimum horizontal stress orientations (Hardebeck and Hauksson, 2001), large outlined arrows are plate motion vectors, and the average orientations for Group-1, Group-2 and La Nacion fault zones are solid black, toothed lines. Large black hatched lines are regional faults.

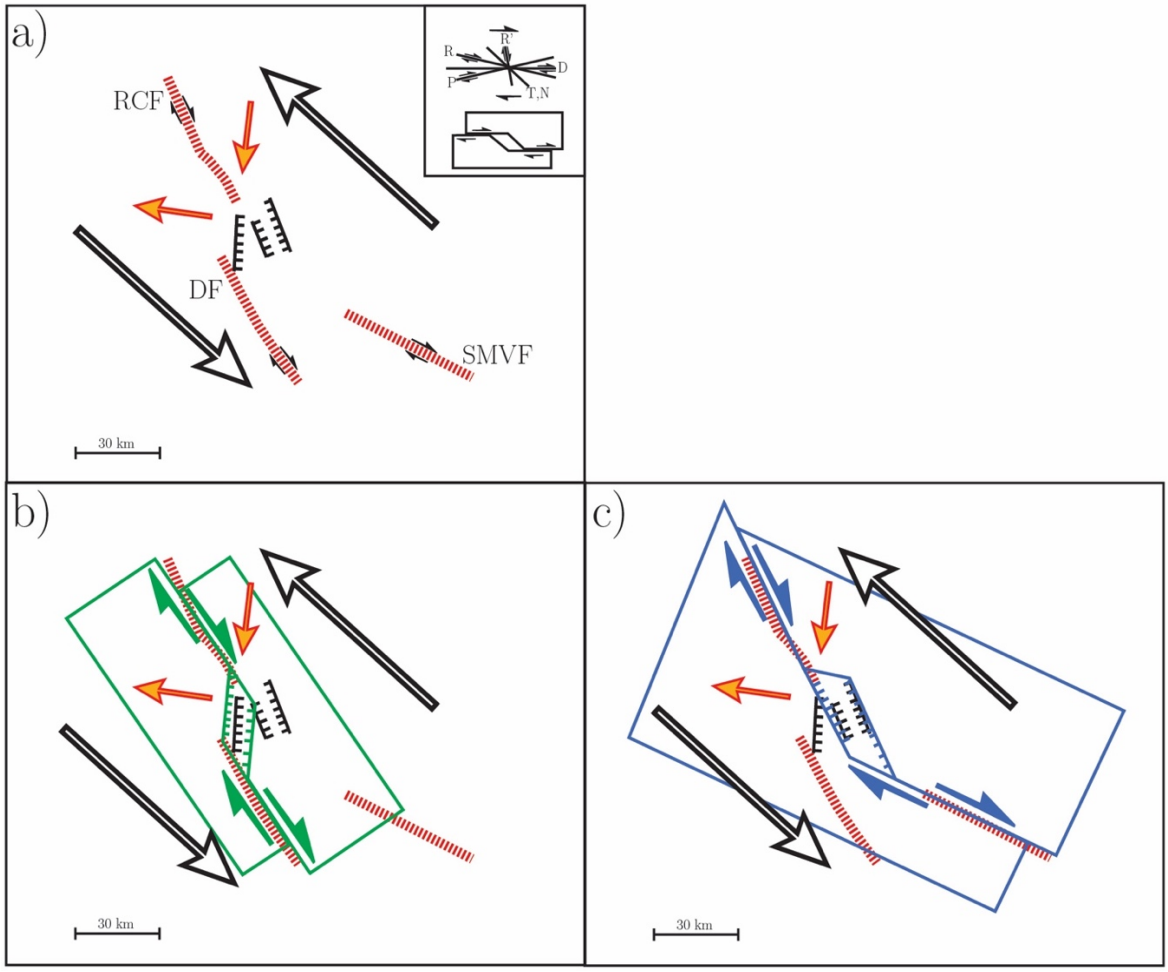

Figure 4.19. Conceptual model for San Diego Bay pull-apart basin. (a) Model parameters. (b) Conceptual model for Group-1 faults. (c) Conceptual Model for Group-2 and La Nacion faults.

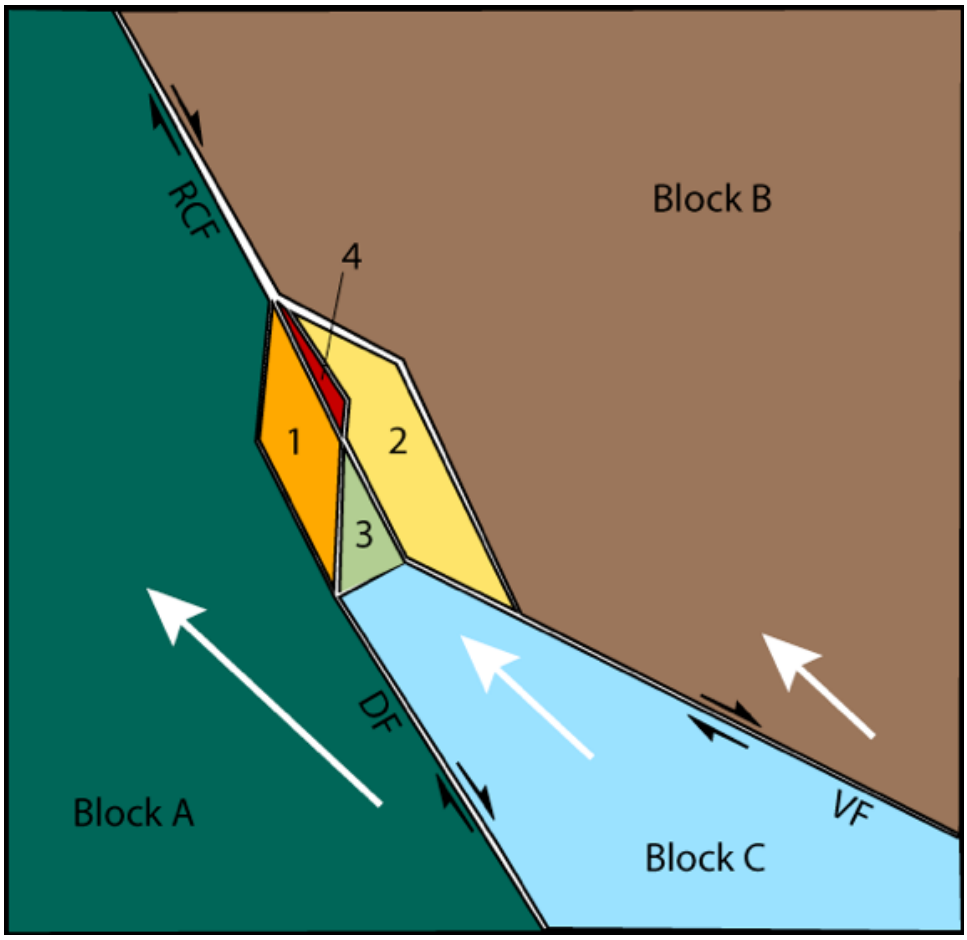

Figure 4.20. Conceptual kinematic block model for the San Diego region. See text for explanation. RCF=Rose Canyon fault, DF=Descanso fault, VF=Vallecitos fault.

5. Conclusion

The material presented in preceding chapters increases our understanding of the Rose Canyon fault and its role in the larger southern California plate boundary. The results presented in this dissertation are based on new datasets compiled using a combination of geological and geophysical observational techniques. The multidisciplinary approach employed to investigate the fault behavior and features of the Rose Canyon fault allows for a better characterization of the seismic hazard in the San Diego-Tijuana region, as well as contributing towards answering fundamental questions in earthquake science such as the variation in earthquake distributions in time and space and what factors control that variation. The following paragraphs summarize the major results of this dissertation.

The results from our paleoseismic study at Old Town show that the Rose Canyon fault has sustained seismic activity with ground rupturing earthquakes throughout the late Holocene and into the Historical period. The last relatively larger magnitude earthquake on the Rose Canyon fault at Old Town was apparently sometime in the mid-1700s. The Old Town paleoseismic record suggest that the Rose Canyon fault has a ~700-800 year recurrence interval for relatively larger magnitude earthquakes (M 6.7-7). The Old Town trenches also contain evidence of a historical rupture that most likely correlates to the May 27th 1862 San Diego earthquake (M ~6), which historical records of ground motion indicate may have initiated on a fault segment beneath San Diego Bay. This could imply that faults in San Diego Bay and the main segment of the Rose Canyon fault can rupture in synchrony. The close correlation in time of dated earthquakes at paleoseismic sites along strike of the Newport-Inglewood-Rose Canyon fault system suggests that the various fault segments communicate stress most likely through a cascading sequence of earthquakes.

The surface velocities of the combined campaign and continuous GPS network indicate a ~3.5 mm/yr gradient across the San Diego region. The results of the preferred double fault homogeneous elastic half-space model indicate that the Rose Canyon fault may be slipping at 2.4 ± 0.5 mm/yr. However, the optimally oriented DESC transect suggests a higher rate of ~2.9 mm/yr. Results from the asymmetric elastic half space model suggest that the oceanic-continental lithospheric boundary present along the northern Newport-Inglewood segment may continue at least as far south as San Diego. Surface velocities relative to site SIO5, which is located on the trace of the Rose Canyon fault point towards a more easterly trend of the fault zone through southern San Diego. Reprocessed MCS data from south San Diego Bay image several northwest oriented faults that are well aligned to provide a fault structure to link the Rose Canyon fault with potential faulting south of San Diego Bay.

The results of the fourth chapter show the value of reprocessed legacy MCS data to investigate fault structures and correlate stratigraphy in urban waterways where new data collection may not be feasible. When combined with the high-resolution chirp profiles, the nested dataset allows for a more comprehensive interpretation of stratigraphy and recency of faulting beneath San Diego Bay. The results of the gridded surface for horizon 5 show several localized depositional centers adjacent to potential sidewall faults. In the southeastern portion of San Diego Bay, fault D1-SB1 looks to be a continuous fault structure connected by relay faults. The D1-SB1 linked fault appears to control deposition in the southern portion of San Diego Bay and is similarly oriented to gravity anomalies beneath the bay.

The San Diego Bay pull-apart basin can be divided into a western and eastern basin based on the different orientation of two groups of faults (Group-1 and Group-2/La Nacion fault zone). Group-1 faults are located in the northwestern portion of San Diego Bay and are well described

by a Rose Canyon–Descanso fault pull-apart basin causing subsidence beneath San Diego Bay. The near parallel orientation of Group-2 and the La Nacion faults to the Rose Canyon fault are in contrast to this model and suggest an additional influence from other regional faults. A potential pull-apart basin between the Rose Canyon and the San Miguel-Vallecitos faults could explain the orientations of the Group-2 and La Nacion faults. However, kinematic analysis of fault orientations and plate motion boundary conditions predict a significant component of strike-slip motion in the eastern basin that is not observed in seismic profiles. Interestingly, the southernmost profiles show several features typically associated with transtension that argue for an increasing component of strike-slip motion and may point towards the early development of a cross-basin fault. The favorable orientation of the Group-2 and La Nacion faults as well as the potential formation of a linked D1-SB1 fault, may be evidence for a Rose Canyon–San Miguel-Vallecitos fault connection, but further work on the nature of faulting in the southern extreme of San Diego Bay and in the Tijuana River Valley is warranted to fully resolve this potential connection.